ACS OMEGA

Open Access

http://pubs.acs.org/journal/acsodf

Review

Definitive Review of Nanobiochar

Abhishek Kumar Chaubey, Tej Pratap, Brahmacharimayum Preetiva, Manvendra Patel, Jonathan S. Singsit, Charles U. Pittman, Jr., and Dinesh Mohan*

Cite This: *ACS Omega* 2024, 9, 12331−12379

Read Online

ACCESS | Metrics & More | Article Recommendations

ABSTRACT: Nanobiochar is an advanced nanosized biochar with enhanced properties and wide applicability for a variety of modern-day applications. Nanobiochar can be developed easily from bulk biochar through top-down approaches including ball-milling, centrifugation, sonication, and hydrothermal synthesis. Nanobiochar can also be modified or engineered to obtain "engineered nanobiochar" or biochar nanocomposites with enhanced properties and applications. Nanobiochar provides many fold enhancements in surface area (0.4−97-times), pore size (0.1−5.3-times), total pore volume (0.5−48.5-times), and surface functionalities over bulk biochars. These enhancements have given increased contaminant sorption in both aqueous and soil media. Further, nanobiochar has also shown catalytic properties and applications in sensors, additive/fillers, targeted drug delivery, enzyme immobilization, polymer production, etc. The advantages and disadvantages of nanobiochar over bulk biochar are summarized herein, in detail. The processes and mechanisms involved in nanobiochar synthesis and contaminants sorption over nanobiochar are summarized. Finally, future directions and recommendations are suggested.

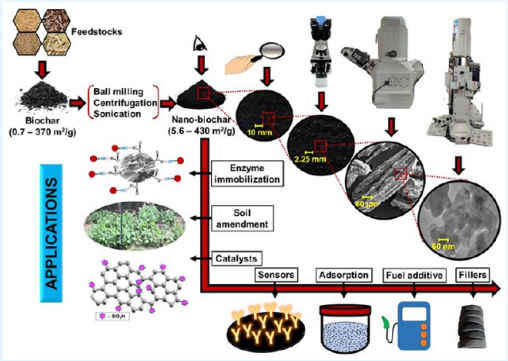

1. INTRODUCTION

Biochar has emerged as a sustainable contributing solution for a wide range of environmental issues, including water pollution, land degradation, accumulating waste, and climate change.[1−9] Biochar is a carbonaceous product of biomass pyrolysis under limited oxygen supply.[10] A wide range of biomass agricultural wastes,[1,9,11,12] animal manures,[1,12,13] municipal wastes,[8,12,14,15] forest residues,[16,12,13,17] and industrial byproducts[12,13,18] can be, and have been, utilized for biochar production. Biochar was initially developed as a soil fertility enhancer and for carbon sequestration.[19−22] Later, biochar was successfully applied for water treatments, photocatalysis, enzyme immobilization, electrodes, supercapacitors, sensor preparation, and as a filler material in construction.[1,2,9,23−26] Still, large scale biochar application has been mainly focused toward agricultural practices and some adsorption applications due to limited or restricted surface functionalities[1,2,19,20,27] needed for many applications. For example, biochar's moderate catalytic performances are related to limited functionality, insufficient surface area, and porosity.[28,29]

Various chemical and morphological modifications can overcome some biochar limitations by enhancing porosity, specific surface area, introducing specific surface functionalities, and removing others, as well as improving selectivity, separability, and structural stability.[30−37] One such approach is developing nanobiochars (particle sizes with at least one dimension <100 nm), which can provide enhanced properties and applicability.[17,38−42] Nanobiochar can be synthesized using ball-milling, sonication, centrifugation, and other techniques.[17,38,40−42] Nanobiochar can also be modified to develop what we call engineered nanobiochars in this review.[39,42,43] Nanobiochar possesses higher specific surface area to mass ratios versus macro or pristine biochar. This property can assist in several applications, including use as an adsorbent, capacitor, reinforcing filler sensor, slow-release fertilizer, photocatalytic material, and fuel additive.[17,38−40,42,43]

Nanobiochar development and use have generated extensive recent interest in the scientific community as an emerging material. A few review articles summarizing nanobiochar development have appeared.[17,38,39,42−46] Nevertheless, a systematic and well-researched review documenting all the dimensions of this topic is needed. Nanobiochar preparation techniques are less explored in the literature.[17,38,39,44] This review covers the full scope of nanobiochar and engineered nanobiochar, while most available reviews only deal with nanobiochar. Insights into nanobiochar and engineered nanobiochar production techniques were compiled, describing their merits and demerits. Bulk biochar and nanobiochar's physicochemical properties are compared. Agents to regenerate

Received: October 7, 2023
Revised: December 23, 2023
Accepted: December 28, 2023
Published: March 4, 2024

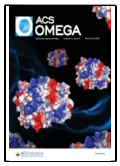

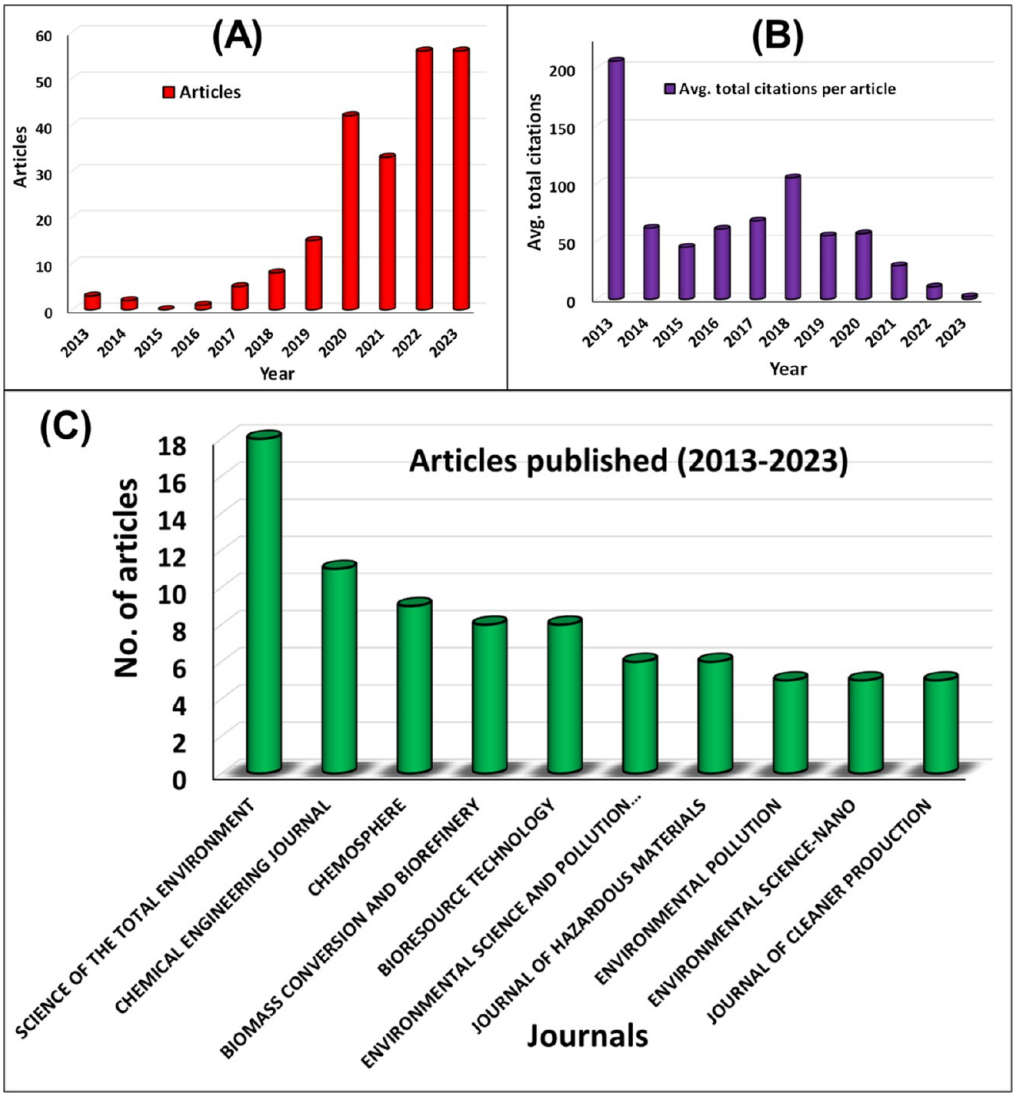

Figure 1. Bibliometric analysis of nanobiochar studies: (A) annual article production, (B) average total citations per article, (C) journal-wise article distribution. Data were collected on December 5, 2023 from Web of Science and processed by bibliometrix package (RStudio).

adsorbent biochar and their operational conditions are also explored. Nanobiochar applications other than environmental remediation are discussed, along with their economic feasibility, advantages over bulk biochar, possible toxic effects on flora and fauna, and future perspectives.

2. BIBLIOMETRIC ANALYSIS

2.1. Data Collection. The web of science core collection was utilized to collect all the data for bibliometric analysis in this study.[47] Data with the keywords "Nanobiochar" OR "Nano-biochar" OR "Biochar nanoparticle" OR "Engineered nano-biochar" OR "Modified nanobiochar" OR "Treated nano-biochar" OR "Biochar nanorod" OR "Nanobiochar composite" OR "Ball milled biochar" OR "Biochar sonication" OR "Biochar centrifugation" OR "Biochar disc milling" OR "Hydrothermal biochar" OR "Biochar carbonization" appearing in the "All Fields" of the English documents were collected on December 5, 2023.

The initial application of biochar, separate from traditional charcoal or activated carbon, in the context of water remediation was documented in the Journal of Colloid and Interface Science in 2007.[48] In this study, biochar was developed as a byproduct through fast pyrolysis of pine wood and oak wood in an auger-fed reactor during biooil production and used to extract heavy metals from water. Following the publication of this research, subsequent studies began exploring the utility of both slow and fast pyrolysis-derived biochars as an alternative to activated carbon for water purification. Prior to this development, biochar had primarily found use in enhancing soil quality and sequestering carbon.

Web of science database provided articles on the above searched keywords started in 2013, and that first article was titled as "Antagonistic Effects of Humic Acid and Iron Oxyhydroxide Grain-Coating on Biochar Nanoparticle Transport in Saturated Sand".[49]

2.2. Analysis Tools. VOSviewer[50] and RStudio's bibliometrix package[51] were employed for visualizing scientific landscapes and science mapping analyses, respectively. Also, data has been analyzed and plotted using OriginPro 2018. The data obtained were downloaded using the "Tab delimited file" and "BibTeX" options for VOSviewer and Rstudio's bibliometrix package, respectively.

2.3. Outcome. A total of 221 documents were collected from 2013 to December 5, 2023, with a 41.42% annual growth

https://doi.org/10.1021/acsomega.3c07804
ACS Omega 2024, 9, 12331−12379

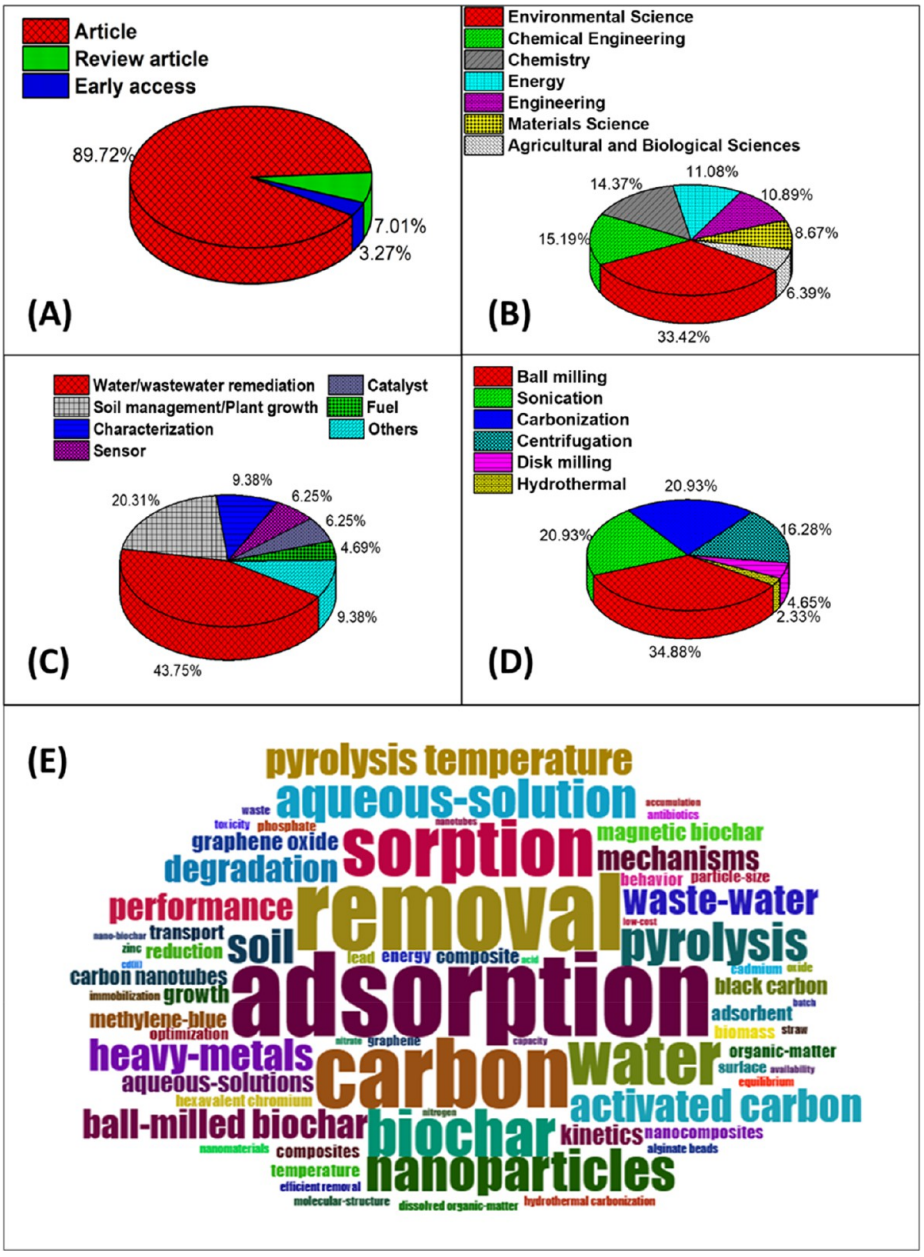

Figure 2. Bibliometric analysis of nanobiochar studies: (A) document types, (B) distribution of publications by science category, (C) nanobiochar application area, (D) nanobiochar preparation methods, and (E) WordCloud. Data were collected and processed on December 5, 2023 from Web of Science.

rate over the decade, showing the nascent stage of nanobiochar research. A total of 881 authors worldwide contributed to nanobiochar related research within this time span. The data were classified based on the annual rate of article production (Figure 1A), average total citations per year (Figure 1B), journal-wise article distribution per decade (Figure 1C), document types (Figure 2A), distribution of articles by science category (Figure 2B), nanobiochar application areas (Figure 2C), nanobiochar preparation methods (Figure 2D), WordCloud (based on keywords plus) (Figure 2E), keyword co-occurrence (Figure 3A), bibliographic coupling among countries (Figure 3B), collaboration among countries with total scientific production (Figure 4), nanobiochar related trend topics (Figure 5), and historiography (Figure 6).

The number of nanobiochar publications has increased over the last 10 years (Figure 1A). The average total citations per article exhibit a higher number of citations for earlier publications (Figure 1B). *Science of the Total Environment* published the most nanobiochar articles, followed by *Chemical Engineering Journal, Chemosphere*, and then *Biomass Conversion and Biorefinery* (Figure 1C). Approximately 89.72% of the published manuscripts are original articles, followed by review articles (~7%) and early access (~3.27%) (Figure 2A). Nanobiochar publications have appeared in a wide variety of science categories. The category of "Environmental Science" was the most frequent, followed by the "Chemical Engineering" and "Chemistry" categories (Figure 2B). Nanobiochars made so far have mostly been applied for water/wastewater remediation (~44%) and this category was followed by soil management/plant growth (20%), characterization (~9%), sensors (~6%), catalysts (~6%), fuels (~5%), and others (~9%) (Figure 2C). Ball-milling is the most applied technique for nanobiochar

https://doi.org/10.1021/acsomega.3c07804
ACS Omega 2024, 9, 12331−12379

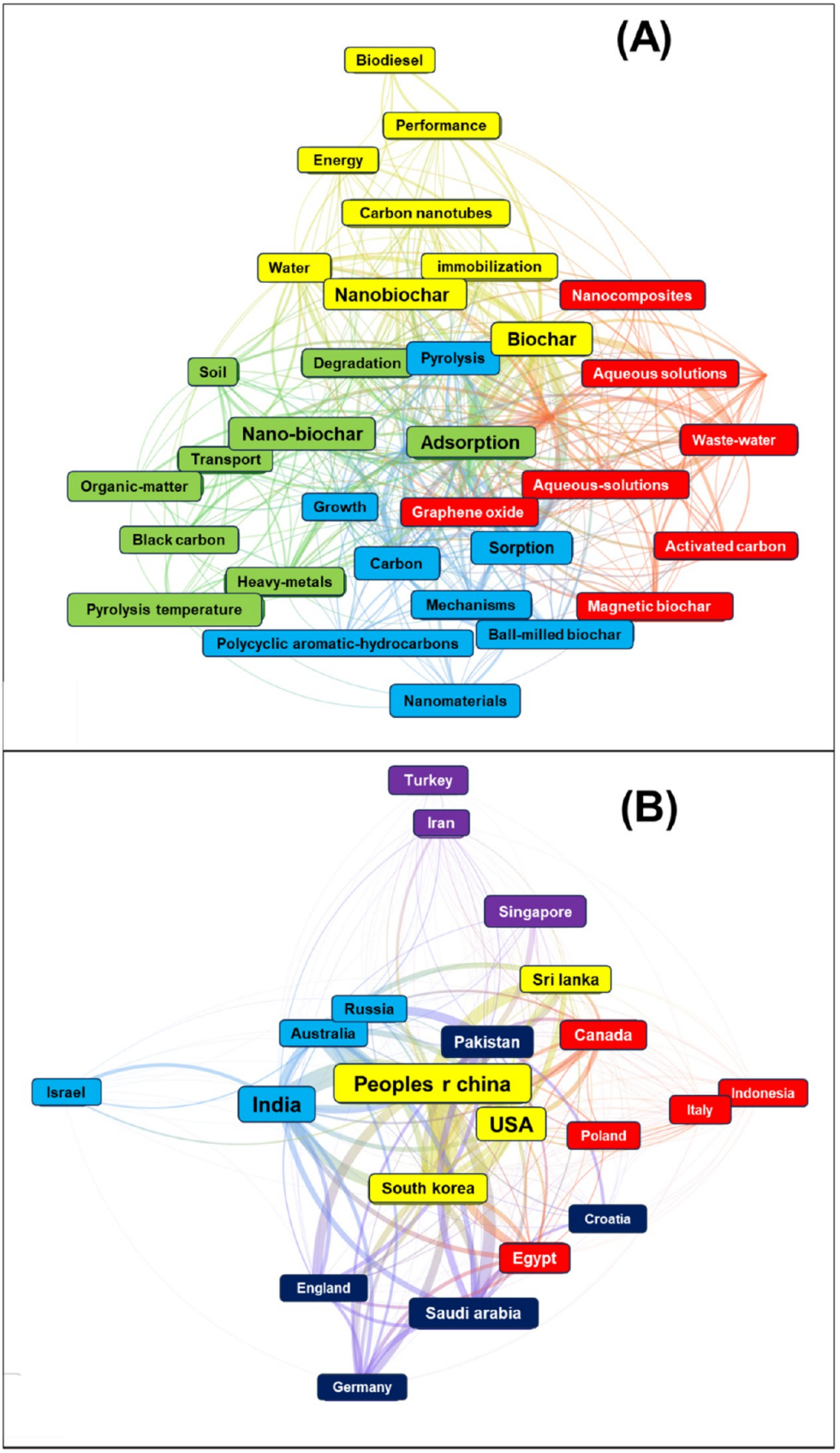

Figure 3. VOSviewer's (A) network visualization for co-occurrence of all keywords and (B) bibliographic coupling among countries from 221 peer-reviewed publications (2013−2023). Each frame represents a keyword, and the size of the frame represents the number of times a pair of keywords appears together in a publication.

https://doi.org/10.1021/acsomega.3c07804
ACS Omega 2024, 9, 12331−12379

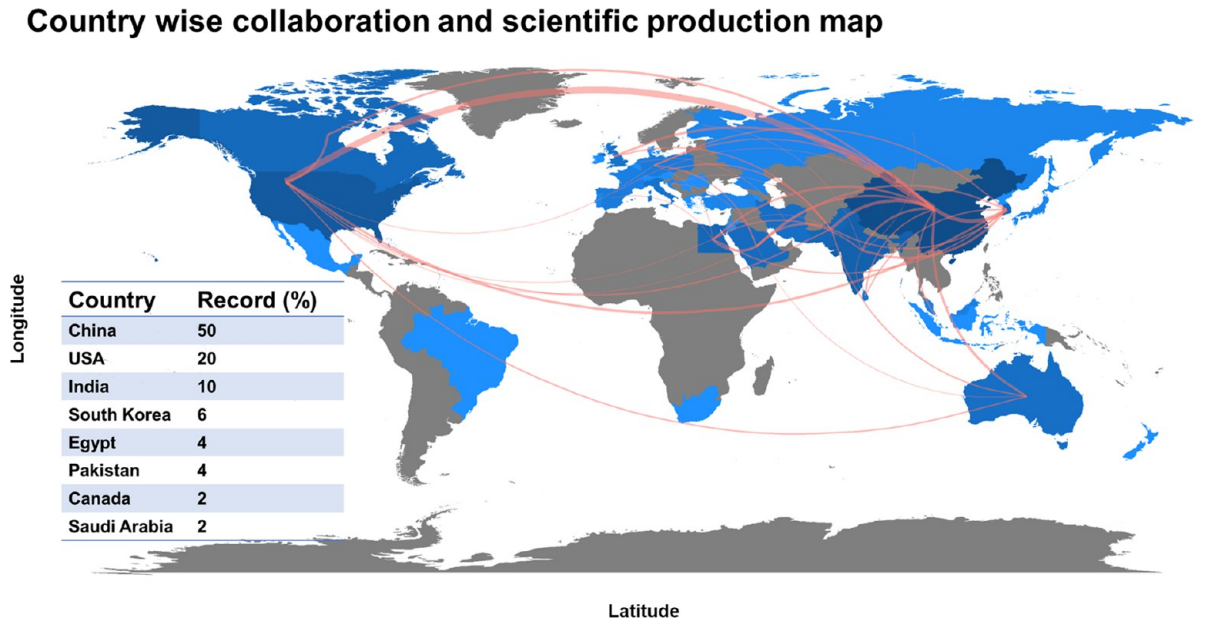

Figure 4. Collaboration among countries with total scientific production on nanobiochar research, prepared by bibliometrix package (RStudio).

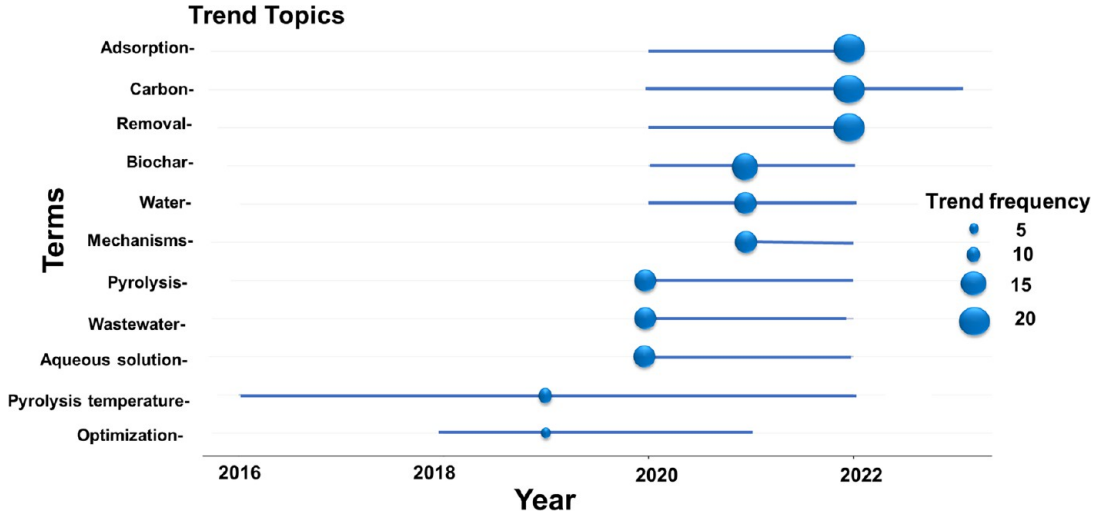

Figure 5. Trend topics related to nanobiochar research from 2016 to 2023, prepared by bibliometrix package (RStudio).

synthesis (~35%), followed by sonication (~21%) and carbonization (~21%) (Figure 2D). The WordCloud illustrates how the less frequent terms are smaller and less obvious, while the more frequent terms are larger and more prominent. The WordCloud is centered around the most frequently mentioned terms, including "Adsorption", "Removal", "Carbon", "Sorption", "Biochar", "Nanoparticles", and "Aqueous solution" each with a frequency of 56, 51, 46, 38, 31, 28, and 26, respectively. The terms with smaller frequencies are "Ball-milled biochar", "Water", "Heavy metals", and "Pyrolysis temperature" (Figure 2E).

VOSviewer's network visualization for co-occurrence of all keywords suggests "biochar", "adsorption", "nano-biochar" or "nanobiochar" and "sorption" are among the most frequently used keywords (Figure 3A). Bibliographic coupling among countries provides connectivity among objects, which is measured on the basis of the number of references they share.[52] The strength of their relatedness (coupling) becomes greater when a document receives more citations.[52] It provides the similarities between the two works' subject matter in the form of documents, sources, authors, organizations, and countries.[52] Here, China dominates and shows more coupling with other countries. India, USA, South Korea, Canada, and Australia were also well related to each other (Figure 3B). The highest percentage of documents were published from China (50%), followed by USA (20%), India (10%), and South Korea (6%) (Figure 4). China shows collaboration with most of the countries contributing literature on nanobiochar (Figure 4).

In a scatter diagram, the trend topic graph plots time on the x axis versus the topic on the y axis.[51] The median of the distribution of occurrences during the time period under consideration is used to determine the reference year for each topic. Pyrolysis temperature (2016−2022) and optimization (2018−2021) were two most trending topics during the initial days of nanobiochar research (Figure 5). From 2020 onward, adsorption, removal, water, wastewater, aqueous solution, mechanism and carbon became trending topics. The chronological citation network is known as a historiograph.[51] Figure 6

https://doi.org/10.1021/acsomega.3c07804
ACS Omega 2024, 9, 12331−12379

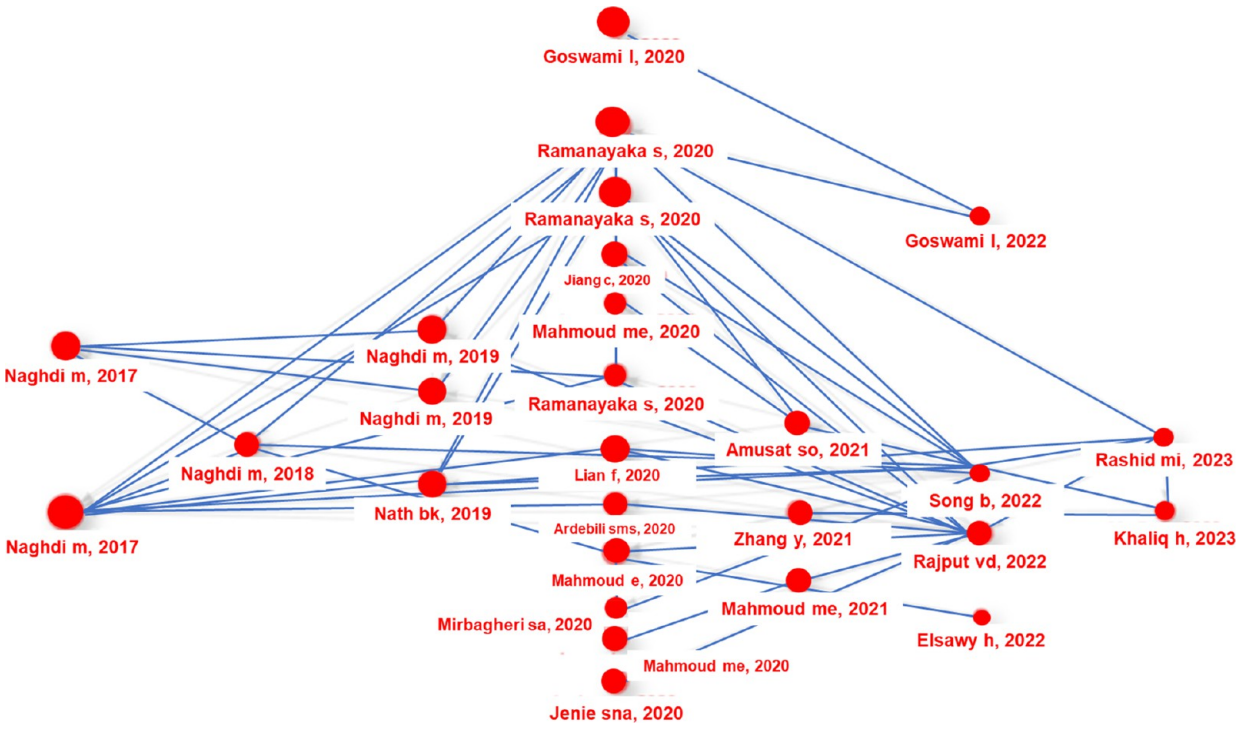

Figure 6. Historiograph of nanobiochar recent research from 2017 to 2023, prepared by bibliometrix package (RStudio).

represents a chronological map (2017−2023) of the most relevant citations for nanobiochar research, resulting from bibliographic collection from web of science. The articles present in Figure 6 are the most influential among the remaining published articles. Early stage articles published in 2017−2019 [Naghdi et al. (2017)[53] and Naghdi et al. (2017),[54] in 2018 Naghdi et al. (2018)[55] and in 2019 Naghdi et al. (2019),[56] Naghdi et al. (2019)[57] and Nath et al. (2019)[58]] are the most cited. In 2020, two articles by Ramanayaka[17,59] are influential, followed by Amusat et al. (2021),[60] Zhang et al. (2021),[61] and Mahmoud et al. (2021)[62] in 2021. Most recently, articles by Rajput et al. (2022)[44] in 2022 and Khaliq et al. (2023)[63] in 2023 are gathering more citations.

3. NANOBIOCHAR PREPARATION

The preparation of nanobiochar is summarized in two subsections. The first covers pristine nanobiochar without any special modifications. The second discusses engineered nanobiochar where specific modifications during preparation are introduced to enhance one or more specific properties. Nanobiochar modifications introduce crucial characteristic properties that enhance effectiveness for target applications. Always under consideration are environmentally friendly methods that save energy and enhance yields during nanobiochar preparation.[17]

3.1. Pristine Nanobiochar. Pristine nanobiochar preparation is possible using ball milling,[41,53,64] sonication,[41,64−66] centrifugation,[67,68] and acidic hydrothermal synthesis.[69−71] These are the most widely used approaches. Other methods have also been reported, including disc milling[59] and thermal flash pyrolysis.[72,73] Ball milling has been the most commonly used technique for preparing nanobiochar. A summary of the nanobiochar and engineered nanobiochar preparation methods appears in Table 1. The most frequently used nanobiochar synthetic methods following ball milling include sonication, centrifugation, and carbonization in that order (Table 1).

3.1.1. Ball Milling. Nanobiochar production by ball milling is an emerging, inexpensive, sustainable, and reproducible method.[74] Several studies used ball milling for the preparation of nanobiochar with enhanced functional characteristics.[13,53,54,75−78] Increase in specific surface area,[79] particle size reduction,[54] enhancement in oxygen-containing surface functional groups,[76] adsorption, and catalytic efficiency proliferations[80] are improved through ball milling as compared to their pristine biochar precursors. The progress in this new area of research is still in development and rising rapidly, along with challenges and opportunities.[38,74] The diagrammatic representation of ball milling procedure and functioning is shown in Figure 7A and B.

Under nonequilibrium conditions, ball milling mechanically reduces the biochar's particle size to an ultrafine or nanoscale level.[79,81] It has been an effective, efficient, and environmentally friendly technique for synthesizing advanced nanomaterials such as nanobiochar.[76,82] The mechanisms of ball milling process include diffusion improvement, strain generation, structural, electronic, and ionic defects, and interactions among the substrates. The kinetic energy needed to rupture or stretch the chemical bonds of large molecules is provided by the movement of milling media and substrates. As a result, solid materials are broken up, elements are produced, glycosidic linkages are broken, and charge transfer occurs.[83,84]

The disintegration of biochar particles to nano level is assisted by the collision between metallic balls inside ball milling chamber.[38,60] The desirable particle size, i.e., up to a grinding limit, can be attained by reducing the agglomeration and varying the ball milling conditions (balls to biochar ratio and milling speed/time).[38,74] The grinding in ball milling is facilitated by colliding particles, where aggregations of particles are a possibility and may contribute toward the enhancement of the apparent particle size.[59,85] Ball milling does not use toxic/

https://doi.org/10.1021/acsomega.3c07804
ACS Omega 2024, 9, 12331−12379

Table 1. Detailed Information on Different Nanobiochar and Engineered Nanobiochar Preparation Methods[a]

Ball milling								
Feedstock precursor	Pyrolysis temp.(°C)/ applied gas	Modification of precursor biochar	Amount of Biochar used (g)	Milling time (h)	Milling speed (rpm)	Milling environment	Ball dia. (mm) /weight (g)	Ball to biochar ratio (weight)
Bamboo[102]	300/N_2	NA	1.8	12	300	Ambient air	NA/180	100:1
	450/N_2							
	600/N_2							
Cow bone meal[103]	300/N_2	NA	3.30	12	300	Deionized water	NA/330	100:1
	450/N_2							
	600/N_2							
Coconut shell[77]	500/N_2	Biochar (coconut, pinenut, and walnut shells) and iron powder (Fe) or iron oxides (α-Fe_2O_3 or Fe_3O_4) were mixed at a mass ratio of 3:1 and then ball milled	NA	6	550	Ambient air	5.6/120	40:1
Pinenut shell[77]								
Walnut shells[77]								
Corn straw[75]	500/NA	NA	4.5	2.5	600	NA	5/NA	NA
Hickory wood chip[76]	300/N_2	NA	1.8	12	300	Ambient air	NA/180	100:1
	450/N_2		3.6					50:1
	600/N_2		9					20:1
Wheat stalk[14]	300, 450, 600/N_2	NA		12	300	Ambient air	NA	100:1
Poplar woodchips[78]	300	3 g biochar was added to 120 mL solution of 3.6 mL water, 114 mL ethanol, and 2.4 mL 3-mercaptopropyltrimethoxysilane (3-MPTS) and then ball milled	3	12	300	Water, ethanol, and 3-MPTS	15−5 −3/300	100:1
Pinewood[53]	525/N_2	NA	5−15	1.6−8.4	575	NA	2.4/NA	4.5:1
Pinewood[54]	525/N_2	NA	10	1.64	575	Ambient air	2.4/45	4.5:1
Pinewood[57]	525/N_2	NA	10	1.6	575	Ambient air	2.4/45	4.5:1
Rice husk[75]	500	NA	4.5	2.5	600	NA	5/NA	NA
Rice husk[104]	300/limited oxygen	NA	NA	24	300	Ambient air	5/NA	100:1
	500/limited oxygen							
	700/limited oxygen							
Sawdust[89]	600/N_2	NA	NA	2−12	NA	Ambient/ water	6−10/NA	NA
Sugar cane bagasse[102]	300/N_2	NA	1.8	12	300	Ambient air	NA/180	100:1
	450/N_2							
	600/N_2							
Wheat straw[104]	300/limited oxygen	NA	24	NA	300	Ambient air	5/NA	100:1
	500/limited oxygen							
	700/limited oxygen							
Hickory wood[13]	300/N_2	NA	NA	12	300	Ambient air	NA	100:1
	450/N_2							
	600/N_2							
Wheat straw[105]	600/N_2	NA	8	NA		Ambient air	6−10/800	100:1
Wood[106]	650/Argon	NA	NA	6	500	Argon	15/10	10:1
Wood saw dust[107]	350/limited oxygen	NA	NA	NA	NA	NA	NA	NA
Pinewood[108]	300−500	NA	NA	4	320	NA	5/NA	30:1
Corn stalk[108]								
Lignin[109]	800/N_2	Nanobiochar mixed with styrene−butadiene rubber (vulcanized at 160 °C)	NA	4	NA	NA	NA	NA
Hickory woodchips[16]	600/N_2	Copper oxide was mixed with biochar and placed inside ball mill	1.8	9	400	Ambient air	NA/90	50:1
Rice husk[58]	NA	Ferrous sulfate heptahydrate (0.3 mol) and urea (1 mol) were ground and added to aqueous paste containing ∼15 g of nanoscale rice husk powder. Slurry was pyrolyzed at 600 °C under reducing conditions.	15.0	NA	500	Ambient air	5/30	NA

https://doi.org/10.1021/acsomega.3c07804
ACS Omega 2024, 9, 12331−12379

Table 1. continued

Ball milling								
Feedstock precursor	Pyrolysis temp.(°C)/ applied gas	Modification of precursor biochar	Amount of Biochar used (g)	Milling time (h)	Milling speed (rpm)	Milling environment	Ball dia. (mm) /weight (g)	Ball to biochar ratio (weight)
Bagasse[110] Hickory chips[110]	450−600/ N_2	1.8 g of biochar mixed with 18 mL ammonium hydroxide (29%) and placed inside ball milling	1.8	12	300	NA	6/180	100:1
Wheat straw[6]	400/N_2 550/N_2 700/N_2	Impregnation of 100 g wheat straw into 1 L solution of 3.4 g $FeCl_2$ and 8.5 g $FeCl_3$ for 24 h. Further, pyrolyzed and ball milled	1.0	12	NA	Ambient air	5/100	NA
Hickory chips[87]	600/N_2	Magnetite addition in 3:1 ratio of biochar	NA	12	500	Ambient air	6/180	100:1
Hickory chips[111]	600	Hickory chips were mixed with $FeCl_3{\cdot}6H_2O$ in 0, 0.5, 1, 2, 5, and 10 (w/w) ratio before pyrolysis	1.8	12	300	Ambient air	NA	100:1
Pine saw dust[112]	300−700	2 g ball milled biochar, 200 agate ball, 2.4 mL water and 76 mL ethanol were mixed in 500 mL agate jar. Further, along with N_2 purging, 1.6 mL 3-MPTS added and 10 pH was maintained using NH_4OH	2	30 h with direction alteration every 6 h	400	Ambient air	15:5:3/200	100:1
Digitalis purpurea[113]	400/N_2	NA	NA	50 h with alteration of direction every 2 h	400	Ambient air	NA/90	50:1
Farmyard manure[114]	500	NA	NA	24	300	NA	3/NA	NA
Wheat straw[115]	550	Obtained biochar were pretreated at −80 °C to improve its grindability	NA	4 h and ball mill machine was rested every 5 min to prevent agglomeration	NA	NA	NA	NA
Wheat straw[116] Rice straw[116] Corn straw[116]	350 and 650	Reduction in H_2	NA	12	350	Ethanol	NA	15:1
Hickory chips[117]	NA	NA	1.0	12	300	Deionized water Sulfuric acid	6/100	100:1

Sonication								
Biomass/ Feedstock precursor	Pyrolysis temp.(°C)/ applied gas	Modification	Biochar used (g)	Dispersion media (pH)	Time (min)	Temperature (°C)	Power	Process repetition (times)
Wheat straw[118] Pine needle[118]	350−550/ anaerobic condition	NA	15	Deionized water (6.8)	30	NA	100W	No
Peanut shell[41] Cotton straw[41] Chinese medicine residues[41] Furfural residues[41]	300−600/ Nitrogen flow	NA	0.7	Deionized water (6.8)	15	25	120W	Yes (5)
Elephant grass[64] Wicker[64] Wheat straw[64]	350−700	NA	3.0	Water	NA	<20	60 kJ	Yes
Pinewood[65]	550−600/ limited oxygen	Acid/alkaline and amine functionalization	3.0	Deionized water	30 s	Ambient	20 kHz/ 700W	No
Corn stalks[119]	450	10 g biochar in 100 mL 1.25 mol/L $MgCl_2$ oscillated for 30 min. 100 mL 2.5 mg/L NaOH were mixed and magnetic stirred for 12 h at 120 rpm at 25 °C and left for 24 h	150	Deionized water	120	Ambient	20 kHz/ 2000 W	No
Cotton straw[66]	600/ Nitrogen	NA	NA	Deionized water	40	40	NA	NA

https://doi.org/10.1021/acsomega.3c07804
ACS Omega 2024, 9, 12331−12379

Table 1. continued

Sonication								
Biomass/ Feedstock precursor	Pyrolysis temp.(°C)/ applied gas	Modification	Biochar used (g)	Dispersion media (pH)	Time (min)	Temperature (°C)	Power	Process repetition (times)
Hardwood and softwood residues[120]	400/ anerobic	Heated with nitric acid at 90 °C for 3 h	0.01	Various solvents	15	3	20W	No
Eucalyptus scrap chips[121]	1200/argon	Particle size reduction using ball mill (300 rpm for 24 h)	0.05	Sodium cholate water	60	10	30% amplitude	No

Acid treated hydrothermal synthesis								
					Hydrothermal conditions			
Biomass/ Feedstock precursor	Pyrolysis temp.(° C)/applied gas	Modification	Biochar used (g)	Sonication (time)	Time (h)	Temp. (°C)	Media	Cooling agent (mL)
Soybean straw[69] Cattle manure[69]	500/Nitrogen	15 mL conc. HNO_3 and 45 mL conc. H_2SO_4	1.0	No	2	Room temperature	Acidic	Deionized Water (1000 mL)
Biochar[70]		75 mL conc. H_2SO_4 and 25 mL conc. HNO_3	2.0	Yes (3h)	24	100	Acidic	Double distilled water (300 mL)
Corn residues and wood[71]	400/Nitrogen 700/Nitrogen	15 mL conc. HNO_3 and 45 mL conc. H_2SO_4	5.0	No	24	25	Acidic	Deionized Water (1000 mL)

Centrifugation								
Biomass/ Feedstock precursor	Pyrolysis temp.(° C)/applied gas	Modification	Biochar used (g)	Dispersion media (volume)	Time (h)	Temperature (°C)	Power	Centrifugation conditions
Rice straw[68]	400 and 700/ anaerobic condition	NA	50	Deionized water (1L)	24	Room temperature	120W	10000 rpm for 30 min
Wood Chips[67] Pine wood[67] Wheat straws[67] Barley grasses[67] Peanuts shells[67] Rice husks[67] Dairy manures[67] Pig manures[67] Sewage sludge[67]	500/N_2	NA	15	Deionized water	24	NA	100W	3500 × *g* for 30 min
Tobacco stems[95]	500/N_2	NA	NA	Double distilled water	NA	NA	NA	3500 × *g*
Rice straw[122]	400 and 700/ anoxic condition	NA	NA	Deionized water	2	Room temperature	NA	10000 rpm for 30 min
Sugar cane[123]	900/N_2	1 g/L biochar was dispersed in double distilled water and ultrasound for 30 min	NA	Double distilled water	12	NA	NA	12000 rpm for 5 min
Wood shreds[124]	550/limited oxygen	NA	NA	Deionized water	2	NA	NA	10000 for 30 min

Carbonization								
							Additional treatment	
Biomass/Feedstock precursor	Pyrolysis temp.(°C)/ applied gas	Modification	Biochar used (g)	Temperature (°C)	Time (min)	pH	Process	Conditions
Microcrystalline cellulose[125]	550/N_2	ZnO	1.76	120	60	7	Centrifuge	5 min at 4000 rpm
Corncob[126]	400/limited oxygen	Triethylenetetramine	12.0	60	120	NA	H_2SO_4	Stirred for 1 h at 1 pH
Artichoke leaves[127]	350	NA	5.0	50−60	60	NA	NaOH	150 mL NaOH (2.0 mol/L)

[a]NA = not available.

hazardous chemicals, provides high atom economy, prevents waste formation from biodegradable products, and consumes only renewable resources.[6,38,54,74,80,86−88]

Biochar ball milling can be performed in two different ways, i.e., dry and wet milling.[38,74,150] Operational convenience and techno-economic analysis are two deciding factors for selecting the milling method.[74] In general, dry ball milling is preferred for

https://doi.org/10.1021/acsomega.3c07804
ACS Omega 2024, 9, 12331−12379

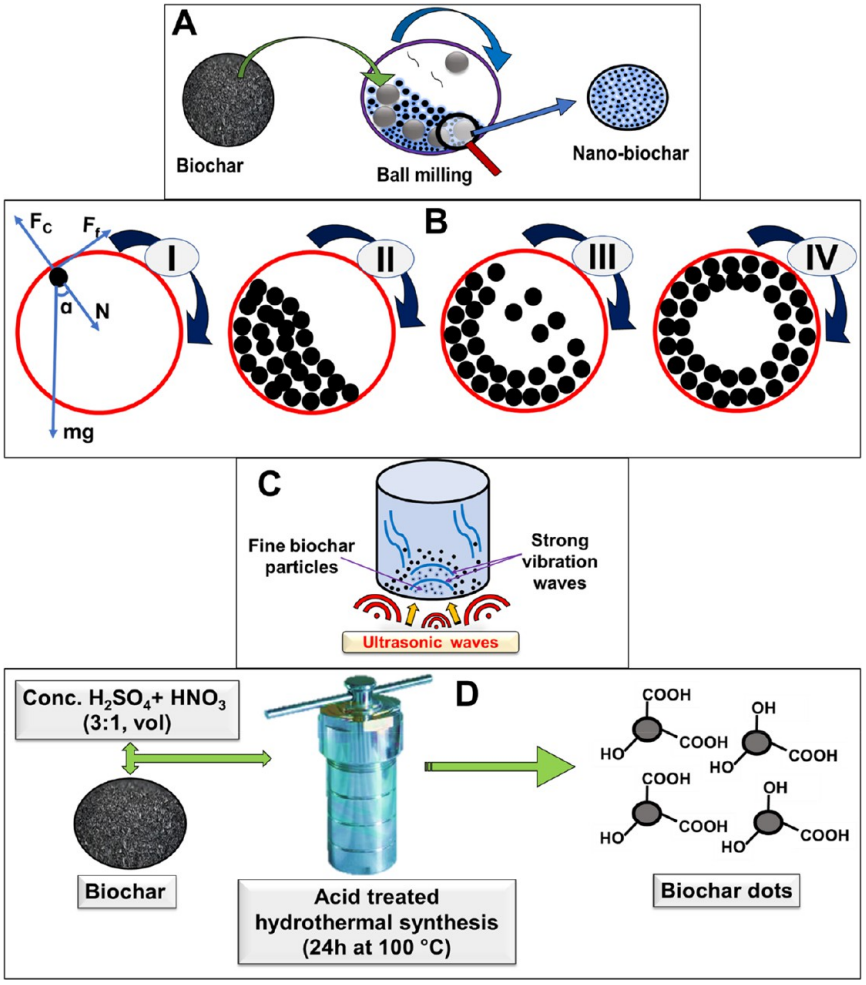

Figure 7. (A) Typical ball milling, (B) ball milling functioning, (I) impact of forces and the types of motion of grinding balls in a ball mill: (II) rolling over; (III) falling; (IV) rolling. Reprinted with permission from ref 60. Copyright 2021 Elsevier. (C) Sonication and (D) acid treated hydrothermal method. Reprinted with permission from ref 70. Copyright 2017 American Chemical Society.

materials that are difficult to subsequently filter.[89,90] Wet milling has shown advantages including higher dispersion of smaller particles, more surface functional group formation, labor-savings, and it is a greener technology.[89] Dry and wet ball milling can prepare biochar with similar yet different properties.[89] In a comparative study, sawdust biochar was ball milled using wet and dry methods.[89] Both wet and dry ball milling produced similar BET surface areas but different structural properties.[89]

The properties of ball-milled biochars derived from different preparation parameters are compared in Table 1. Preparation variables in Table 1 include precursor type, pyrolysis temperature (°C), the gas applied, various modifications used to engineer the nanobiochar (if given), biochar weight (g), milling time (h), milling speed (rpm), milling environment, ball diameter (mm)/weight (g), and ball-to-biochar weight ratio. A wide variety of feedstocks have been converted to biochar and then ball-milled to reduce particle size. Feedstocks include bamboo, coconut shell, pine nutshell, walnut shells, corn straw, hickory woodchips, poplar woodchips, pinewood, rice husk, sawdust, sugar cane bagasse, wheat straw, wood feedstock, wood sawdust, and lignin (Table 1).

3.1.2. Sonication. The physical modification of biochar using ultrasound irradiation is an efficacious route to enhance its adsorption capacity for various contaminants (Figure 7C).[38] Fine particles adhering to the surface or embedded in the pores of the biochar are exfoliated by sonication to produce nanobiochar.[26] To produce a desired particle size distribution, sonication of biochar can be repeated several times to generate a nanobiochar.[41,64] Sonication utilizes high-energy ultrasound waves to disintegrate a biochar's particles present in a suspension.[41,91,92] The solvent media carries the ultrasound, which impinges on particle surfaces via microcavitation that produces short-lived, very high temperatures and shockwaves. A typical sonication method involves dispersion of prepared biochar in a solvent, which is subjected to sonication using an ultrasonic transducer. After sonication, the suspension's larger particles can be gravity-settled, filtered, or centrifuged to obtain a supernatant containing biochar nanoparticles.[40,64,67,93]

The shockwaves caused by ultrasound irradiation increase the microporous area of biochar via mechanical damage, which opens blocked pores and enhances carbon structural exfoliation. The fine fragments, either embedded in pores or adhered to the surface of biochars, are also exfoliated during sonication.[41] This damage causes mineral matter exposure at the surface and distribution from pores, leading to the improved sorption efficacy.[65] Nanobiochar yield rises with increased sonication time and depends on the amount of heterogeneous carbon in bulk biochar.[41] Sonication of biochar facilitates uniform surfaces and unclogs pores.[66,94] Nanobiochar properties may be altered

https://doi.org/10.1021/acsomega.3c07804
ACS Omega 2024, 9, 12331−12379

with changes in sonication temperature, power, amplitude, and probe size.[38,64] Previous sonication studies have employed biochars made from wheat straw, pine needles, peanut shells, cotton straw, furfural residues, elephant grass, wicker, and pinewood at 300 to 700 °C with variations in sonication power (Table 1). The dearth of literature in the field of biochar sonication has not permitted general conclusions to be drawn about the optimization of process parameters.[38]

3.1.3. Centrifugation. In addition to ball milling and sonication, centrifugation is often used during nanobiochar preparation.[40,67,68,93,95] Carbonization and centrifugation are commonly discussed separately, but one literature analysis describes the involvement of both in combination to produce nanobiochar.[38] Centrifugation in a solvent is a straightforward method for separating highly dispersed nanoparticles.[96] To obtain desired nanoparticle size ranges, several rounds of centrifugation are required. Centrifugation is employed up to an enhanced gravity effect of 100,000 rpm (roughly 800,000 × g). This is suitable for sedimentation of micron-sized species down to the smallest nanoparticles.[97] The mechanism of nanobiochar preparation depends on the intrinsic particle properties of different biochars, such as size, density, surface functions, and shape. These cause varied sedimentation velocities.[97]

Typically, grinding is performed followed by centrifugation to obtain nanobiochar fractions. One study used two major feedstock classes, i.e., plant-based wastes and municipal wastes, to make biochars at 500 °C under nitrogen for 2 h. Plant-based wastes included pine wood, wood chips, barley grasses, wheat straws, peanut shells, and rice husks, while municipal wastes employed were dairy manures, pig manures, and sewage sludge.[67] To prepare micron-sized biochar particles, 15 g of biochar was added to a beaker (500 mL) containing deionized (DI) water in a 3% (wt./wt.) ratio. It was stirred for 1 min; then ultrasonicated for 30 min, followed by stirring for 10 min. The particles obtained was allowed to settle for 24 h to separate <1 μm particle sizes according to Stokes Law. After the particles in solution settle, these are called micron-size biochar particles. The nano sized biochar particle suspensions prepared were then further centrifuged for 30 min at 3500 × g to separate 1 μm to 100 nm particles, leaving a supernatant that contains particle size fractions <100 nm. All these micron and nano sized biochar particle suspensions were freeze-dried to provide respective biochar powders, which were then stored in a desiccator.[67] A clear demarcation of the size distribution was observed. Micron-sized biochar particles had hydrodynamic diameters dominantly <1000 nm with a wide range of size distributions from 70 to 1000 nm, and nano sized biochar particles were <100 nm. The varied size distribution of micron- and nanosized biochar fractions resulted from the use of different feedstocks because of their nonuniform compositions and densities.[67] In another study, rice straw biomass was powdered (2.0 mm mesh) and pyrolyzed under an oxygen deficiency at 400 and 700 °C for 2 h. The resulting biochar particles were further ground and sieved (150 μm mesh). A mixture of biochar particles and deionized water was held for 2 h to settle the particles based on Stoke's law. Then, the topmost suspension layer was taken from the mixture, centrifuged (at 10,000 rpm) for 30 min, and a 100−350 nm biochar fraction size was obtained.[68]

3.1.4. Hydrothermal Synthesis. Acid-treated hydrothermal synthesis is another path to synthesize smaller biochar nanoparticles (average particle size ∼3−6 nm).[69−71] The acid-treated hydrothermal biochars are often termed "biochar dots", "biochar nanodots", or "biochar nanoparticles".[69−71] At present, only a handful of studies report synthesizing nanobiochar using acid-treated hydrothermal synthesis.[69−71] The obtained biochar nanodots can be used for various environmental applications. Compared to grinding and sonication, hydrothermal synthesis does not require a high energy input and produces relatively smaller biochar particles.[69] Hydrothermal synthesis is also useful to optimize nanobiochar synthesis conditions by systematically changing the time, temperature, and aqueous environments used during hydrolysis.[69] A typical acid-treated hydrothermal synthesis procedure is shown in Figure 7D. Biochar, prepared at 500 °C from cattle manure and soybean straw at 500 °C under nitrogen, was ground and passed through a 60-mesh sieve. This biochar (1 g, homogenized) was immersed in 15 mL conc. HNO_3 and 45 mL conc. H_2SO_4 for 2 h at room temperature in a hydrothermal reactor. Then, this mixture was added to 1000 mL deionized water.[69] The suspension was filtered through a 0.22 μm membrane filter and oven-dried for 48 h at 65 °C.[69] The process yielded biochar nanodots of 2−10 nm in size. This drastic reduction in size is due to the oxidative hydrolysis during acid digestion, which is determined by the nitric and sulfuric acid concentrations used to alter the biochar microstructure by oxidation.[69]

A comparative study of the physicochemical properties of biochar nanoparticles produced by sonication/centrifugation versus acid-treated hydrothermal synthesis was evaluated.[71] For hydrothermal synthesis, biochar (∼5 g) was weighed and passed through fine sieves of 270-mesh (53 μm). Then, this biochar was treated with conc. H_2SO_4 (45 mL) and conc. HNO_3 (15 mL) in a 3:1 ratio to carry out the oxidation at 25 °C for 24 h. The acid-biochar mixture was diluted to 1000 mL using deionized water, stirred for 1 min and left for 2 h. The suspension formed was filtered through a 0.22 μm membrane filter, and the filtrate was washed several times with deionized water to pH 6.[71] The sonication/centrifugation method employed 3 g of biochar with the same starting particle size as the hydrothermally made sample (<53 μm). This sample was mixed with deionized water in a 3% (wt./wt.) ratio, sonicated for 30 min, stirred for 1 min, and then held for 2 h. This suspension was centrifuged (8500 rpm) for 30 min, and the supernatant was oven-dried at 80 °C.[71] Biochar nanoparticle production yield was ∼10-times higher in hydrothermal method (0.365−0.589%) vs sonication/centrifugation (0.035−0.075%). These two methods exhibited different particle size distributions. The sonication/centrifugation sample gave 91.53 to 172.6 nm hydrodynamic sized biochar nanoparticles.[71] Centrifugation created nanoparticles with variable sizes due to fragmentation[98] but the acid-treated hydrothermal method provided relatively uniform particles with a "rather lower size" range (hydrodynamic size of 89.71 to 152.9 nm).[71] The biochar nanoparticles produced from the hydrothermal method had higher surface polarity, stability, more surface functional groups, and the highest surface area (51.2 to 167.7 m^2/g).[71] Biochar nanoparticles produced using sonication/centrifugation had lower surface areas from 19.1 to 34.3 m^2/g. The ash content was higher for biochar nanoparticles prepared via sonication/centrifugation vs the hydrothermal route.[71] Increasing ash content, in sonication/centrifugation, probably results from salt build-up during the extraction of biochar nanoparticles. Acid treatment, in contrast, removes inorganic materials and reduces the amount of ash found in the biochar nanoparticles.[71,99] The hydrothermal method proved to be a cost-effective, simple, and quick biochar nanoparticle-producing method.[69] To develop biochar nanoparticles on a large scale,

https://doi.org/10.1021/acsomega.3c07804
ACS Omega 2024, 9, 12331−12379

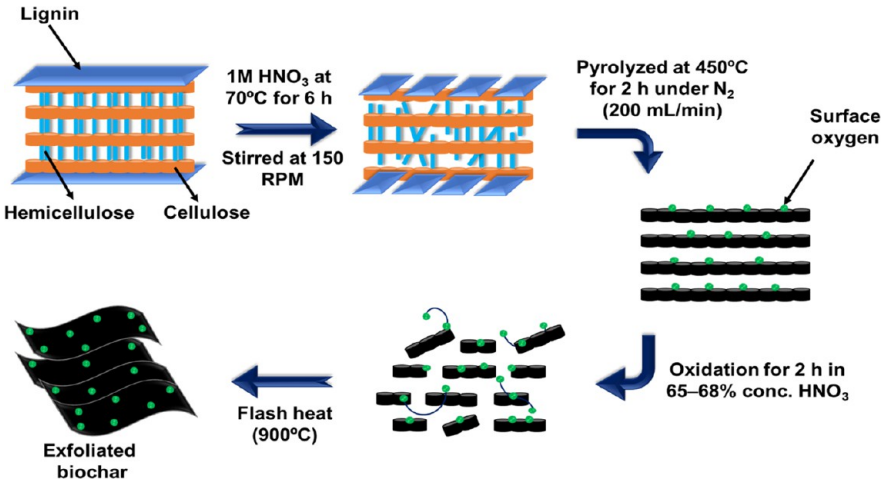

Figure 8. Schematic illustration of the synthesis technique for the functionalization of exfoliated wheat straw biochar nanosheets by a thermal flash pyrolysis method. Reprinted with permission from ref 73. Copyright 2022 Elsevier.

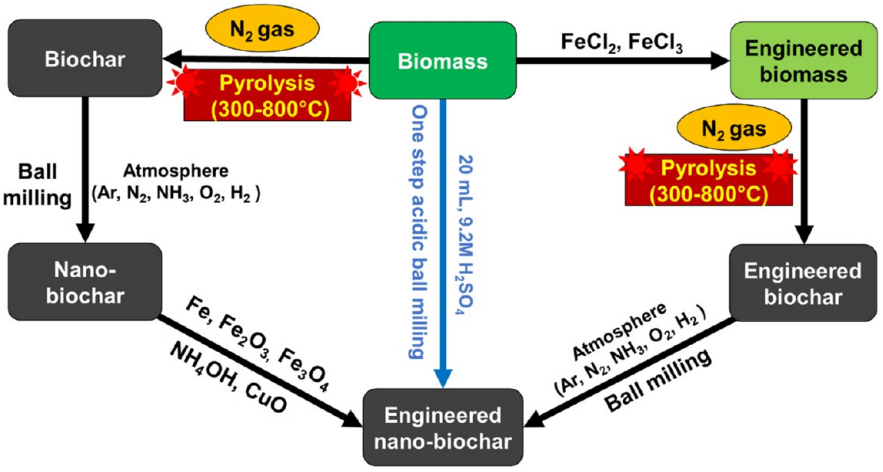

Figure 9. Example ball mill-assisted syntheses of nanobiochar and engineered nanobiochar.

substantial study is needed, and special consideration must be given to the creation of novel strategies.[69]

3.1.5. Other Preparation Methods. Other nanobiochar preparation methods include thermal flash heating,[72,73] disc milling,[59] and conventional grinding.[100] Only limited reports of nanobiochar syntheses using these methods exist in the literature. For example, the application of double-disc milling process to produce nanobiochar is very limited, primarily due to its high operations cost.

Disc milling has an advantage of providing an enhanced nanobiochar quality via shear and attrition stress and a more uniform nanobiochar size and shape.[59] In ball milling, particles collide and grind. As they aggregate, the apparent particle size increases. The nanobiochar produced by double-disc milling was evaluated to remove a wide range of contaminants.[59] These included antibiotics, herbicides, and potentially toxic elements.[59] Biochar (< 3 mm) obtained as a gasification byproduct of *Gliricidia sepium* was preconditioned at −80 °C for 3 days and then mechanically ground dry with a disc mill.[53,59] Disc mill was again used to grind both dried biochar and a biochar ethanol suspension for 2 min at a speed of 1000 rpm.[59,101] Next, the colloidal biochar obtained (5 g) was dispersed in ethanol (100 mL) and centrifuged at 2000 rpm for 10 min. After removing the separated solids, the supernatant containing biochar nano fractions was further sonicated for 30 min (at 50 kHz) and vacuum-dried at 50 °C. These nanobiochar particles had a BET surface area, diameter, and length of 28 m^2/g, 50−150 nm, and <1 μm, respectively.[59] Surface area is approximately ten-times lower than original macro-scale biochar, which may be the combined effect of fracturing macro, meso, and micropores boundaries during size reduction. The graphitic particle character, the existence of nanopores, and the method used to make the nanoparticles determine the surface area.[59] This nanobiochar gave enhanced adsorption capacities for all the adsorbates tested, including oxytetracycline (520 mg/g), glyphosate (83 mg/g), Cr(VI) (7.46 mg/g), and Cd(II) (922 mg/g) from aqueous media.[59] The adsorption capacities per unit area (mg/m^2) for oxytetracycline, glyphosate, Cr(VI), and Cd(II) were 18.6, 2.96, 0.27, and 32.9, respectively.[59]

The lignin coating on wheat straw was partially oxidized along with cellulose prior to pyrolysis to biochar (Figure 8). Then thermal-flash heating was conducted, which provided exfoliated biochar nanosheets (Figure 8). These types of synthesis methods are less explored.[72,73] The first step of thermal-flash heating is the pretreatment of wheat straw biomass (particle size, 2 mm) with 1 M HNO_3 (50 mL) at 70 °C for 6 h. The pretreated wheat straw biomass was filtered and dried at 80 °C for 24 h and then pyrolyzed at 450 °C for 2 h under a N_2 environment (200

https://doi.org/10.1021/acsomega.3c07804
ACS Omega 2024, 9, 12331−12379

mL/min).[73] In the second step, 2−3 g of pretreated biochar was oxidized with 20 mL 65−68% conc. HNO_3 for 2 h, suction filtered, and then flash-treated using a muffle furnace at 900 °C without N_2 gas to cause structural exfoliation.[73] Exfoliated nanobiochar exhibits a higher BET surface area (421.24 m^2/g) and pore size (3.98 nm) than pristine biochar, which had a 3.81 m^2/g BET surface area and a 2.05 nm pore size.[73] The thallium adsorption capacity was 9-times greater on exfoliated nanobiochar than pristine biochar.[73]

The conventional grinding process to prepare micro/nano biochar powder is a simple technique utilizing grinding and sieving.[100] Small pieces of biomass (pitch pine) waste were dried at 90 °C for 3 h to remove moisture and ground to a fine powder using a universal high-speed smashing machine. This powder was pyrolyzed for 2 h at 600 °C inside a sealed steel pot with limited oxygen and cooled to room temperature.[100] To obtain ultrafine biochar powders, a planetary type grinding mill (with variable frequency) was used for 2 h. Finally, 200-mesh screen (stainless steel) with a mesh size of 74 μm was used to obtain biochar micro/nanopowders.[100] This powdered micro/nano biochar was used to prepare electrodes, sensors, fuel briquettes (pellets), biofertilizers, and adsorbents.

3.2. Engineered Nanobiochar. Engineered nanobiochar can be prepared by either pre- or post-treatment methods.[39,42,43] To further enhance the selectivity and diverse applicability, nanobiochars were engineered/modified with different chemicals such as hematite,[77] magnetite,[6,77,87] zerovalent iron,[77] ammonium hydroxide (nitrogen),[110] copper oxide,[16] acids (sulfuric, nitric, and hydrochloric acid),[53,57] thiol,[78] and styrene−butadiene rubber (Figure 9).[109] Modifications can add new material surfaces to the existing nanobiochar. These may adsorb impurities that biochar does not, or they may release nutrients or other chemicals into soils. Modification may cause reactions on the biochar's surfaces, which generate new functional groups, which modify surface behavior, influencing adsorption uptake, dispersion of nanoparticles, or reactions in the media to which they are added. Until now, very few studies have reported the production and application of engineered nanobiochar (Table 1). Ball milling has also been selected frequently for preparing engineered nanobiochar.[6,16,54,56,77,78,87,110,128] Ball milling to modify nano-BC could be done simultaneously with the biochar to nanobiochar size reduction or after this process as a separate additional milling step with an additive. For example, 3 g of poplar wood chip-based biochar was ball milled with a mixture of 3.6 mL water, 114 mL ethanol, and 2.4 mL 3-MPTS (3-mercaptopropyltrimethoxysilane) to produce engineered nanobiochar in a single step.[74]

3.2.1. Nitrogen Doping. Nitrogen doping has provided enhancements in the amount of active surface sorption sites, basicity, and provided excess positive surface charges onto engineered nanobiochar, which resulted in enhanced contaminants sorption.[110,129,130] In particular, heavy metals sorption was improved by (a) creating active N-functional group sites to which the metals could undergo complexation; (b) enhancing basicity of biochar due to N-doping increases adsorption of acidic pollutants e.g., CO_2 and SO_2; and (c) forming positive biochar surface charges by N-doping to promote sorption of negatively charged contaminants (such as reactive red dye) via electrostatic interactions.[110] N-doped biochar has also been employed as a catalyst in various chemical reactions to degrade sulfamethoxazole, orange G, phenol, and bisphenol A.[131] For example, ethanol (50 mL) and 1 g of reed biomass (0.2 mm) were mixed, agitated (0.5 h), and sonicated (1 h). Then, 1 g of NH_4NO_3 was added to the above suspension. It was heated at 85 °C for 4 h while being stirred. The NH_4NO_3 and reed biomass mixture was pyrolyzed, at a rate of 15 °C per min, for 90 min in N_2 at different constant temperatures between 400−1000 °C.[131] N-doped biochar at 900 °C produced a 6.5-fold and 39-fold faster sulfamethoxazole degradation rate than pristine biochar and N-doped biochar pyrolyzed at 400 °C, respectively.[131]

Ball milling is often done under N_2 to avoid air (O_2) oxidation of the biochar surface. Conversely, purposeful nitrogen doping can be achieved by adding chemicals such as ammonium hydroxide and ammonium nitrate. In one study, N-doped carbon nanoparticles were synthesized using graphite powders and N_2 gas in a high-energy rolling ball mill (300 kPa) at room temp.[132] In brief, four hardened steel balls (2 cm) were added to a milling jar (300 mL) containing 2 g of the graphite powders in a ratio of 1:132 (graphite to ball mass ratio). This mixture was milled at 150 rpm for 24 h. After that, milled samples were pyrolyzed for 3 h at 700 °C in a horizontal tube furnace with 25 °C/min ramp rate. The atmosphere of horizontal tube furnace was maintained by a 0.05 L/min gas flow rate of 85% N_2/15% H_2 mixture.[132] The N-doped carbon nanoparticles obtained were utilized as an electro-catalyst for oxygen reduction reactions.[132]

Nitrogen doping of ball milled bagasse and hickory chip biochars was performed to improve the sorption of reactive red dye and carbon dioxide.[110] Initially, both biomasses were oven-dried (80 °C), ground to 0.5−1 mm, and pyrolyzed under nitrogen at 450 or 600 °C for 2 h.[110] Biochars (1.8 g each) were milled in a planetary ball mill inside agate jars (500 mL) with 180 g agate balls (6 mm dia.) for 12 h at 300 rpm. The rotation direction was alternated every 3 h. Nitrogen doping of the biochars was facilitated by ball milling 1.8 g of already ball milled biochar mixed with 18 mL ammonium hydroxide (29%) under the same conditions.[110] After this milling, the N-doped ball milled biochars were washed with deionized water in vacuum filtration units until the filtrate was almost neutral and dried for 48 h at 80 °C.[110] Biochars originally pyrolyzed at 450 °C achieved higher surface N-doping (2.41−2.65%) than those pyrolyzed at 600 °C (1.18−1.82%). This was due to the lower amount of O-containing functional groups present in biochar pyrolyzed at 600 °C versus that present when pyrolysis temperature was 450 °C.[110] Oxygenated surfaces function from the start of most pathways leading to nitrogen introduction. Example pathways to N-doped biochar by ball milling are provided in eqs 1−6.[110,133]

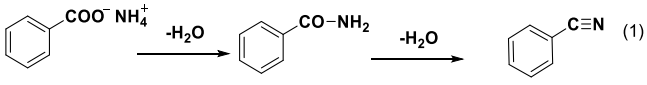

(1)

O-containing surface functional groups (e.g., lactones, pyrones (ether-type), and carbonyls) can react with ammonia to form the other N species that have been reported in carbon materials.[133] Temperature is a key factor for the formation of other functional groups (eqs 1−6). Nitriles are formed at 180 °C by amide dehydration, for example. Amine groups are formed at initial carboxyl and hydroxyl sites on biochar at temperatures below 300 °C. Pyridinic-type nitrogens are generated from ether functions in the medium temperature range between 300 and 500 °C.[133] Increasing the ball milling velocity (≥500 rpm) or raising pressure have resulted in the formation of various N species.[133] Four types of nitrogen-containing functions (pyridinic, pyrrolic, graphitic N, and N-oxides) were generated in

https://doi.org/10.1021/acsomega.3c07804
ACS Omega 2024, 9, 12331−12379

carbon nanoparticles after ball milling nitrogen with graphite powders at 300 kPa, followed by pyrolysis for 3 h at 700 °C.[132] Another report suggests three nitrogen functions (pyridinic N, pyrrolic N, and graphitic N) were formed on nitrogen-doped graphene, which was made by ball milling melamine with graphene for 48 h at 500 rpm.[134] Therefore, adjusting the ball milling operating parameters can lead to formation of various N species in N-doped biochars.[110] Eqs 1−6 provide example nitrogen-containing surface functional group generation by reacting ammonia with various oxygen functional groups as a function of temperature.[110,133]

Carboxylic acids can react at room temperature with NH_3 to form ammonium salts, which dehydrate thermally to amides and nitriles at about 180 °C (eq 1):[133]

Lactones can generate lactams with NH_3 and then decarbonylate to a pyrrole at high temperatures (450 °C), as given in eq 2.

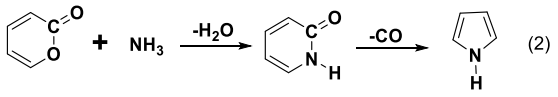

(2)

Lactams can also dehydrate after protonation to form pyridinic groups. In eq 3, HCN is formed by thermolysis of an amide to a nitrile by loss of water. The subsequent loss of HCN provides the proton needed for the lactam to pyridine conversion (at 615 °C):[133]

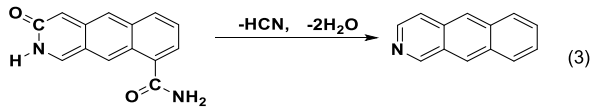

(3)

Furthermore, temperatures above 150 °C can dehydrate adjacent carboxyl groups into carboxylic anhydrides, which then form an imide after reacting with NH_3. Decarboxylation of the imide groups produces pyridines at around 395 °C, with CO_2 evolution as shown in eq 4:[133]

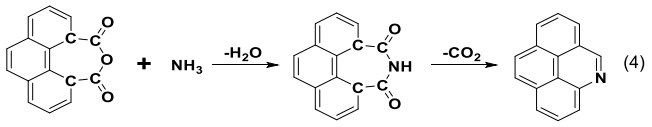

(4)

Phenolic compounds can form anilines, as shown in eq 5, at temperatures below 300 °C:[133]

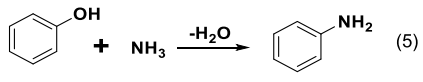

(5)

Elevated temperatures facilitate reactions between NH_3 and ethers via dehydration. Further, pyridine-like nitrogen can be seen on the periphery of the carbon layers after dehydrogenation, as shown in eq 6:[133]

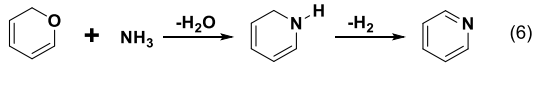

(6)

Ammonia decomposition to N_2 + H_2 begins above 500 °C. Also, a very small amount of HCN forms above 450 °C.[133]

3.2.2. Thiol Functionalization. 3-Mercaptopropyltrimethoxysilane (3-MPTS) is commonly used to add thiol functions to modified adsorbents.[78,135,136] It releases methanol in exchange for surface bound hydroxyl groups of adsorbents including smectite, metal oxides, and SiO_2.[135,137−139] It can also react with water to release methanol and form oligomeric siloxanes, which are also bound to surfaces. Either way, strong surface adhesion bonds $-CH_2CH_2CH_2S-H$ functions onto surfaces.[140] The sorption of Hg was assisted via ligand exchange and complexation on engineered biochar because the thiol groups provide surplus adsorption sites, creating strong sulfur binding to mercury. Also, biochar surfaces become more net negatively charged by the acidic thiol functions. This supports electrostatically induced sorption of cationic contaminants or heavy metals.[135]

Chemical impregnation and ball milling were used to prepare thiol-modified adsorbents.[78] 3-MPTS solutions were used to provide the surface thiol functionalization.[78] Poplar wood chip biochar was prepared at 300 °C. A ball mill agate jar was charged with 3g biochar suspended in a 120 mL solution of water, ethanol, and 3-MPTS (3.6 mL water, 114 mL ethanol, and 2.4 mL 3-MPTS). Alternatively, dropwise addition of 3-MPTS provides better mixing with biochar.[78] Agate balls (300 g) with diameters of 15−3 mm were added into this mixture in a mass ratio of 2:5:3. After placing the agate jar inside the ball mill, it was operated for 12 h at 300 rpm, with its rotation direction altered after every 6 h.[78] Biochar-to-ball mass ratios (1:100, 1:50, and 1:20), ball milling duration (3, 6, 12, 30, and 48 h), and various biochar amounts (3, 6, and 15 g) were evaluated. Rotation speeds of 300, 400, and 600 rpm were also investigated for biochar (3 g) mixed with agate balls (300 g) for 12 h. Finally, product biochars were washed with deionized water and ethanol 3 times and freeze-dried for 48 h.[78] Biochar that was modified with thiol after ball milling showed greater removal capacities (320.1 mg/g and 104.9 mg/g) than chemical treatments before ball milling with 3-MPTS (175.6 mg/g and 58.0 mg/g) for Hg^{2+} and CH_3Hg^+, respectively.[78]

3.2.3. Metal Impregnation. Metal dispersion on nanobiochar can be performed through pretreatment of the biomass precursor or post-treatment after nanobiochar preparation.[39,45,46,58,141,142] The pretreatment method involves immersing the biomass feedstock in a metal ion solution. Conversely, post-treating applies metal impregnation after nanobiochar preparation.[39] Metal, metal oxide, and metal hydroxide impregnated nanobiochar composites were developed via these routes for enhanced contaminants removal and other applications.[39,45,46,58,141,142] For example, iron oxide impregnated biochar nanocomposites showed both magnetic properties and enhanced removal of contaminants such as arsenic.[143−145] Porous biochar facilitates dispersion and strong adherence of iron oxide particles, which expands the iron oxide surface area.[145] A promising As(V) removal capacity of 6.80 mg/g was achieved by corn straw biochar impregnated with iron.[146]

A post-treatment preparation of iron oxide-permeated rice husk nanobiochar employed ∼15 g of dried rice husks that were ball milled (50 mL container) with 30 g of 5 mm diameter stainless-steel balls at 500 rpm to form nanoscale rice husk powders.[58] These nanoscale rice husks (15 g) were mixed with 0.3 mol $Fe_3(SO_4)_2{\cdot}7H_2O$ and 1 mol urea paste and pyrolyzed at 600 °C under reducing conditions via a one-pot pyrolytic technique at different residence times.[58] The Fe_3O_4-impregnated engineered nanobiochar prepared using a 5 h residence time showed better arsenic removal capacity. TEM images revealed nano-Fe_3O_4 clusters present in the nanobiochar matrices and the Fe_3O_4 nanoparticles were surrounded by graphite layers.[58] The reactions involved in the formation of

https://doi.org/10.1021/acsomega.3c07804
ACS Omega 2024, 9, 12331−12379

Table 2. Pros and Cons of Different Nanobiochar Preparation Methods

Preparation methods	Advantages	Disadvantages
Ball milling[17,38,54,74,104]	- No harmful chemicals required - Large scale applicability - Requires low energy - Low-cost production - Does not damage microcrystalline biochar structure - Easy to change ball milling environment - Reproducible - High efficiency - No waste generation	- Possibilities of particle's aggregation - Issues of purity and homogeneity - Mostly confined to laboratory only - Little data available on financial viability and environmental concerns
Centrifugation[38]	- Simple method - Enhances zeta potential/dispersibility of nano-biochar	- Multiple centrifugations required to get desired nanoparticle - Costly - Lower nanobiochar yields reported
Sonication[38]	- Provides uniform surfaces - No clogging of pores - Requires shorter reaction times - High purity	- Excessive ultrasound exposure may damage tissue - Large scale production may increase the manufacturing cost
Carbonization[38]	- Easy surface modification	- High energy consumption due to high temperature requirement (activation) - Generates hazardous gases - Additional treatment needed to get nanosize particles
Modification with chemical treatments[38]	- Provides engineered nanobiochar with desired surface properties - Improves affinity toward selected contaminants	- Acidic treatment can corrode walls of nano- biochar micropores lowering surface area - Additional chemical cost required - Use of hazardous chemicals sometimes reported

different iron oxide and hydroxide species on the biochar surfaces are given below in eqs 7−10:

$$2Fe(OH)_2 + H_2O + {}^1/_2O_2 \rightarrow 2Fe(OH)_3 \quad (7)$$

$$Fe(OH)_3 \rightarrow FeOOH + 2H_2O \quad (8)$$

$$Fe(OH)_2 + 2FeOOH \rightarrow Fe_3O_4 + 2H_2O \quad (9)$$

$$2Fe(OH)_2 + {}^1/_2O_2 \rightarrow Fe_2O_3 + 2H_2O \quad (10)$$

3.3. Advantages and Disadvantages of Different Preparation Methods. Nanobiochar preparation is most often accomplished by a top-down approach, where biochar particle sizes are reduced progressively to the nanoscale. This is most commonly carried out by ball milling in recent studies.[17] Surface modification to engineer different properties has been explored. Surface tailoring has been performed by oxidization, chemical impregnation, and coating functional nanoparticles.[38] Each method described here has its own unique merits as well as demerits. To quickly summarize the advantages and disadvantages of nanobiochar preparation methods, including ball milling, sonication, centrifugation, carbonization, and chemical treatment-based modifications, see Table 2.

As mentioned above, ball milling is generally the preferred method for nanobiochar preparation because it seldom needs to use harmful chemicals. It can be scaled up, and has high atom and mass efficiency. Aggregation of particles at certain conditions and presence of some impurities and heterogeneities are possible ball milling drawbacks. Centrifugation is a straightforward and simple method to separate different biochar particle sizes by sedimentation. It must be used with some other method that gives size reduction of particles. Thus, grinding, sonication, ball milling or other methods can form a particle size range, and nanosized particle fractions can be separated by centrifugation. Centrifugation is a solvent-assisted method for nanobiochar preparation since sedimentation proceeds through a liquid medium. It provides highly dispersed nanoparticles with improved zeta potentials.[38,96] To get the desired biochar particle sized fractions, multiple rounds of centrifugation are required, making this process costly. It is hard to scale up to large nanobiochar weights. Nanobiochar yields obtained by centrifugation are lower compared to those fractions obtained from direct ball milling.[38,42] Sonication is frequently used because it provides uniform surfaces, less pore clogging, and high purity nanobiochar in less reaction time compared to other methods.[38] The disadvantages of sonication include difficulty in upscaling to mass production, which further adds to production cost. Excess exposure to ultrasound may be dangerous to health.[38] An increase in tissue temperatures upon exposure to ultrasound occurs at intensities above 3 W/cm^2 resulting in tissue injury. Usually, the surface of the bones is where this happens most often.[147]

Engineered nanobiochar preparation usually requires using chemicals to develop specific desired surface properties and improved affinity toward selected contaminants (Table 2). Chemical application is associated with disadvantages, including the possible exposure to hazardous chemicals and wall corrosion in nanobiochar micropores. This further enhances the overall cost of engineered nanobiochar production.[38]

4. CHARACTERISTIC NANOBIOCHAR PROPERTIES

Biochar with different characteristic properties has been applied in diverse fields such as adsorbents, sensors, soil conditioners, and carbon sequestration.[1−5,8,9,20,148] Feedstock used and preparation conditions, play key roles in the successful production of desired biochar properties.[1−3,9] As expected, nanobiochar will have characteristics derived from the precursor macro-biochar from which they were derived by particle size reduction. However, several of the nanobiochar properties will differ, including surface area, pore volume, pore size, and zeta potentials.[17,40,93] These changes arise during particle size

https://doi.org/10.1021/acsomega.3c07804
ACS Omega 2024, 9, 12331−12379

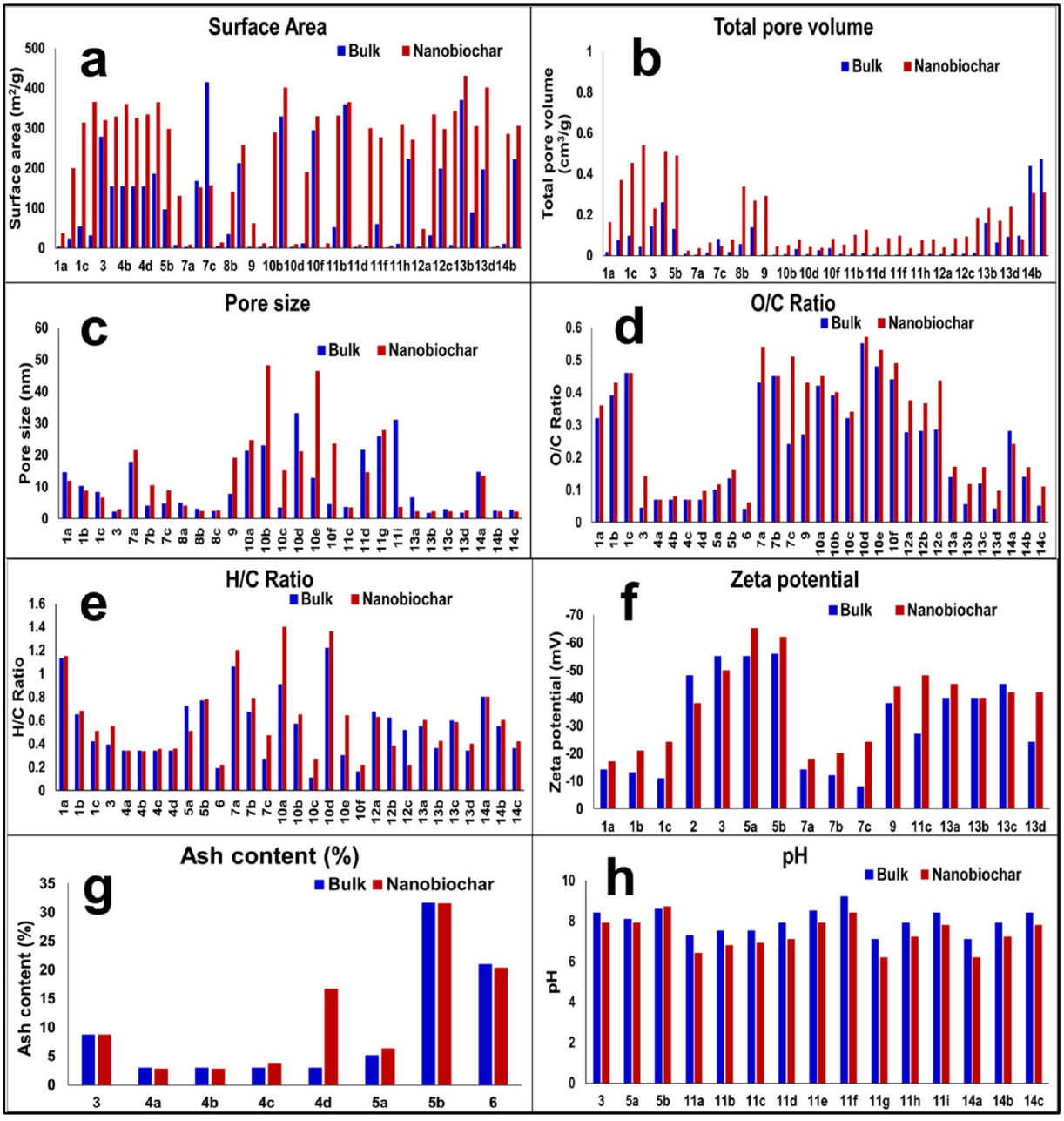

Figure 10. Comparison between bulk and nanobiochar (synthesized using ball milling) properties i.e., (a) surface area, (b) total pore volume, (c) pore size, (d) O/C ratio, (e) H/C ratio, (f) zeta potential, (g) ash content and (h) pH. All information related to the feedstock, precursor pyrolysis temperature, nanobiochar preparation conditions, and sample numbers on *x*-axis are given in Table 3. Data obtained (Table 3) with permission from refs 103, 77, 87, 105, 284, 14, 78, 104, 76, 6, 110, 13. Copyright 2020, 2016, 2020, 2019, 2020, 2020, 2020, 2019, 2018, 2020, 2019, 2020 Elsevier, respectively. Data obtained (Table 3) with permission from ref 89. Copyright 2019 Taylor and Francis.

reduction as well as specific influences of the nanobiochar preparation techniques. For example, changing the biomass feedstock can influence the resulting biochar particle sizes and the nanobiochar composition (e.g., carbon (%), minerals, surface functional groups, aromatic clusters, zeta potential, colloidal stability, and ash content). Feedstock changes cause key changes in % carbon, mineral contents, functional groups available, aromatic cluster content, zeta potential, and colloidal stability based on particle sizes (bulk, micron, and nano).[67]

This section deals with the characteristic nanobiochar properties versus those of its macro counterpart's properties based on the method of the nanobiochar's preparation by ball milling (Figure 10), sonication (Figure 11), and centrifugation (Figure 12). All data related to the characteristic properties of nanobiochar prepared via these three methods are summarized in Table 3. In addition, Table 3 also has information on the *x*-axis (sample numbers) for Figures 10, 11, and 12. Surface area, total pore volume, pore size, O/C ratio, H/C ratio, zeta potential, ash content, and pH are given for ball milled nanobiochars and their pristine precursors (Figure 10a–h). Surface area, O/C ratio, H/C ratio, zeta potential, pH, and ash content of each nanobiochar versus its pristine biochar precursor were also compared for nanobiochar synthesis by sonication (Figure 11a–f) and centrifugation (Figure 12a–f).

4.1. Surface Area. Nanobiochar pore properties can be a deciding factor for the extent of its different applications. The

https://doi.org/10.1021/acsomega.3c07804
ACS Omega 2024, 9, 12331−12379

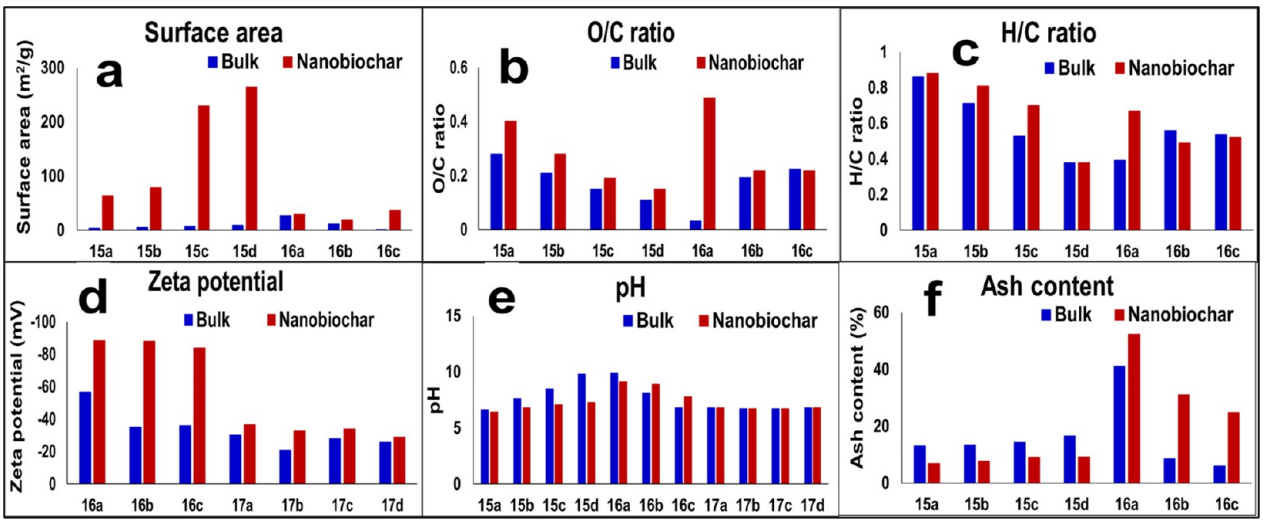

Figure 11. Comparison between precursor bulk and product nanobiochars (synthesized using sonication) properties i.e., (a) surface area, (b) O/C ratio, (c) H/C ratio, (d) zeta potential, (e) pH, and (f) ash content. All information related to the feedstock, precursor pyrolysis temperature, nanobiochar preparation conditions, and sample numbers on *x*-axis are given in Table 3. Data obtained (Table 3) with permission from refs 118, 151. Copyright 2013 and 2018 American Chemical Society, respectively. Data obtained (Table 3) with permission from ref 152. Copyright 2016 Elsevier.

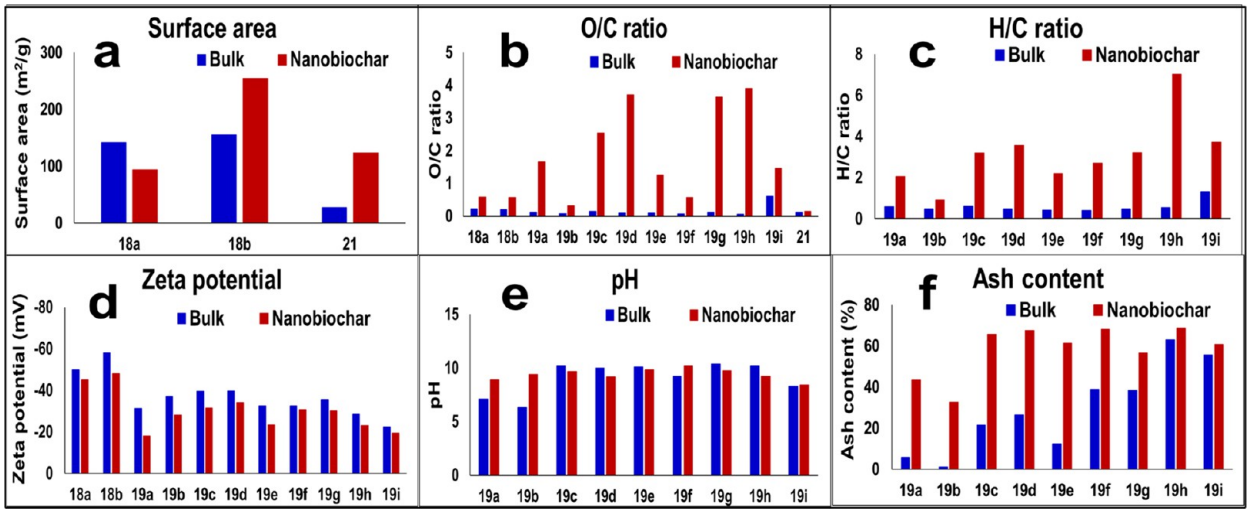

Figure 12. Comparison of the properties of bulk versus nanobiochar (synthesized by centrifugation fractions of bulk samples) i.e., (a) surface area, (b) O/C ratio, (c) H/C ratio, (d) zeta potential, (e) pH, and (f) ash content. All information related to the feedstock, precursor pyrolysis temperature, nanobiochar preparation conditions, and sample numbers on *x*-axis are given in Table 3. Data obtained (Table 3) with permission from refs 67, 153. Copyright 2019 and 2019 Elsevier, respectively. Data obtained (Table 3) with permission from ref 68. Copyright 2020 American Chemical Society.

pore properties (surface area, pore volume, and pore size) of bulk and nanobiochars have been widely explored after preparation by ball milling, but less explored for other preparation methods like sonication and centrifugation. Figure 10a summarizes changes in surface areas of different bulk biochars and their corresponding nanobiochars prepared by ball milling of those bulk samples. Large increases in surface area were reported (up to 97-fold) after ball milling compared to the pristine biochar (Figure 10a).[104] For example, the surface area of cow bone biochar increased from 2.76, 22.90, and 52.78 m^2/g in three pristine samples to 35.49, 199.5, 313 m^2/g after ball milling. These biochars were originally prepared at 300, 450, and 600 °C and ball milling increased surface areas by 12.9-, 8.7-, and 5.9-fold, respectively.[103] Raising pyrolysis temperature and applying ball-milling enhanced both the external as well as internal surface areas of the resulting nanobiochar. Raising pyrolysis temperatures (from 300 to 600 °C) releases more volatiles and exposes hidden biochar matrix pores to increase surface area.[103,149] The surface area of hickory wood biochar also increased from 1.4 to 29.1 fold after ball milling.[13]

A change in milling time and a wet vs dry milling environment can affect nanobiochar's surface properties.[89] Mechanical ball milling produced a ∼ 200% increase in the surface area for sawdust ball milled biochar. The "before ball milling" surface area (154 m^2/g) rose to 325 m^2/g after mechanical ball-milling (at 2 h wet milling), 334 m^2/g (at 12 h wet milling), 328 m^2/g (at 2 h dry milling), and 360 m^2/g (at 12 h dry milling).[89] Different biomass feedstocks give biochars that respond differently to ball milling. Pristine corn straw biochar (185 m^2/g) and rice husk biochar (96 m^2/g) were ball milled at 600 rpm for 2.5 h to generate nanoscale biochars with 100−600 nm particle sizes and surface areas of 364 m^2/g and 298 m^2/g, respectively.[75] The surface area of coconut shell biochar increased from 30.9 m^2/g to 365 m^2/g after ball milling.[77] A

https://doi.org/10.1021/acsomega.3c07804
ACS Omega 2024, 9, 12331−12379

Table 3. Comparison between Pristine and Nanobiochar Physicochemical Properties[a]

Precursor biomass	Pyrolysis conditions	Ball milling conditions	Surface area (m^2/g) (P/N)	Folds increase in surface area	Total pore volume (cm^3/g) (P/N)	Pore size (nm) (P/N)	O/C Ratios (P/N)	H/C Ratio (P/N)	Zeta value (mV) (P/N)	pH (P/N)	Ash content (P/N)	Sample no. on X axis
Ball milling												
Cow bone meal[103]	Pyrolyzed under N_2 flow of 200 mL/min at 300 °C	Wet milling (ball to biochar ratio 100:1) at 300 rpm for 12 h, then ball milled biochar was 5 min centrifugated at 9000 rpm	2.7/35.5	12.8	0.017/0.163	14.48/11.7	0.32/0.36	1.14/1.15	−14/−17	NA	NA	1a
	450 °C		22.9/199.5	8.7	0.074/0.367	10.15/8.67	0.39/0.43	0.66/0.70	−13/−21			1b
	600 °C		52.8/313	5.9	0.097/0.453	8.22/6.46	0.46/0.46	0.44/0.54	−11/−24			1c
Coconut shell[77]	500 °C for 1.5 h under nitrogen flow	40:1 (ball to biochar ratio) milled for 6h at 550 rpm	30.9/365	11.8	0.042/0.54	NA	NA	NA	−48/−38	NA	NA	2
Hickory chips[87]	600 °C for 6 h (nitrogen flow)	Planetary ball mill with 6 mm agate balls (100:1)	277.4/319.1	1.15	0.14/0.23	2.09/2.82	0.044/0.142	0.392/0.55	−55/−50	8.4/7.9	8.7/8.7	3
Sawdust[89]	600 °C for 2 h at 10 °C/min ramp rate in N_2	Ball milled with 6–10 mm ball diameter for 2 h	154/328	2.13	NA	NA	0.069/0.069	0.341/0.34	NA	NA	2.91/2.8	4a
		12 h	154/360	2.34	NA	NA	0.069/0.080	0.341/0.34		NA	2.91/2.8	4b
		Wet ball milled (1 g BC:3 mL water) for 2 h	154/325	2.11	NA	NA	0.069/0.069	0.341/0.35		NA	2.91/3.8	4c
		12 h	154/334	2.17	NA	NA	0.069/0.096	0.341/0.35		NA	2.91/16.7	4d
Corn straw[75]	500 °C for 2 h at 5 °C/min rate	Planetary ball milling (diameter 5 mm at 600 rpm for 150 min	185/364	1.97	0.26/0.51	NA	0.1/0.115	0.72/0.51	−55/−65	8.1/7.9	5.13/6.3	5a
Rice husk[75]			96/298	3.11	0.13/0.49	NA	0.134/0.161	0.77/0.78	−56/−62	8.6/8.7	31.55/31.5	5b
Wheat straw[105]	600 °C for 1 h under 100 mL/min N_2 flow rate	Milling of 8 g biochar and 800 g ZrO_2 ball (6–10 mm dia.) for 5 min.	6.9/130	18.89	0.007/0.0225	NA	0.04/0.06	0.19/0.22	NA	NA	20.91/20.3	6
Poplar woodchips[284]	Ambient atmosphere at 300 °C	200 rpm for 24 h for 1 g biochar with 100 g agate ball (3–15 mm dia.)	1.2/7.9	6.55	0.003/0.034	17.80/21.5	0.43/0.54	1.06/1.20	−14/−18	NA	NA	7a
	500 °C		167/151	0.90	0.013/0.063	4.02/10.40	0.45/0.45	0.67/0.79	−12/−20	NA	NA	7b
	700 °C		415/156	0.38	0.081/0.045	4.61/8.83	0.24/0.51	0.27/0.47	−8/−24	NA	NA	7c
Wheat stalk[14]	Pyrolyzed in N_2 at 300 °C	Ball to biochar ratio 100:1 with 300 rpm for 12 h	3.9/13.5	3.46	0.0174/0.076	4.84/4.03				NA	NA	8a
	450 °C		33.7/139.9	4.15	0.0544/0.3366	3.0/2.27	NA	NA	NA	NA	NA	8b
	600 °C		211.6/257.5	1.22	0.1370/0.2678	2.28/2.41				NA	NA	8c

https://doi.org/10.1021/acsomega.3c07804
ACS Omega 2024, 9, 12331−12379

Table 3. continued

Precursor biomass	Pyrolysis conditions	Ball milling conditions	Surface area (m^2/g) (P/N)	Folds increase in surface area	Total pore volume (cm^3/g) (P/N)	Pore size (nm) (P/N)	O/C Ratios (P/N)	H/C Ratio (P/N)	Zeta value (mV) (P/N)	pH (P/N)	Ash content (P/N)	Sample no. on X axis
Ball milling												
Poplar wood chips[78]	Pyrolyzed at 300 °C for 3 h	3 g biochar was mixed with 2.4 mL 3-MPTS and milled at 300 rpm for 12 h	1.8 / 61.3	33.52	0.003 / 0.291	7.76 / 19.05	0.27 / 0.43	NA	−38 / −44	NA	NA	9
	At 300 °C for 2 h		1.2 / 10.8	8.64	0.002 / 0.043	21.3 / 24.6	0.42 / 0.45	0.91 / 1.40		NA	NA	10a
Wheat straw[104]	At 500 °C for 2 h		2.9 / 289	96.98	0.005 / 0.050	23 / 48.1	0.39 / 0.40	0.57 / 0.65		NA	NA	10b
	At 700 °C for 2 h	Planetary ball milling, ball to biochar powder ratio (1:100) Stainless steel balls of size 5 mm, operational speed 300 rpm for 24 h	328 / 401	1.22	0.031 / 0.076	3.42 / 15.1	0.32 / 0.34	0.11 / 0.27	NA	NA	NA	10c
	At 300 °C for 2 h		1.8 / 9.3	5.16	0.004 / 0.04	33.1 / 21.0	0.55 / 0.57	1.22 / 1.36		NA	NA	10d
Rice husk[104]	At 500 °C for 2 h		10.8 / 190	17.59	0.024 / 0.036	12.7 / 46.3	0.48 / 0.53	0.30 / 0.64		NA	NA	10e
	At 700 °C for 2 h		294 / 329	1.12	0.035 / 0.08	4.46 / 23.5	0.44 / 0.49	0.16 / 0.22		NA	NA	10f
Sugar cane bagasse[76]	For 2 h at 300 °C		0 / 10.8	10.8	0.007 / 0.052	NA / 31.7	NA	NA	NA	7.3 / 6.4	NA	11a
	450 °C		51 / 331	6.5	0.008 / 0.099	NA / 3.6	NA	NA	NA	7.5 / 6.8	NA	11b
	600 °C		359 / 364	1.01	0.009 / 0.125	3.6 / 3.4	NA	NA	−27 / −48	7.5 / 6.9	NA	11c
Bamboo[76]	300 °C	Planetary ball milling, Ball diameter 6 mm, Operational speed of 300 rpm in ambient air with rotation and direction altered every 0.5 h	2 / 8.3	4.15	0.005 / 0.038	21.1 / 14.5	NA	NA	NA	7.9 / 7.1	NA	11d
	450 °C		4.7 / 299	63.62	0.003 / 0.083	NA / 3.5	NA	NA	NA	8.5 / 7.9	NA	11e
	600 °C		59 / 276	4.68	0.002 / 0.097	NA / 3.7	NA	NA	NA	9.2 / 8.4	NA	11f
Hickory chips[76]	300 °C		0.8 / 5.6	7	0.004 / 0.034	25.9 / 27.8	NA			7.1 / 6.2		11g
	450 °C		9.8 / 309	31.53	0.007 / 0.074	NA / 3.6	NA	NA	NA	7.9 / 7.2	NA	11h
	600 °C		222 / 270	1.22	0.006 / 0.079	31.1 / 3.6	NA			8.4 / 7.8		11i
Wheat straw[6]	Engineered biomass pyrolyzed in N_2 at 400 °C for 2 h	Magnetic wheat straw biochar was ball milled (5 mm ball dia.) with 100:1 ball to biochar ratio	2.9 / 47.2	16.1	0.004 / 0.038	NA	0.277 / 0.375	0.675 / 0.63	NA	NA	NA	12a
	550 °C		31.1 / 333.4	10.7	0.007 / 0.083		0.28 / 0.366	0.624 / 0.38		NA	NA	12b

https://doi.org/10.1021/acsomega.3c07804
ACS Omega 2024, 9, 12331−12379

Table 3. continued

Precursor biomass	Pyrolysis conditions	Ball milling conditions	Surface area (m^2/g) ($\frac{P}{N}$)	Folds increase in surface area	Total pore volume (cm^3/g) ($\frac{P}{N}$)	Pore size (nm) ($\frac{P}{N}$)	O/C Ratios ($\frac{P}{N}$)	H/C Ratio ($\frac{P}{N}$)	Zeta value (mV) ($\frac{P}{N}$)	pH ($\frac{P}{N}$)	Ash content ($\frac{P}{N}$)	Sample no. on X axis
Ball milling												
Hickory chips[110]	700 °C	Planetary ball milling, 6 mm ball dia, Ball to mass ratio 10:1, operated at 300 rpm for 12 h	198.6/296.3	1.5	0.006/0.091		0.285/0.436	0.515/0.22				12c
	At 450 °C for 2 h		7.4/342	46.5	0.012/0.184	6.61/2.16	0.139/0.171	0.55/0.602	−40/−45	NA	NA	13a
	600 °C		370/430	1.16	0.158/0.232	1.71/2.16	0.055/0.116	0.362/0.42	−40/−40	NA	NA	13b
Bagasse[110]	At 450 °C for 2 h		88.5/304	3.44	0.063/0.17	2.86/2.22	0.119/0.170	0.598/0.58	−45/−42	NA	NA	13c
	600 °C		196/401	2.04	0.09/0.238	1.81/2.38	0.041/0.097	0.34/0.397	−24/−42	NA	NA	13d
Hickory wood[13]	For 2 h in nitrogen atmosphere at 300 °C	Planetary ball milling, Ball to mass ratio (1:100) operated at 300 rpm	0.8/5.6	7	0.096/0.08	14.6/13.4	0.28/0.24	0.80/0.80	NA	7.1/6.2	NA	14a
	450 °C		9.8/284.7	29	0.44/0.304	2.45/2.13	0.14/0.17	0.55/0.60		7.9/7.2	NA	14b
	600 °C		221.5/304.8	1.4	0.471/0.307	2.71/2	0.05/0.11	0.36/0.42		8.4/7.8	NA	14c

Precursor biomass	Pyrolysis conditions	Nanobiochar preparation conditions	Surface area (m^2/g) ($\frac{P}{N}$)	Folds increase in specific surface area	Total pore volume (cm^3/g) ($\frac{P}{N}$)	Molar O/C ratio ($\frac{P}{N}$)	H/C ratio ($\frac{P}{N}$)	Zeta potential (mV) ($\frac{P}{N}$)	pH ($\frac{P}{N}$)	Ash Content ($\frac{P}{N}$)	Sample no. on X axis
Sonication											
Peanut shell[151]	For 2 h under N_2 flow in a tube furnace at 300 °C	0.7 g bulk biochar with 35 mL deionized water dispersed for 15 min at 25 °C under sonication at 120 W	3.7/63.6	17.3	NA	0.28/0.4	0.86/0.88	NA	6.61/6.40	13.1/6.89	15a
	400 °C		4.7/78.6	16.5		0.21/0.28	0.71/0.81	NA	7.59/6.80	13.4/7.68	15b
	500 °C		7.4/230	31.4		0.15/0.2	0.53/0.70	NA	8.48/7.08	14.3/8.93	15c
	600 °C		8.8/264	29.9		0.11/0.15	0.38/0.38	NA	9.81/7.27	16.5/9.16	15d
Wheat straw[152]	350−700 °C in an oxygen poor atmosphere (<1% O_2)	3 g biochar was added to 80 mL water and ultrasonic vibrator was used to disperse the biochar	26.3/29.6	1.1	0.025/0.0002	0.03/0.48	0.39/0.67	−56.65/−88.40	9.9/9.1	41.14/52.35	16a
Wicker[152]			11.4/18.2	1.6	0.006/0.00014	0.19/0.22	0.559/0.49	−34.87/−87.94	8.1/8.9	8.53/30.97	16b
Miscanthus[152]			0.7/36.4	47.9	0.001/0.0007	0.24/0.22	0.537/0.52	−36.12/−83.6	6.8/7.8	6.0/24.74	16c
Wheat straw[118]	Under anaerobic conditions at 350 °C	15 g biochars were sonicated in 500 mL deionized water for 30 min to prepare nanobiochar suspension	65	NA	NA	NA	1.289	−30.1/−36.6	6.8/6.8	NA	17a

https://doi.org/10.1021/acsomega.3c07804
ACS Omega 2024, 9, 12331−12379

Table 3. continued

Precursor biomass	Pyrolysis conditions	Nanobiochar preparation conditions	Surface area (m^2/g) $\left(\frac{P}{N}\right)$	Folds increase in specific surface area	Total pore volume (cm^3/g) $\left(\frac{P}{N}\right)$	Molar O/C ratio $\left(\frac{P}{N}\right)$	H/C ratio $\left(\frac{P}{N}\right)$	Zeta potential (mV) $\left(\frac{P}{N}\right)$	pH $\left(\frac{P}{N}\right)$	Ash Content $\left(\frac{P}{N}\right)$	Sample no. on X axis
Sonication											
Pine needle[118]	550 °C		205	NA	NA	NA	1.478	$\frac{-20.6}{-32.9}$	$\frac{6.7}{6.7}$		17b
	350 °C		30	NA	NA	NA	1.20	$\frac{-28.0}{-34}$	$\frac{6.7}{6.7}$		17c
	550 °C		83	NA	NA	NA	0.721	$\frac{-25.6}{-28.9}$	$\frac{6.8}{6.8}$		17d
Centrifugation											
Rice straw[68]	At 400 °C	Nano biochar was separated by centrifugation method	$\frac{141.3}{93}$	0.66	$\frac{0.089}{0.356}$	$\frac{0.22}{0.58}$	NA	$\frac{-50}{-45}$	NA	NA	18a
	700 °C		$\frac{155.3}{254}$	1.6	$\frac{0.101}{0.575}$	$\frac{0.20}{0.57}$		$\frac{-58}{-48}$			18b
Wood chips[67]						$\frac{0.11}{1.66}$	$\frac{0.58}{2.05}$	$\frac{-31.4}{-17.9}$	$\frac{7.05}{8.90}$	$\frac{5.73}{43.4}$	19a
Pine wood[67]						$\frac{0.08}{0.32}$	$\frac{0.48}{0.91}$	$\frac{-37.0}{-28.0}$	$\frac{6.30}{9.40}$	$\frac{0.91}{32.6}$	19b
Wheat straw[67]						$\frac{0.14}{2.54}$	$\frac{0.61}{3.20}$	$\frac{-39.6}{-31.6}$	$\frac{10.2}{9.69}$	$\frac{21.4}{65.5}$	19c
Barley grass[67]						$\frac{0.09}{3.71}$	$\frac{0.49}{3.56}$	$\frac{-39.8}{-34.0}$	$\frac{10.0}{9.17}$	$\frac{26.4}{67.3}$	19d
Peanut shell[67]	At 500 °C	Nanoparticles were separated using centrifugation	NA	NA	NA	$\frac{0.10}{1.25}$	$\frac{0.42}{2.18}$	$\frac{-32.4}{-23.4}$	$\frac{10.1}{9.82}$	$\frac{12.2}{61.3}$	19e
Rice husk[67]						$\frac{0.05}{0.58}$	$\frac{0.39}{2.71}$	$\frac{-32.3}{-30.6}$	$\frac{9.20}{10.2}$	$\frac{38.9}{68.2}$	19f
Dairy manure[67]						$\frac{0.12}{3.65}$	$\frac{0.48}{3.23}$	$\frac{-35.5}{-30.2}$	$\frac{10.4}{9.76}$	$\frac{38.5}{56.6}$	19g
Pig manure[67]						$\frac{0.05}{3.89}$	$\frac{0.53}{7.04}$	$\frac{-28.4}{-22.9}$	$\frac{10.2}{9.22}$	$\frac{62.9}{68.5}$	19h
Sewage sludge[67]						$\frac{0.61}{1.45}$	$\frac{1.30}{3.72}$	$\frac{-22.3}{-19.4}$	$\frac{8.31}{8.43}$	$\frac{55.6}{60.8}$	19i
Tobacco stem[95]	Pyrolyzed at 500 °C with a N_2 carrier	Centrifugation at 3500 *g*	$\frac{NA}{21.1}$	NA	NA	$\frac{NA}{0.109}$	$\frac{NA}{0.434}$	$\frac{NA}{-72.5}$	$\frac{NA}{9.79}$	NA	20
Rice hull[153]	Carbonized at 600 °C in limited oxygen	Centrifuged at a rate of 10,000 rpm for 30 min	$\frac{27.1}{123}$	4.5	$\frac{0.036}{0.062}$	$\frac{0.11}{0.14}$	NA	NA	NA	NA	21

[a] *P* = Pristine biochar, *N* = Nanobiochar, NA = Not available.

https://doi.org/10.1021/acsomega.3c07804
ACS Omega 2024, 9, 12331−12379

rare decline in a biochar's surface area after ball milling has also been reported.[103] Poplar woodchips biochar prepared at 500 and 700 °C, with surface areas of 167 and 415 m^2/g, lost surface after ball milling to 151 and 156 m^2/g, respectively. This might be due to destruction of part of the original pore structure by ball milling.[103]

Surface area variations of different bulk biochars and their corresponding nanobiochars prepared using sonication are plotted in Figure 11a. Nanobiochars exhibited from 1.13- to ∼48-fold surface area increases versus their precursor macro-biochars. Biochars prepared using wheat straw, wicker, and miscanthus had surface areas of 26.27, 11.38, and 0.76 m^2/g, respectively. These rose to 29.56, 18.25, and 36.39 m^2/g, respectively, after sonication (60 kJ energy output with 80% amplitude).[64] In this sonication, 3 g biochar was dispersed in 80 mL water using a probe-type ultrasonic vibrator.[64]

Nanobiochar was generated via sonication of previously made peanut shell biochar that had been pyrolyzed at 300, 400, 500, and 600 °C. These nanobiochars had large enhancements in their surface areas exhibiting 17.3-, 16.6-, 31.3-, and 29.9-fold rises as their particle sizes dropped into the nano level during sonication.[41] BET surface areas of peanut shell nanobiochar also increased with a rise in the pyrolysis temperature of their precursor biochars.[41]

A clear trend for the isolation of nanobiochar fractions with larger surface areas is achieved after centrifugation (Figure 12a). After centrifugation, a maximum 4.55-fold increase in surface area of nanobiochar is reported as compared to bulk biochar (Figure 12a). For instance (sample no. 18b), the BET surface area increased from 155.31 m^2/g to 253.90 m^2/g for bulk biochar and nanobiochar prepared at 700 °C, respectively.[68] However, a reduction in the BET surface area, from 141.25 m^2/g to 93.18 m^2/g, of nanobiochar occurred after centrifugation of the rice husk biochar prepared at 400 °C.[68] The reduction in the BET surface area indicates the role of pyrolysis temperature.[68]

4.2. Total Pore Volume and Pore Size. The total pore volumes of bulk and nanobiochars were also compared (Figure 10b). Higher total pore volumes were observed for ball milled biochars than their pristine counterparts (Figure 10b). Increases in the pyrolysis temperatures to make the pristine biochars increase pore volumes for both pristine and ball milled biochars (Figure 10b). For example, the total pore volumes of pristine and ball milled cow bone meal biochars were 0.017/0.163, 0.074/0.367, and 0.097/0.453 cm^3/g in the samples pyrolyzed at 300, 450, and 600 °C, respectively.[103] Ball-milling increases the biochar's external surface area by decreasing the grain size and also increases its internal surface area by exposing the pore networks.[76,103] For example, a remarkable increase in total pore volume was reported going from unmilled (0.042 cm^3/g) to ball milled biochar/Fe_3O_4 (0.54 cm^3/g).[77]

Similarly, total pore volumes also increased from 0.089 and 0.101 cm^3/g for pristine biochar prepared from rice straw at 400 and 700 °C, respectively, to 0.356 and 0.575 cm^3/g for its nanobiochar prepared by centrifugation.[68] Similarly, rice hull nanobiochar prepared by ball milling its biochar pyrolyzed at 600 °C has an enhanced BET surface area (27.1 to 123.2 m^2/g). This nanobiochar's total pore volume increased to 0.062 from 0.036 cm^3/g.[153] On rare occasions, a reduction in total pore volume after ball milling is reported in literature.[13] The total pore volumes of 0.096, 0.436, and 0.471 cm^3/g of the hickory wood biochars prepared under nitrogen gas at 300, 450, and 600 °C all declined after ball milling to 0.079, 0.304, and 0.307 cm^3/g, respectively.[13]

The comparison of pore sizes of bulk biochars with their corresponding nanobiochars made using ball milling is illustrated in Figure 10c. No clear trend was reported for pore sizes, as a few studies revealed an increase in pore size after ball milling, while other studies showed a decline in pore size. Only limited studies exist on pore properties (surface area, pore volume, and pore size) of nanobiochar prepared using centrifugation or other methods.

4.3. O/C Ratio and H/C Ratio. Molar elemental ratios are useful to estimate the aromaticity (H/C ratio) and polarity (O/C ratio) of biochars and nanobiochars.[40,64] Lower H/C ratios imply higher aromaticity and more advanced carbonization of the bulk and nanobiochars. Lower O/C ratios reflect a less-polar nature of the biochar/nanobiochar.[89] Raising biochar pyrolysis temperature increases aromaticity but lowers the polar characteristics. Macro- and nanobiochar H/C and O/C ratios of less than 1 indicate less availability of organic residues.[64] These characteristics further help improve sorption capacity of many aqueous contaminants.[5] How the O/C ratios of bulk versus their corresponding ball milled nanobiochars compare is shown in Figure 10d. O/C ratios for bulk biochar range from 0.04 to 0.55 versus 0.06 to 0.75 for ball milled biochar (see Figure 10d). Most nanobiochars have higher O/C ratios after ball milling their precursors, but not always (see example 14a in Figure 10(C). O/C ratios of cow bone meal biochar pyrolyzed at 300, 450, and 600 °C increased from 0.32, 0.39, and 0.46 before to 0.36, 0.43, and 0.46, respectively, after ball milling.[103] A decrease in C (wt %) content increases O/C ratios, resulting in forming more oxygen-containing surface functional groups. A slight decrease of C (wt %), during wet ball milling, might be associated with the structures of oxygen-containing groups (C = O, in ester and carboxyl groups, etc.) that were disrupted. Small fused-ring aromatics, aliphatic carbon, and carboxyl carbon in the biochar- dissolved organic carbon (DOC) or the tar particles could be released into aqueous solutions from biochar pores.[79,103,110,154] H/C ratios of different biochars and their counterpart nanobiochars prepared using ball-milling are compared in Figure 10e. No clear trends appeared. A few studies showed distinct rise in the H/C ratio (sample 10a, Figure 10e) after ball-milling, but most H/C ratios remained almost constant with a few showing small drops. Bulk biochar H/C ratios ranged from 0.11 to 1.22, while ball-milled biochar showed H/C ratios of 0.22 to 1.40 (Figure 10e).

Most studies reported sonication increases the O/C and H/C ratios of the resulting nanobiochars (Figure 11b and Figure 11c). Molar O/C ratios increased from 0.032 and 0.193 to 0.487 and 0.217, respectively, when wheat straw and wicker biochars were sonicated to nanobiochars.[64] However, decreases O/C ratio when miscanthus bulk biochar (0.224) is sonicated to nanobiochar (0.217).[64] The H/C ratio increased from 0.392 to 0.667 for the wheat straw biochar after sonication. Conversely, H/C dropped from 0.559 and 0.537 to 0.491 and 0.521, respectively, upon sonication of wicker and miscanthus biochars.[64] The wheat straw nanobiochar (prepared via sonication) was less carbonized and less aromatic vs its macro particle precursors, indicating that its nanobiochar composition was less strongly pyrolyzed.[64] In this sonication, wheat straw biochar was physically dispersed using a probe-style ultrasonic vibrator. It was placed 2 cm below the biochar suspension's surface using a 13 mm-diameter probe tip.[64] Micro peanut shell biochars have higher degrees of dehydration and demethylation than their nanobiochars.[41] These same nanobiochars produced at pyrolysis temperatures from 300 to 600 °C have larger molar

https://doi.org/10.1021/acsomega.3c07804
ACS Omega 2024, 9, 12331−12379

H/C and O/C ratios after sonication. Their O/C precursor ratios increase from 0.28, 0.21, 0.15, and 0.11 for samples pyrolyzed at 300, 400, 500, and 600 °C to 0.40, 0.28, 0.19, and 0.15, respectively, after sonication. Similarly, H/C ratios for these same biochars rose, respectively from 0.86, 0.71, 0.53, and 0.38 to 0.88, 0.81, 0.70 and 0.38.[41]

The O/C and H/C ratios of nanobiochars prepared using centrifugation of bulk biochar are compared in Figure 12b and c, respectively. O/C and H/C ratios tend to rise for nanobiochar after centrifugation. Examples include nanobiochars from wood chips, pine wood, wheat straw, barley grass, peanut shell, rice husk, dairy manure, pig manure, and sewage sludge.[67,68] Nanobiochars obtained from rice straw biochar precursors via centrifugation were found to have higher O/C ratios compared to their bulk precursors. These bulk samples were highly carbonized (more aromatic) before smaller particle sizes were isolated by sedimentation.[68] The O/C ratio for bulk samples increased from 0.22 and 0.20 to 0.58 and 0.57 for the sedimented nanobiochars when the bulk samples were pyrolyzed originally at 400 and 700 °C, respectively.[68] Higher O/C ratios signify the possibility of more polar functional groups on higher area nanobiochar surfaces. These higher O/C ratios also agree with the higher surface hydrophilicities of nanobiochars versus their bulk precursors.[68] With decrease in size from bulk to nano, both O/C and H/C ratios increased as bulk samples were converted to nanobiochars.[67] As with rice straw biochar, rice hull biochars, which are rich in SiO_2. This causes a rise in O/C ratio as bulk particle sizes were reduced to nanobiochar by centrifugation.[67,153] This biochar was prepared at 600 °C when the O/C ratio was 0.114. The resulting nanobiochar's O/C ratio was 0.138.[153]

4.4. Zeta Potential. Particle surface charges are estimated through zeta potential measurements. These reflect the stability of nanobiochar colloidal solutions.[38] High zeta potentials lead to lower nanobiochar particle agglomeration and higher dispersion.[38] The relationship of zeta potential (mV) and the stability behavior of the colloid particle is summarized in Table 4.

Table 4. Stability Behavior of the Colloid Particles with Respect to Zeta Potential[a]

Zeta potential (mV)	Stability behavior of the particles
0 to ±5	Rapid coagulation or flocculation
±10 to ±30	Incipient instability
±30 to ±40	Moderate stability
±40 to ±60	Good stability
>±61	Excellent stability

[a]Reprinted with permission from ref 155. Copyright 2019 Rice University.

Ball milling bulk biochar decreases the zeta potential values (negative mV) (Figure 10f). This decrease in the zeta potential of ball-milled biochars corresponds to an increase in oxygenated surface functions that effectively reduces biochar's positive charge. That would benefit the sorption of cationic aqueous contaminants.[103] Bulk biochar zeta potentials range from −8 to −56 mV. These decrease after ball milling from −17 to −65 mV (Figure 10f).

Sonication, like ball milling, of bulk biochar lowers the zeta potentials of the resulting nanobiochar (Figure 11d). During size reduction, the zeta potential value decreased significantly from −56.65, −34.87 and −36.12 mV to −88.40, −87.94, and −83.60 mV, respectively, for wheat straw, wicker, and miscanthus biochars prepared at 700 °C.[64] Similarly, the zeta potential value becomes more negative when nanobiochars are prepared from wheat straw by pyrolysis at 350 and 550 °C.[118] Bulk wheat straw biochar zeta potentials changed from −30.1 and −20.6 mV to −36.6 and −32.9 mV in the nanobiochars, respectively, when the bulk samples were prepared at 350 and 550 °C.[118] Conversely, zeta potentials increased (became more positive) from −34.0 and −28.9 mV to −28.0 and −25.6 mV when bulk pine needle biochars prepared at 350 and 550 °C were sonicated to nanobiochars.[118]

Centrifugation of bulk biochar has separated nanobiochars with higher zeta potentials as shown in Figure 12d. Zeta potentials changed from −50 and −58 mV to −45 and −48 mV with a change in their size from bulk to nano for two bulk rice husk biochars prepared at 400 and 700 °C, respectively.[68] Another study demonstrated zeta potential variations with changes in the particle size and type of feedstock.[67] Overall, the zeta potentials of nanobiochars sedimented from variety of bulk biochar feedstocks, including wood chips, pine wood, wheat straw, barley grass, peanut shell, rice husk, dairy manure, pig manure, and sewage sludge, via centrifugation were 1.73 to 13.4 mV less negative compared to their corresponding microbiochars.[67] Thus, the nanobiochar suspensions had lower stability than the starting microbiochars. Among all feedstock-derived micro- and nano- biochars mentioned above, were found to have lower zeta potential values of −39.6 mV and −31.8 mV, respectively.[67] Zeta potentials were higher at −22.3 mV and −19.4 mV for micro and nanobiochar derived from sewage sludge, respectively.[67] Micro and nanobiochars derived from feedstocks like wood, agricultural wastes, and herbs possess zeta potential values above −30 mV.[67] These higher zeta potential magnitudes of micro and nano plant-derived biochars were attributed to higher surface phenolic and carboxylic group content in these biochars, as confirmed by FTIR spectra.[67]

4.5. pH. Nanobiochars prepared by ball-milling were found to have lower pH values versus their bulk precursors (Figure 10h).[13,87,102] This lower pH is attributed to the introduction of oxygen containing carboxyl, phenolic, and hydroxyl groups on the ball-milled biochar.[13,87] Reductions in pH ranging from 0.6 to 0.9 occurred as ball milling converted bulk sugar cane bagasse, bamboo, and hickory chip biochars to nanobiochars.[102] The bulk precursors had been pyrolyzed at 300 to 600 °C.[102] These results are consistent with others[13,76,156] indicating oxygenated functions are added during ball milling that lower pH. Similarly, the pH of ball-milled biochar prepared from hickory chips at 600 °C decreased to 7.9 from 8.4 before size reduction.[87] The pH values of ball-milled nanobiochars, which were made from different hickory chip biochars pyrolyzed at 300, 450, and 600 °C dropped from 7.1, 7.9, and 8.4 to 6.2, 7.2, and 7.8, respectively.[13]

The pH decreases for some nanobiochars made by sonicating bulk biochar (Figure 11e). Some pH drops were significant.[41] Peanut shell biochar made from 300 to 600 °C had low pH values due to low ash and high-oxygenated functional group content. When sonicated to nanobiochar, the bulk samples prepared at 300, 400, 500, and 600 °C with respective pH values of 6.61, 7.59, 8.48, and 9.81 gave reduced pH values of 6.40, 6.80, 7.08, and 7.27, respectively.[41] Similarly, nanobiochar prepared by sonicating wheat straw biochar exhibited a lower 9.1 pH versus a 9.9 pH for the bulk biochar.[64] However, pH lowering after sonication is not universal. The pH of nanobiochar prepared from bulk wicker and miscanthus biochars by

https://doi.org/10.1021/acsomega.3c07804
ACS Omega 2024, 9, 12331−12379

Table 5. Sorption of Aqueous Contaminants Using Nanobiochars and Engineered Nanobiochars[a]

							Equilibrium isotherm studies		Kinetic studies			
Adsorbate	Adsorbent	Surface area (m^2/g)	Adsorbent dose (g/L)	pH	Temp. (°C)	Adsorbate conc. (mg/L)	Isotherm models	Langmuir monolayer capacity (mg/g)	pseudo-first order rate constant(h^{-1})	pseudo-second order rate constant (g/mg/h)	Possible removal pathways	Adsorbent regeneration, if any (No. of adsorption/desorption cycles)
Arsenic[58]	Iron oxide rice husk nanobiochar	1736.8	10	7−12	25	0.01−10	Sips, Langmuir, Freundlich	5987	26.4	1.32	Strong covalent	Yes (5)
Hg(II)[78]	Thiol-modified nanobiochar	61.3	0.04	7	25	1.0−25	Langmuir, Freundlich	320.1	0.1	5.4×10^{-3}	Chemical precipitation, surface complexation, electrostatic attraction	Yes
Pb(II)[100]	Micro/nanobiochar (upper layer)	NA	NA	7	25	20−180	Langmuir	55.56	NA	NA	NA	No
	Micro/nanobiochar (lower layer)							41.7				
Hg(II)[6]	Ball milled magnetic nanobiochar	296.3		2−9	NA	1−150	Langmuir, Freundlich	127.4	0.326	9.75×10^{-3}	Surface complexation, electrostatic attraction, Hg-cπ bond formation	Yes (5)
Hg(II)[78]	Ball milled thiol modified biochar	61.3	0.04	7	25	1−25	Langmuir, Freundlich	320.1	0.1	5.4×10^{-3}	Electrostatic attraction, ligand exchange, surface complexation	Yes (5)
MeHg[78]						0.1−8		104.9	0.10	3.8×10^{-2}		
Cr(VI)[170]	Novel ball milled pyrite/biochar	82.9	0.1−1.0	3−11	25	10−120	Langmuir, Freundlich	134		0.0013	Surface complexation, electrostatic attraction	No
Cr(VI)[172]	Ball milled iron loaded biochar	241	0.5	5	22	18−50	Langmuir, Freundlich	48.1	3.94	1.55×10^{-4}	Electrostatic interaction	No
NH_4^+[119]	Nano-Mg-biochar	153.2	0.2−10	3−11	25	5−200	Langmuir, Freundlich, Elovich	23.8	0.012	0.001	Ligand exchange, Electrostatic attraction, ion exchange	No
Cr(VI)[188]	Nanobiochar enriched diamine derivative	6.9	0.25−4	2−12	15-60	10	Langmuir, Freundlich, Temkin, Dubinin−Radushkevich	79.3	0.834	15.0	Ione pair	Yes (5)
Ni(II)[76]	Ball milled bagasse biochar	270	0.2−1.0	6	20	10−200	Freundlich, Langmuir and Redlich-Peterson	114.4	NA	NA	Electrostatic interaction, cation-π interaction, surface complexation	No
Cr(VI)[174]	Novel ball milled Fe^0-biochar	29.7	0.5−5	2.5−11	20	20−200	Langmuir, Freundlich, Sips	17.5	NA	NA	Surface complexation	Yes (4)
Cu(II)[182]	Tri metallic surface engineered nanobiochar	NA	0.05−0.35	2−9	20-60	50−350	Langmuir, Freundlich, Redlich-Peterson, Fritz Schlunder	220.4	2.4	0.06	Surface interaction, metal-ion interaction	Yes (10)
Pb(II)[182]								185.4	2.4	0.06		
Pb(II)[189]	Nanosized activated sludge biochar	78.8	1−5	2−10	25	1−5	Langmuir, Freundlich	3.202×10^{-3}	NA	NA	NA	No
Cd(II)[190]	High performance nanobiochar	176.8	1	5.5	25	30−200	Langmuir, Freundlich	70.6	0.03	0.01	Precipitation, complexation	No
Cu(II)[103]	Micronano- nitrogenous ball milled bone biochar at 300 °C	35.5	0.5	5	25	5−200	Langmuir, Freundlich	159.3	NA	NA	Cation exchange, Surface complexation, cation-π interaction, precipitation, Electrostatic interaction	No
Pb(II)[103]						5−400		339.3				
Cd(II)[103]						5−200		66.3				
Cu(II)[103]	Micronano- nitrogenous ball milled bone biochar at 450 °C	199.5				5−200		184.3				
Pb(II)[103]						5−400		428.8				
Cd(II)[103]						5−200		122.1				
Cu(II)[103]	Micronano- nitrogenous ball milled	313.1				5−200		217.6				
Pb(II)[103]						5−400		558.9				

https://doi.org/10.1021/acsomega.3c07804
ACS Omega 2024, 9, 12331−12379

Table 5. continued

Adsorbate	Adsorbent	Surface area (m^2/g)	Adsorbent dose (g/L)	pH	Temp. (°C)	Adsorbate conc. (mg/L)	Equilibrium isotherm studies: Isotherm models	Equilibrium isotherm studies: Langmuir monolayer capacity (mg/g)	Kinetic studies: pseudo-first order rate constant(h^{-1})	Kinetic studies: pseudo-second order rate constant (g/mg/h)	Possible removal pathways	Adsorbent regeneration, if any (No. of adsorption/desorption cycles)
Cd(II)[103]	bone biochar at 600 °C					5−200		165.8				
Cd(II)[59]	Dendro nanobiochar	28	1.0	7	30	5−300	Langmuir, Freundlich, Hill, Temkin, Redlich-Peterson	NA	NA	NA	NA	No
Cr(VI)[59]				3.75		1−25		NA				
Methylene blue[102]	Ball milled bagasse biochar prepared at 450 °C	331	0.16	4.5	20	50	Langmuir, Freundlich	213				No
				7.5				354				
Reactive red[111]	Mesoporous ball milled iron loaded biochar	48.3	1.0	3	25	0−250	Langmuir, Freundlich	68.8	2472	11.4	Electrostatic attraction,	Yes (3)
				7.5				90.1	4080	124.2		
Titan yellow[117]	Hickory chips acidic ball milled biochar	5.7	0.167	NA	25	30−65	Langmuir, Freundlich	NA	0.58	0.003	Intraparticle diffusion	Yes (5)
Carbamazepine[57]	Pine wood derived nanobiochar	47.3	0.1	6	25	0.5−20 × 10^{-6}	Langmuir, Freundlich	0.04	1.2	95.2	NA	No
Prednisolone[188]	Nanobiochar enriched diamine derivative	6.9	0.25−4	2−12	15-60	5−100	Langmuir, Freundlich, Temkin, Dubinin−Radushkevich	21.9	0.246	3.156	Ion pair	Yes (5)
Tetracycline hydrochloride[14]	Wheat straw ball milled biochar	139.9	0.2	4−11	25	5−30	Langmuir, Freundlich	96.69	24.1	0.44	Surface adsorption, Pore filling	No
Glyphosate[59]	Dendro nanobiochar	28	1	6	30	5−250	Langmuir, Freundlich, Hill, Temkin, Redlich-Peterson	NA	NA	NA	Chemisorption	No
Oxytetracycline[59]			1	4.75		10−500		NA	NA	NA		
Sulfapyridine[191]	Ball milled biochar	NA	NA	3.5−8.5	25	10	Langmuir, Freundlich	57.9	3.4	0.125	$\pi-\pi$ interaction, H- bonding, hydrophobic interaction, electrostatic interaction	No
Sulfamethoxazole[191]			NA					100.3	1.9	0.127		
Diethyl phthalate[75]	Nano scale biochar prepared from Corn straw	364	2	6	25	0−500	Langmuir, Freundlich	25.5	0.102	2.04 × 10^4	Pore filling, H-bonding, $\pi-\pi$ EDA	No
	Nano scale biochar prepared from Rice husk	298						20	0.162	2.04 × 10^4		
Tetracycline[6]	Ball milled magnetic biochar	296.3	0.4	2−9	24	1−150	Langmuir, Freundlich	268.3	0.379	1.48 × 10^{-2}	Chemisorption, intra particle diffusion, external mass transfer	Yes (5)
17β-estradiol[192]	Magnetic nanobiochar prepared at 400 °C	166.9	0.1	3−9	25-40	0.6−3.0	Langmuir, Freundlich	50.2	75.6	18	H-bonding	Yes (5)
	Magnetic nanobiochar prepared at 600 °C	339.1						41.7	102	28.2	H-bonding	
	Magnetic nanobiochar prepared at 800 °C	321.7						34.1	70.2	31.2	$\pi-\pi$ interaction	

[a]NA = not available.

https://doi.org/10.1021/acsomega.3c07804
ACS Omega 2024, 9, 12331−12379

sonication, increased from 8.1 and 6.8 to 8.9 and 7.8, respectively.[64]

A few studies have shown no such change in pH after sonication.[75,118] For example, the pHs of corn straw and rice husk biochars prepared at 500 °C insignificantly changed from 8.1 and 8.6 to 7.9 and 8.7 after size reduction.[75] These differences in pH changes occurring after sonication illustrate feedstock influences on the pH during size reduction.[64] A study of nanobiochars prepared by sonication from wheat straw and pine needles did not find any change in pH upon reduction in particle size.[118]

The pH changes found after using centrifugation to separate nanobiochars from larger particle sizes do not exhibit any clear pattern (Figure 12e). The pH values of wood chip, pine wood, rice husk, and sewage sludge nanobiochars increased from 7.05, 6.30, 9.20, and 8.31 for the bulk biochars to 8.90, 9.40, 10.02, and 8.43, respectively, after centrifugation.[67] Conversely, the pH values decreased from starting sample values 10.2, 10.0, 10.1, 10.4, and 10.2 to values after centrifugation 9.69, 9.17, 9.82, 9.76, and 9.22, respectively, for biochars derived from wheat straw, barley grass, peanut shell, dairy manure, and pig manure, respectively.[67] Centrifugation of tiny particles could cause the loss of inorganic sulfur, calcium, and phosphorus compounds, which might lower the pH as sedimentation leaves only smallest particles in the liquid.[67] The pH value of centrifuged nanobiochar also depends on the composition of the feedstock.[67]

4.6. Ash Content. The ash content of bulk biochar and nanobiochar is a critical component. It is an indirect estimate of mineral availability and plays a crucial role in determining the properties and applications.[38] Ash content of different bulk biochars and their respective nanobiochars, produced via ball milling is compared in Figure 10g. Ball-milling usually does not cause any significant change in nanobiochars' ash content versus its parent bulk biochar. Ash precursors are present throughout its structure, so this lack of size sensitivity might be expected. However, a few studies showed slightly higher ash contents in nanobiochar prepared using ball-milling.[89] Sawdust biochar (pyrolyzed for 2 h at 600 °C under N_2) was wet ball milled (1 g biochar/3 mL water) for 2 and 12 h and gave ash contents of 3.79 and 16.7%, respectively, vs pristine biochar (2.91%), as shown in samples no. 4c and 4d of Figure 10g.[89] The loss of dissolved organic carbon during wet ball milling, may be the cause of increasing ash content in nanobiochar due to significant mineral weight contribution.[89]

The ash content of nanobiochar, prepared by sonicating bulk biochar, can increase or decrease versus that in the bulk (Figure 11f).[41,64] Reduction in ash content occurred in bulk peanut shell biochars after sonication. Bulk ash content dropped from 13.1, 13.4, 14.3, and 16.5% to 6.89, 7.68, 8.93, and 9.16% in the nanobiochars from sonication, respectively, of four samples. The bulk biochar precursors were pyrolyzed at 300, 400, 500, and 600 °C, respectively.[41] This ash content drop suggests that minerals were separated or dissolved by extraction during the nanobiochar size reduction via sonication (sample no. 15a−d, Figure 11f).[41] However, the opposite trend (increased ash content) was obtained when nanobiochar was obtained from sonicating bulk wheat straw, wicker, and miscanthus biochars.[64] Ash content increased from 41.14, 8.53, and 6.0% for the three bulk biochars to 52.35, 30.97, and 24.74% for their sonicated nanobiochars prepared from wheat straw, wicker and miscanthus feedstock, respectively (sample no. 16a−c, Figure 11f).[64]

Nanobiochar separated by centrifugation has much higher ash contents than its bulk precursors (Figure 12f). As particle size drops from bulk sizes to the nano level, the ash content increases.[67] However, the increase in ash content was also a function of feedstock. Ash content increased greatly when bulk to nanobiochar conversions by centrifugation were conducted on biochars prepared from plant biomass (wood, herbs, and agricultural wastes).[67] Ash contents increased from 5.73 → 43.4, 0.91 → 32.6, 21.4 → 65.6, 26.4 → 67.3, 12.2 → 61.3, 38.9 → 68.2, 38.5 → 56.6, 62.9 → 68.5 and 55.6 → 60.8% by centrifugation of biochars prepared from wood chips, pine wood, wheat straw, barley grass, peanut shells, rice husks, dairy manure, pig manure, and sewage sludge, respectively.[67] The ash content increases from bulk biochar to nanobiochar as the particle sizes get smaller.[67] This pattern was particularly pronounced for biochar made from plant biomass sources such as herbs, wood, and agricultural waste. Here the ash levels rose significantly while the particle sizes decreased (nanobiochar > bulk biochar).[67] These increases were predominantly a result of the accumulation of inorganic salts and hydrated ions during centrifugation and extraction.[67] Ash concentrations in nanobiochar were only marginally higher than those in bulk biochar for manure and sludge biochars from municipal sources. This could be because the mineral components in these biochars were exceedingly small (nanosize) or the ash in nanobiochar from municipal sources was not further concentrated.[67]

5. NANOBIOCHAR APPLICATIONS

Since nanobiochar is derived from biochar, they have many applications in common, including adsorption of organic and inorganic contaminants from aqueous solutions[17,58,67,102,103] and their immobilization in soil,[17,44] soil conditioning, soil fertility enhancement,[44,157] plant growth promotion,[18,94,158] enzyme immobilization,[55] catalysts,[159,160] and sensor development.[123,161] These applications and others make nanobiochar a sustainable replacement option for many costly nanomaterials.[40,43,64,123,161,162] Applications are summarized in the sections below.

5.1. Sorption of Aqueous Contaminants. *5.1.1. Heavy Metals.* The removal of many heavy metals by aqueous sorption has been a main research interest for nanobiochar application.[6,17,58,78,87,103] Adsorption studies of Cd(II), Cu(II), Pb(II), Hg(II), Ni(II), As(V), and Cr(VI) by nanobiochar are summarized in Table 5.[6,58,78,103] High sorption capacities by nanobiochars result from high specific surface areas, variable surface functionalities, graphitic nature, and humic acid like components.[17]

Heavy metal sorption capacities on nanobiochar are influenced by the number of surface functional groups per unit surface area, the aqueous pH, zeta potential, surface pH of zero surface net charge (PZC), and cation exchange capacity of the nanobiochar.[6,17,58,78,103] Since many factors affect heavy metal sorption on nanobiochar, detailed sorption mechanisms are seldom known, and they may vary for a given heavy metal.[6,17,58,78,103] Existing literature has invoked surface complexation, intraparticle diffusion, electrostatic attraction, ligand exchange, surface adsorption, and cation-π interactions as occurring during heavy metal uptake on nanobiochar.[6,17,58,78,103] Sorption of heavy metals by nanobiochar is not attributed to a single step; rather, it is governed by the combination of all steps in the process.[6,17,58,78,103] The uptake of a metal may involve many different types of surface bound structures. For example, surface complexation, cation−π

https://doi.org/10.1021/acsomega.3c07804
ACS Omega 2024, 9, 12331−12379

interaction, and electrostatic interaction were all suggested for Ni(II) adsorption on nanobiochar.[76] Each type of structure likely has several major geometric variations and different solvation interactions. For example, the adsorption of Hg(II) was considered to occur via multiple surface-bound structures when equilibrium was reached.[6] Defining a true rigorous adsorption mechanism, while often mentioned is beyond the reach for all adsorption studies, because all the individual reactions and steps, their equilibria and all activation barriers and intermediates cannot be defined.

A maximum sorption of 1.2 mg/g and 10 mg/g was observed for Cr(VI) and Cd(II), respectively, at pH 4 and 9, respectively, using the graphitic nanobiochar (28 m^2/g) prepared by disc milling of woody biochar. This biochar was a byproduct of gasification (at 700 °C) of *Gliricidia sepium*.[59] In aqueous media, Cd(II) mainly exists as a cation (Cd^{2+}) at pH 6−8 and has a capacity to bind with the nanobiochar in a nonspecific manner.[59] However, above pH 11, all cadmium exists as its hydroxy complex. Hence, Cd(II) binds to the negatively charged surface of this nanobiochar (PZC = 7.4).[59] Cr(VI) was sorbed at pH 4.0, during which it takes the form of the negatively charged ($Cr_2O_7^{2-}$) entity, while the nanobiochar surface carries a positive charge (as PZC = 7.4). Ca^{2+} present on the nanobiochar surface provide good binding sites for the negatively charged $Cr_2O_7^{2-}$ via electrostatic attraction.[59] Surface complexation with the surface functional groups like C=O and C−O present on nanobiochar may lead to reduction of the strongly oxidizing dichromate ions to Cr^{3+}, as confirmed by XPS spectroscopy.[59] The relative peak area intensity of oxygen containing functional groups like carboxyl, carbonyl, and hydroxyl on the surface of nanobiochar decreased with Cr(VI) removal from solution. This suggests that these oxygen functional groups played a role in supplying electrons for the reduction of Cr(VI) during the sorption process. Further, coordination bonding between the nanobiochar surface functional groups was identified by the XPS high resolution C 1s and N 1s spectra. Following the interaction of Cd(II) with nanobiochar, the deconvoluted C 1s peaks for C−O, C=O and O=C−C^- binding energies increased from values of 283.9, 285.5, and 287.3 eV to 284.8, 286.4, and 288.7 eV, respectively. This confirms the formation of oxygen-bearing functional groups such as phenolic and carboxylic in nanobiochar. A marginal binding energy increase was observed in the O 1s C=O peak transition from 530.8 to 532.5 eV, and in O 1s C=O shifting from 285.5 to 286.4 eV. This implies that the oxygen coordinated to Cd^{2+} donating some electron density to the Cd ion. Further, C=O[$Cr(CO)_6$] or C−Cr bond formation was also observed at 287.5 eV. Similarly, the involvement of C−N and C−NH_2 in Cd adsorption is demonstrated by a slight binding energy increase observed as the transition from 399 to 401 eV.[59]

Sorption of the Cu(II), Pb(II), and Cd(II) onto the ball-milled bone biochar follows the L-shaped adsorption isotherm, indicating possible occurrence of homogeneous or heterogeneous precipitation during the sorption.[103] Excellent sorption capacities of 287.6, 558.9, and 165.8 mg/g for Cu(II), Pb(II), and Cd(II), respectively, were achieved using the ball milled bone biochar.[103] Pseudo first order and pseudo second order kinetic models were applied. The pseudo second order model better fits the adsorption data.[103] The uptake of Cu(II), Pb(II), and Cd(II) onto ball-milled bone biochar surfaces is facilitated through a combination of surface complexation, precipitation, ion-exchange, electrostatic interactions, and coordination of heavy metals with π electrons. These processes, whether operating individually or synergistically, contribute to the efficient uptake of metals.[103,163,164] The uptake of Cu(II) and Cd(II) on the ball milled bone biochar was fast (equilibrium time of 90 min) as compared to Pb(II) (equilibrium time of 200 min).[103] This difference in metal ion sorption kinetics on the ball milled bone biochar might occur at active nitrogen and oxygen functions and hydroxyapatite present on the ball milled bone biochar.[165,166]

The solution pH influences the adsorbent's surface charge and the sorbate's speciation, which combined to change the heavy metal uptake capacity in aqueous media.[103] Heavy metal sorption on the ball-milled nanobiochar depends on temperature,[103] zeta potential reduction, which, after ball-milling, exposes of various oxygen and nitrogen surface functional groups that remove aqueous heavy metals.[105,167] Cd^{2+} and Co^{2+} sorption increased as solution pH rose from 2 to 7. At pH < pH_{pzc}, the adsorbent surfaces are protonated, leading to net of positively charged surfaces. This results in metal cation repulsion.[168] Increasing solution pH > pH_{pzc} causes net negative surface charge on ball milled bone biochar that attracts heavy metal cations, increasing the nanobiochar's sorption capacity.[168] For example, at pH (<4), competition between the proton and Cd(II) for the adsorption sites decreases metal cation removal capacity.[169] At pH > 7, the sorption capacity decreases owing to the precipitation or formation of hydroxide complexes, carbonates, or phosphates.[169] Similarly, Cr(VI) removal represents negative metal oxyanions. Metal oxyanion removal is facilitated by acidic aqueous solution. The removal capacity of Cr(VI) increased to 136 mg/g from 43.0 mg/g as the pH dropped from 11 to 3.[170] In aqueous solution, Cr(VI) predominantly exists as $HCrO_4^-$ between a pH range of 1 to 6, transitioning to CrO_4^{2-} at pH > 6. The pH at the zero-point charge for BM-FeS_2@BC (6.4) was determined to be less than that of FeS_2 (7.0). At solution pH levels of 3.0 and 5.0, the surface of BM-FeS_2@BC becomes positively charged, leading to adsorption of $HCrO_4^-$ onto the surface via electrostatic attraction.[171] However, at higher pH competition between Cr(VI) (CrO_4^{2-}), and −OH exists for the adsorption sites and a $Cr_X Fe_{(1-X)}$ OOH and $Cr_XFe_{(1-X)}(OH)_3$ precipitate will deposit onto the iron surface, leading to reduced removal (eqs 11 and 12):[170]

$$XCr^{3+} + (1 - X)Fe^{3+} + 3H_2O = Cr_XFe_{(1-X)}(OH)_3(s) + 3H^+ \quad (11)$$

$$XCr^{+} + (1 - X)Fe^{3+} + 2H_2O = Cr_XFe_{(1-X)}OOH + 3H^+ \quad (12)$$

A biochar/iron oxide composite was prepared by mixing 25 g of hickory chip biomass in a $FeCl_3$ (175) solution. This solution was prepared by dissolving 27.05 g of $FeCl_3{\cdot}6H_2O$ in 100 mL of deionized water and left to interact for a period of 2 h. Subsequently, the solution was subjected to drying at 80 °C for 24 h. The preprocessed biomass was pyrolyzed in a furnace for 1 h at 600 °C. The ball milled composite of biochar and iron oxide was produced by grinding the respective composites using the planetary ball mill (for 4 h at 500 rpm).[172] This adsorbent doubled the Cr(VI) removal capacity (48.1 mg/g) versus parent unmilled biochar.[172] Cr(VI) kinetic data were better fitted to the Elovich model.[172,173]

Nanobiochar's oxygen-containing functional groups (−OH, O=C−O, C=O, and C−O) and surface pores contributed to

https://doi.org/10.1021/acsomega.3c07804
ACS Omega 2024, 9, 12331−12379

Cr(VI) removal via chemisorption and electrostatic attraction.[82] In aerobic conditions, ball milled pyrite/biochar composites released Fe^{2+} and S^{2-} upon the reaction with dissolved oxygen (eq 13).[170,174,175] Since the amount of dissolved oxygen is limited in the closed environment, the oxidation of Fe(II) to Fe(III) was slow and limited, only occurring at the initial stage of the reaction (eq 14):[170,176]

$$2FeS_2 + 2H_2O + 7O_2 \leftrightarrows 2Fe^{2+} + 4SO_4^{2-} + 4H^+ \quad (13)$$

$$4Fe^{2+} + O_2 + 4H^+ \leftrightarrows 4Fe^{3+} + 2H_2O \quad (14)$$

With passage of time, sulfide and Fe^{2+} ions on the ball milled pyrite/biochar surface reduce the Cr(VI) to Cr(III) as per eqs 15 and 16:

$$3FeS_2 + 3HCr_2O_7^- + 21H^+ \leftrightarrows 3Fe^{3+} + 6S^0 + 3Cr^{3+} + 12H_2O \quad (15)$$

$$HCrO_4^- + 3Fe^{2+} + 7H^+ \leftrightarrows Cr^{3+} + 3Fe^{3+} + 4H_2O \quad (16)$$

At higher pH levels, −OH competes with Cr(VI) for adsorptive sites, leading to a reduction in adsorption.[170] Cr(III) and Fe(III) precipitated as Fe or Cr (oxy)hydroxides onto the ball milled pyrite biochar composites and may eventually inactivate the biochar surface.[170,177] The Fe^{3+} generated could react with more FeS_2, giving Fe^{2+} which then reduces Cr^{6+} to Cr^{3+} (see eqs 17 and 18):[178]

$$FeS_2 + 14Fe^{3+} + 8H_2O \leftrightarrows 15Fe^{2+} + 2SO_4^{2-} + 16H^+ \quad (17)$$

$$3FeS_2 + 15HCr_2O_7^- + 57H^+ \leftrightarrows 3Fe^{3+} + 6SO_4^{2-} + 15Cr^{3+} + 36H_2O \quad (18)$$

Temperature also plays a crucial role during the adsorption.[103] Cu(II), Pb(II) and Cd(II) sorption onto ball-milled bone biochar increased with a rise in temperature.[103] Heavy metal adsorption increased at high temperature due to an increase in the intraparticle diffusion rate of metals within the pores of ball milled biochar. Also, higher rates of intraparticle diffusion by heavy metals occurs.[103] These adsorptions were spontaneous ($-\Delta G°$ values) at 25 to 55 °C.[103] $\Delta G°$ values for the Pb(II) sorption onto the bone biochar prepared at 600 °C were −22.96, −23.97, −24.98, and −26 kJ/mol at 25, 35, 45, and 55 °C, respectively. These values become more negative for the ball milled bone biochar prepared at same temperature as the values changes to −24.94, −26.39, −27.85, and −29.31 for the sorption at 25, 35, 45, and 55 °C, respectively.[103] Bone char adsorption of heavy metals is characterized by spontaneity and is thermodynamic favorable. The enthalpy values were positive (endothermic).[103]

Maximum adsorption capacities of 13.5−38 mg/g for nickel (at an initial Ni(II) conc. of 50 mg/L) were achieved for the ball milled nanobiochar prepared from a variety of plant feedstocks, including bamboo, sugar cane bagasse and hickory wood chip bulk biochars pyrolyzed in the 300−600 °C temperature range.[76] For each biochar feedstock, the precursor prepared at 600 °C showed greater adsorption capacity, when ball milled to its nanobiochar, compared to feedstocks prepared at lower temperatures (300 and 450 °C).[76] More volatiles were released during the preparation of biochar at higher temperature, resulting in higher porosity and internal surface area versus those prepared at lower temperatures.[76,179] Ball milling led to a decrease in the nanobiochar's pH by introducing oxygen-containing functional groups (carboxyl and hydroxyl) on the biochar surface.[102] Ball milled nanobiochar showed higher sorption capacity for Ni(II) (114.4 mg/g) than other [except activated carbon (187 mg/g)] commonly used adsorbents such as, Fe_2O_3 carbon foam (13.8 mg/g), H_2SO_4 activated carbon (37.2 mg/g), *chlorella sorokiniana* (60.5 mg/g), and glycine functionalized graphene oxide (36.6 mg/g).[76]

Ball milled nanobiochar also proved to be an effective adsorbent for aqueous Hg(II).[6] An excellent removal capacity of 127.4 mg/g was achieved by the Fe_3O_4 loaded nanobiochar prepared from iron impregnated (8.5 g $FeCl_3$ and 3.4 g $FeCl_2$) wheat straw (100 g) at 700 °C.[6] The Hg(II) adsorption was pH dependent. Both adsorbate speciation and adsorbent surface charge are affected as solution pH changes. Various Hg(II) species like $HgCl_2$, $HgCl^+$, $Hg(OH)_2$, and HgCl(OH) are present over the solution pH range 0−12.[6] In the low experimental pH range of 2−9 (pH_{PZC} = 4.43), protonation of the surface functional groups occurs. Both H^+ and Hg^{2+} compete for the adsorption sites causing a progressive decline in the removal capacity of Hg(II) as pH becomes acidic and goes to 2.[180,181] Hg(II) adsorption in the pH range of 4−8 remains same. Then, it decreased further with an increase in pH above 8. The Hg(II) adsorption capacity decreased from 99.92 to 79.95 mg/g as the ionic strength rose from 0 to 0.5 mol/L $NaNO_3$. This implies an apparent competition between surface physical and/or specific adsorption and electrostatic attraction for the same adsorption sites. This indicates a limited contribution of electrostatic attraction to Hg(II) adsorption. Hg(II) adsorption was postulated to occur via Cπ-Hg(II) bond interactions at the graphitic carbon surface and by complexation between −COOH (or $-COO^-$ depending on pH) groups and Hg(II).[6]

An effective adsorbent was generated through entrapment of ball-milled biochar in Ca-alginate beads.[80] This combination significantly improves cadmium's adsorption capacity from 40.0 (ball milled biochar) to 227.1 mg/g (Ca-alginate entrapped ball milled biochar).[80] Cd^{2+} is adsorbed by ion exchange with protons from carboxylic acid functions.[80] Two carboxylate anions from the alginate form bidentate cadmium complexes.[80] Ball-milled and modified ball-milled also proved to effectively increase the Cr(VI) aqueous adsorption capacity.[170] Ball-milled pine wood biochar with pyrite (FeS_2) significantly raises the Cr(VI) removal capacity by 3−25-times that of pristine and ball-milled biochar.[170] Cr(VI) removal occurs by adsorption/surface complexation (∼8%) and reduction/precipitation (∼92%).[170]

Another hybrid adsorbent nanobiochar, amino functionalized silica coated Co/Fe/Mn nanobiochar, was prepared from *Cynodon dactylon* plant residue.[182] It exhibited specific amine and silica groups on its surface and was also superparamagnetic.[182] This engineered nanobiochar adsorbent had 185.4 mg/g and 220.4 mg/g sorption capacities for aqueous Pb(II) and Cu(II) ions, respectively.[182] The nanobiochar hybrid was recycled up to 15 times and after each batch sorption, this nano sorbent could be separated by using an external magnet. Nearly 85% and 60% adsorption capacities were still achieved after 10 and 15 adsorption−desorption cycles, respectively.[182]

5.1.2. Dyes. Nanobiochars have successfully removed aqueous dyes. These sorbents include ball milled bagasse biochar,[76] mesoporous ball milled iron-loaded biochar,[111] and hickory chips acidic ball milled biochar.[117] Both pristine and engineered nanobiochars have been used to remove both cationic and anionic dyes.[102,110,111,117] For example, ball-milled

https://doi.org/10.1021/acsomega.3c07804
ACS Omega 2024, 9, 12331−12379

nanobiochar prepared from bagasse pyrolyzed at 450 °C had a methylene blue removal capacity of 392 mg/g.[102] This adsorption's capacity increased from 216 to 318 mg/g as solution pH rose from 1.8 to 6.6. A further increase in pH to 7.5, only decreased the sorption capacity to 293 mg/g, but then the capacity rose to 392 mg/g at pH 9.8.[102] This ball-milled bagasse biochar sorbent, prepared at 450 °C was as good or better than activated carbon (270 mg/g),[183] graphite oxide (351 mg/g),[184] a biochar/AlOOH composite (85 mg/g),[167] or graphene coated biochar (174 mg/g).[185]

Engineered nanobiochar offered enhanced removal of anionic dyes due to the reduction in these sorbents' zeta potential and point of zero charge.[79,110,111,117] For example, N-doped ball milled biochar showed very efficient uptake of reactive red from the aqueous media.[110] Reactive red removal capacities of 22, 27.4, 31.3, and 37.4 mg/g were achieved for the N-doped ball milled biochar prepared from bagasse and hickory chips at 450 and 600 °C, respectively.[110] Authors observed the biochars prepared at 450 °C were more efficiently N-doped versus those prepared at 600 °C because a reduction of the oxygen-containing surface functions occurred as pyrolysis temperature rose. Most N-doping onto the biochar surface was due to −CN and $-NH_2$ groups, formed at −OH and −COOH surface sites.[110]

Modifications during the ball milling process can enhance the adsorption capacity of ball milled biochar several fold for the dyes.[117] For example, facile one step acidic ball milling approach using sulfuric acid was designed to fabricate a porous biochar directly from hickory wood without any further heat treatment.[117] It provided excellent removal (182.3 mg/g) of titan yellow dye. This capacity was 23-times higher than that of plain ball milled biochar (8.1 mg/g).[117] Ion exchange and electrostatic interaction were the main attractions governing titan yellow uptake onto the acid-modified ball milled hickory chip biochar.[117]

Iron-loaded ball milled hickory chip biochar was prepared by adding $FeCl_3{\cdot}6H_2O$ and hickory chips to distilled water, followed by drying, pyrolysis, and ball milling.[111] The iron-loaded ball milled nanobiochar adsorbed aqueous reactive red (sorption capacity: 90.1 mg/g at pH 7.5) at a sorption rate of <0.25 h versus carbon-based adsorbents which required equilibrium times of hours (up to 2.5 h).[111] The high kinetic rate constant (k_2 = 2.07 g mg^{-1} min^{-1}) was attributed to an increase in surface area of ball milled iron loaded precursor biochar.[111] Methylene blue also adsorbed onto the ball milled bagasse biochar prepared at 450 °C very rapidly during the first 10 min, achieving equilibrium in 8 h versus 16 h for the unmilled biochar.[102] The fast kinetics resulted from enlarged surface areas, pore openings and altered pore networks induced by ball milling. This facilitated intraparticle diffusion.[102] The iron oxide-loaded biomass transformed to β-FeOOH during biochar-forming pyrolysis as determined using XRD.[111] β-FeOOH played a very important role in adsorption by increasing the biochar's zeta potential, which facilitates the electrostatic interactions between β-FeOOH-loaded ball-milled biochar and reactive red dye.[111,186]

Solution pH plays a key role in reactive red and methylene blue sorption on nanobiochar and a significant role in determining the sorption pathway.[102,111] For example, electrostatic attractions attract and bind methylene blue to ball milled nanobiochar. A portion proceeds through electrostatic interaction between aromatic portion of methylene blue polynuclear aromatic regions of the biochar at pH 4.5.[102] At pH 7.5, both π−π and electrostatic interactions occur and contribute to sorption, leading to its highest adsorption capacity of 392 mg/g.[102] The reactive red dye sorption on β-FeOOH-loaded ball milled biochar increases as pH rises from 2 to 8, and then sorption drops with a further increase in pH from 8 to 10.[111] Protonation of biochar surface functional groups and dissociation of six sulfonate groups in reactive red contribute to the observed removal capacity changes with variations in pH.[111]

Ball milled biochar prepared from bulk hickory chip biochar pyrolyzed at 300−600 °C were modified using H_2O_2 oxidation. This treatment enhanced the methylene blue removal capacity to 310 mg/g from 185 mg/g before H_2O_2 oxidation.[61] Batch adsorption studies, characterization, and model simulations all demonstrated that ball milling significantly enhanced the specific surface area, while H_2O_2 treatment introduced the oxygen-containing functions to the biochar surface.[61] Oxygen functions help enhance electrostatic interactions with methylene blue, leading to enhanced adsorption.[61,102] The larger specific surface area of the ball milled samples also favors the methylene blue sorption via weak van der Waals forces, H-bonding, as well as π−π attractions[61,74] The oxygen-containing functional groups on the H_2O_2-modified ball milled biochar interact with methylene blue through electrostatic interactions, promoting the adsorption as well as adding H-bonding and ion exchange interactions.[102,187]

5.1.3. Emerging Contaminants. Pesticides, pharmaceuticals, new industrial chemicals, personal care products, endocrine disruptors, and synthetic hormones are categorized as contaminants of emerging concern or emerging contaminants.[4,5,148] Conventional technologies often do not efficiently remediate them.[148] Nanobiochar prepared from a variety of feedstocks has been able to successfully remove oxytetracycline,[59] carbamazepine,[53] glyphosate,[59] sulfamethoxazole,[191] 17β-estradiol,[192] sulfapyridine,[191] and tetracycline.[6] Woody nanobiochar was prepared from precursor woody biochar, a byproduct of *Gliricidia sepium* gasification, collected from the Dendro thermal power plant in Sri Lanka. Nanobiochar monolayer adsorption capacities of 520 and 83 mg/g were obatined for oxytetracycline and glyphosate, respectively.[59] The sorptive interaction between oxytetracycline or glyphosate with nanobiochar appears to be indicative of a physisorption process facilitated by electrostatic and van der Waals attractions. Within the experimental pH range from 3 to 7, several surface functional groups present on nanobiochar, including phenolic −OH, Si−O, and aldehyde/ketone C=O, may acquire negative charge. This implies that the coordination and covalent binding of the positively charged end of oxytetracycline's zwitterionic form (within the pH range 3.5−7.5) to the negatively charged functional groups on the nanobiochar surface is chemisorption. Cationic and zwitterionic forms of glyphosate are absent within the experimental pH range of 1−2, so likelihood of chemisorptive binding between glyphosate and nanobiochar can be dismissed.[59,129] Similarly, multiple sorption interactions, including π−π interaction, hydrophobic interaction, electrostatic interaction, and H-bonding, were also claimed for sulfapyridine and sulfamethoxazole adsorption onto ball-milled hickory chips and or pyrolyzed bamboo biomass, which had then been ball milled.[191]

These sorbents also removed the antibiotics sulfapyridine and sulfamethoxazole with 100 and 58 mg/g capacities, respectively.[191] Removal efficiencies of sulfapyridine and sulfamethoxazole increased from 39.8 and 33.4% to 89.6 and 83.3% after the ball-milling step due to the enhanced specific surface area and

https://doi.org/10.1021/acsomega.3c07804
ACS Omega 2024, 9, 12331−12379

the increase in surface functional groups.[191] The enhanced surface functionalities (−CH_2 at 2920 cm^{-1}, C=O/C=C at 1696 and 1597 cm^{-1} and aromatic −C=O at 1262 cm^{-1}) introduced during ball-milling enhanced the nanobiochar's affinity toward sulfonamide and sulfapyridine through H-bond formation.[191] The Langmuir isotherm better fitted the adsorption data obtained for sulfapyridine and sulfamethoxazole, giving R^2 values of 0.98 and 0.96, respectively.[191] This nanobiochar showed adsorption capacities comparable to other biochar-based adsorbents, including H_3PO_4-activated bamboo biochar (88.10 mg/g)[193] and giant reed biochar (4.92 mg/g)[194] for the sulfamethoxazole and carbon nanotube-modified biochar (27.90 mg/g) for the sulfapyridine.[195]

Carbamazepine was successfully adsorbed using ball-milled pine wood nanobiochar.[57] This nanobiochar removed approximately 95% of the carbamazepine after a 3 h contact time. The authors claimed this indicated rapid mass transfer.[57] Enhancements in pore size, pore structure, and surface functionality assisted this rapid equilibration.[57] Aqueous pH optimization significantly impacts adsorption by influencing the adsorbent surface charge and the adsorbate's speciation.[57,191] Increasing pH from 3 to 8 enhances the carbamazepine adsorption efficiency by nearly 2.3-times.[57] Solution pH also influenced sulfapyridine and sulfamethoxazole adsorption through variations in electrostatic interaction.[172] Sulfamethoxazole and sulfapyridine (with pK_a values of 2.3 and 8.4, respectively) removal does not change in the pH range of 3.5−6.5. Raising the solution pH increased the fraction of sulfonamides' anionic forms, causing electrostatic repulsion, resulting into a decrease in removal efficiency. Sulfamethoxazole does not exhibit any removal at pH 8.5.[191]

Altering adsorbent dose and adsorbate concentration also affect sorption.[56,57,196] For example, increasing ball-milled pine wood nanobiochar dose from 0.2 to 1.0 g/L increased carbamazepine removal from 53 to 87%.[57] Increasing the adsorbent's dose to some levels will no longer increase adsorption capacity due to the overlapping of adsorption sites and/or adsorbent aggregation.[57,197]

Ball-milled iron-loaded wheat straw biochar (BMBC700) removed 99% of tetracycline from aqueous solution within 12 h.[6] Its adsorption isotherm best fits the Langmuir model, with an adsorption capacity of 268.3 mg/g.[6] Tetracycline sorption was postulated to adhere to the sorbent through H-bonding, electrostatic attractions, and $\pi-\pi$ interactions.[6] Following tetracycline adsorption, the intensity of the XPS peak associated with the O−C=O group diminished, indicating the interaction between the tetracycline molecule and the ester as well as −COOH carboxylic acids groups of BMBC700 during adsorption. The C=C peak in the HR-XPS spectra of ball milled wheat straw biochar shifted from 284.4 to 284.6 eV, while the O−C=O (288.4 eV) peak vanished after adsorption of tetracycline onto the BMBC700. This confirmed the involvement of these functional groups during sorption.[6] Intraparticle diffusion and external mass transfer were rate controlling adsorption steps.[6] The $\pi-\pi$ stacking interactions were possible between aromatic rings in the tetracycline and the adsorbent's carbon matrix.[198] Moieties present in tetracycline could serve as proton acceptors (−C=O, $-N(CH_3)_2$) or as both proton acceptors and donors (−OH, $-NH_2$, and $-CONH_2$) within H-bonded adsorbed structures.[199]

Fe_3O_4-modified nanobiochar obtained from the pyrolysis of bagasse at 400−800 °C provided excellent aqueous 17β-estradiol removal.[192] Initially, bagasse biomass underwent pyrolysis at temperature range of 400−800 °C for 1 h at 7 °C/min, followed by grinding, which produced biochar nanoparticles after size screening techniques. Subsequently, Fe_3O_4 nanobiochar was prepared through a coprecipitation in an oxygen free environment, ensured by nitrogen purging.[192] Nanobiochar (3.3 g) was suspended in 300 mL ultrapure water and sonicated at 70 °C. Then, successively, 1.37 g of $FeSO_4 \cdot 7H_2O$ and 2.67 g of $FeCl_3.6H_2O$ were added to the suspension, which was maintained at 70 °C for 10 min. Next, 10.97 mL of $NH_3 \cdot H_2O$ solution was added, and the mixture was incubated for 90 min at 300 rpm. The resultant precipitate was resuspended in ultrapure water for later use after being rinsed three times with deionized water.[192] This ball-milled nanobiochar had a 14.5-times higher specific surface area compared to its precursor.[192] That enhanced its adsorption capacity.[192] Fe_3O_4-modified nanobiochar prepared at 400, 600, and 800 °C had specific surface areas of 167, 339, and 322 m^2/g, respectively. Langmuir capacities of 50, 42, and 34 mg/g were obtained for 17β-estradiol sorption onto the Fe_3O_4-modified nanobiochar prepared at 400, 600, and 800 °C, respectively.[192] Fe_3O_4-modified nanobiochar prepared at 400 °C exhibited more oxygen-containing surface functional groups than the Fe_3O_4-modified nanobiochars prepared at 600 and 800 °C. These numerous functions facilitated the formation of hydrogen bonds, while the lower pyrolysis temperature gave less aromatic structure available for $\pi-\pi$ interactions. Consequently, the sorption of 17β-estradiol onto Fe_3O_4-modified nanobiochar prepared at 400 °C involved dominant hydrogen bond interactions. As pyrolysis temperature rose beyond 600 °C, the molecular composition of biochars undergoes a increasingly transformed into crystalline inflexible graphene sheets. Indeed, when prepared at 800 °C, a greater abundance of graphene sheets existed versus nanobiochar prepared at 400 °C. The aromatic rings located at the center of graphitic sheets are more electron deficient, while the carbon rings nearer to the edges are more electron rich.[200−202] Hence, these aromatic sheets provide $\pi-\pi$ interaction sites for electron-rich aromatic rings in sorbates. Thus, the dominant interaction between the Fe_3O_4-modified nanobiochar prepared at 800 °C was a $\pi-\pi$ interaction between 17β-estradiol and graphitic surface.[192]

A number of one-,[173] two-,[173,203−209] and three-parameter[173] isotherms were applied to explain contaminant equilibrium sorption. The Langmuir adsorption isotherm was sufficient for the low surface coverage range while a Freundlich, Sips, Toth, or any other model can be used for wider concentration ranges.[173]

Equilibrium sorption data for various nanobiochars and engineered nanobiochars were fitted to several two-parameter isotherm models,[173] namely Freundlich (eq 19),[210] Langmuir (eq 20),[211] and Temkin (eq 21),[212] as well as three-parameter isotherm models,[173] including Sips (Langmuir−Freundlich) (eq 22),[213] Toth (eq 23),[214] Redlich-Peterson (eq 24),[215] Radke-Prausnitz (eq 25),[216] and Koble-Corrigan (eq 26).[217] The constants obtained for different contaminants using these models are summarized in Table 5.

Two parameter isotherm models:

$$q_e = K_F C_e^{1/n} \tag{19}$$

$$q_e = \frac{Q^0 b C_e}{1 + b C_e} \tag{20}$$

https://doi.org/10.1021/acsomega.3c07804
ACS Omega 2024, 9, 12331−12379

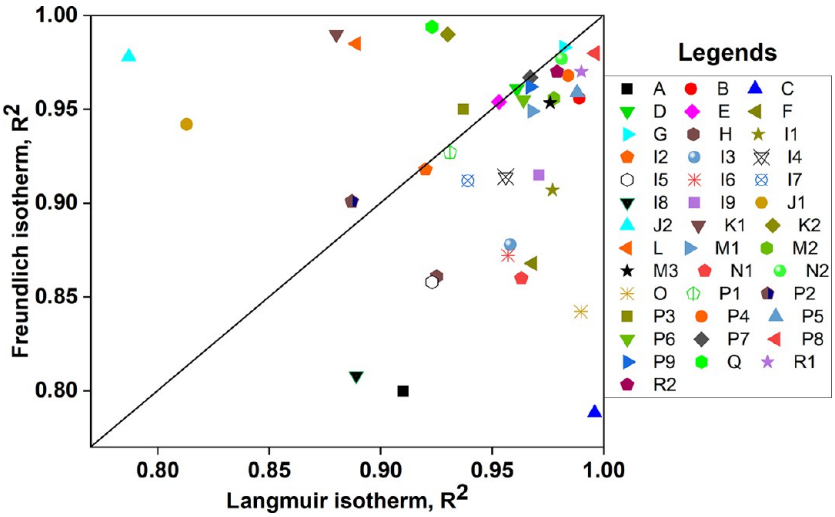

Figure 13. Comparative evaluation of Langmuir and Freundlich regression coefficients obtained for different aqueous contaminants on nanobiochars or engineered nanobiochars. (A) Iron oxide permeated rice husk;[58] (B) Thiol-poplar wood;[78] (C) Iron loaded wheat straw;[6] (D) Thiol-poplar wood;[135] (E) Pyrite-pine wood;[170] (F) Iron oxide-Hickory chips;[172] (G) Bagasse;[102] (H) Corn stalks;[190] (I1−3) Cow bone at 300 °C (I4−6) 450 °C (I7−9) 600 °C;[103] (J1−2) Bagasse;[76] (K1−2) Iron loaded-Hickory chips;[111] (L) Pine wood;[57] (M1−3) Wheat straw;[14] (N1−2) Hickory chips;[191] (O) Wheat straw[6] nanobiochar prepared by ball milling. (P1−3) Bagasse at 400 °C (P4−6) 600 °C (P7−9) 800 °C;[192] (Q) Dendro nanobiochar prepared by centrifugation.[59] (R1−2) Surface engineered-agro plant nanobiochar prepared by hydrothermal.[182] Data obtained with permission from refs 58, 78, 6, 135, 170, 172, 102, 190, 103, 76, 111, 57, 14, 191, 192, 59, 182. Copyright 2019, 2020, 2020, 2019, 2021, 2021, 2018, 2023, 2020, 2018, 2021, 2019, 2020, 2020, 2018, 2020, 2022 Elsevier, respectively.

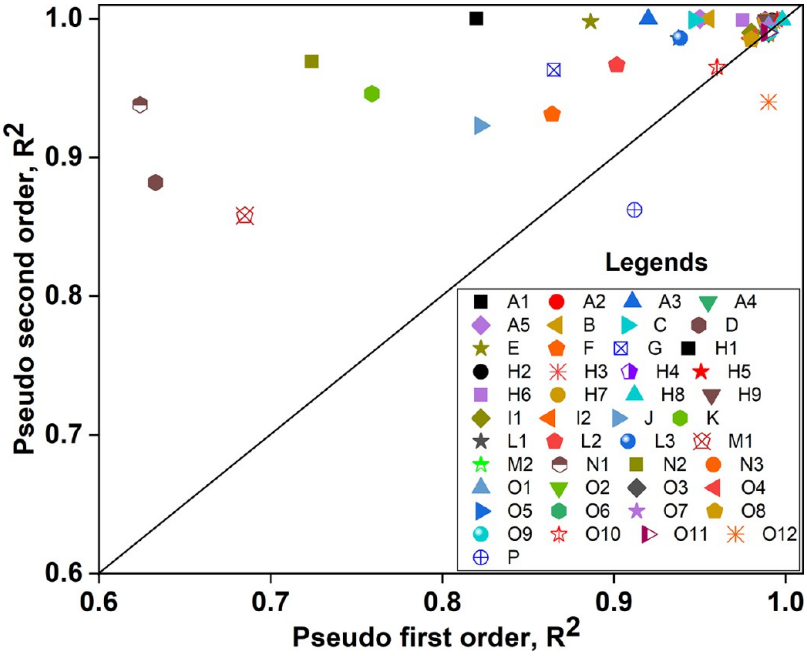

Figure 14. Comparative evaluation of Pseudo-first order and Pseudo-second order regression coefficients obtained for different aqueous contaminants on nanobiochars or engineered nanobiochars. (A1−5) Iron oxide permeated rice husk;[58] (B) Thiol-poplar wood;[78] (C) Iron loaded wheat straw;[6] (D) Iron oxide-Hickory chips;[172] (E) wheat straw;[6] (F) Bagasse;[102] (G) Corn stalks;[190] (H1−3) Cow bone at 300 °C (H4−6) 450 °C (H7−9) 600 °C;[103] (I1−2) Iron loaded-Hickory chips;[111] (J) Hickory chips;[117] (K) Pine wood;[57] (L1−3) Wheat straw;[14] (M1−2) Hickory chips;[191] (N1−3) Bagasse nanobiochar prepared by centrifugation.[192] (O1−6) Surface engineered-agro plant [Cu:20−120 mg/L], (O7−12) [Pb:20−120 mg/L] nanobiochar prepared by hydrothermal method.[182] (P) Mg-modified corn stalk nanobiochar prepared by sonication.[119] Data obtained with permission from refs 58, 78, 6, 172, 102, 190, 103, 111, 117, 57, 14, 191, 192, 182, 119. Copyright 2019, 2020, 2020, 2021, 2018, 2023, 2020, 2021, 2022, 2019, 2020, 2020, 2018, 2022, 2023 Elsevier, respectively.

$$q_e = \frac{RT}{b_{Te}} \ln(a_{Te} C_e) \quad (21)$$

$$q_e = \frac{K_s C_e^{\beta s}}{1 + a_s C_e^{\beta s}} \quad (22)$$

Three parameter isotherm models:

https://doi.org/10.1021/acsomega.3c07804
ACS Omega 2024, 9, 12331−12379

Table 6. Nanobiochar Regeneration Using Different Eluents[a]

Adsorbent	Adsorbent dose (g)	Adsorbate	Adsorbate conc. (mg/L)	Adsorbate vol. (mL)	pH	Regenerating agents	Removal efficiency of the adsorbent after each desorption andregeneration cycles (mg/g) (if available)
CSL-NanoB[62]	0.3	Cd(II)	0.1M	30	7.0	0.1 M HCl	1st cycle = 128.8 mg/g, 2nd cycle = 128.8 mg/g, 3rd cycle = 123.2 mg/g, 4th cycle = 112 mg/g, 5th cycle = 106.4 mg/g
	0.3	Sm(III)	0.1M		7.0		1st cycle = 97.5 mg/g, 2nd cycle = 97.5 mg/g, 3rd cycle = 90 mg/g, 4th cycle = 82.5 mg/g, 5th cycle = 67.5 mg/g
SBMGO[221]	0.03	Cu(II)	NA	25	1.2	HCl (pH 1.2; volume 25 mL)	86%
	0.03	Cr(VI)	NA	25		0.5 M NaOH	92%
Ball milled Fe biochar[111]	NA	Reactive red 120	NA	NA	3	1 M NaOH	47.9 mg/g
	NA		NA	NA	7.5		54.6 mg/g
Mg/Zr coffee nanobiochar[222]	NA	Phosphate	NA	NA	NA	NaOH	96.2%
	NA		NA		NA	HCl	94.7%
Artichoke leaves nanobiochar[127]	0.25	Metformin hydrochloride	10	100	NA	0.1 M HCl (100 mL)	1st cycle = 81.7%, 2nd cycle = 81.2%, 3rd cycle = 80.5%, 4th cycle = 80%, 5th cycle = 78.5%
Ball-milled magnetic nanobiochars[6]	0.02	Tetracycline	NA	NA	NA	0.2 M NaOH (20 mL)	5th cycle = 90.55 mg/g
	0.02	Hg(II)	NA		NA	0.5 M Na_2S(20 mL)	5th cycle = 87.36 mg/g
Nanobiochar with ethylenediamine[188]	0.25	Cr(VI)	10	100	NA	0.1 M HCl (100 mL)	1st cycle = 93%, 2nd cycle = 92.5%, 3rd cycle = 91%, 4th cycle = 89%, 5th cycle = 85%
	0.25	Prednisolone	25		NA		1st cycle = 90%, 2nd cycle = 87%, 3rd cycle = 84%, 4th cycle = 80%, 5th cycle = 75%
Magnetic ball-milled BC[87]	NA	Methylene blue	NA	NA	NA	Anhydrous ethanol	1st cycle = 90.1%, 2nd cycle = 86.7%, 3rd cycle = 84.8%, 4th cycle = 82.3%, 5th cycle = 81.9%
Twice ball milled magnetic biochar[223]	0.2	Methylene blue	20	NA	NA	Ethanol	1st cycle = 80%, 2nd cycle = 76.7%, 3rd cycle = 74.8%, 4th cycle = 70.1%

[a]NA = not available.

$$q_e = \frac{K_T C_e}{(a_T + C_e)^{1/n}} \quad (23)$$

$$q_e = \frac{K_R C_e}{1 + a_R C_e^{\beta}} \quad (24)$$

$$q_e = \frac{a_{RP} r_R C_e^{\beta_R}}{a_{RP} + r_R C_e^{\beta_R - 1}} \quad (25)$$

$$q_e = \frac{a C_e^{\beta}}{1 + b C_e^{\beta}} \quad (26)$$

where q_e is the quantity of contaminant sorbed per unit of nanobiochar weight (mg/g). C_e is the contaminant's equilibrium concentration (mg/L) in the solution. Constant n is adsorption intensity. K_s, a_s and β_s are the Sips isotherm constants. K_T (mg/g) and a_T (L/mg) are the Toth isotherm constants. K_R (L/g) and a_R (L/mg)$^{\beta}$ are the Redlich-Peterson isotherm constants. a_{RP}, r_R and β_R are the Radke-Prausnitz isotherm constants. The Koble-Corrigan isotherm model incorporates three parameters, a, b, and β.

Furthermore, the regression coefficients (R^2) were collected for the Langmuir and Freundlich models. A plot of the $R^2_{Freundlich}$ and $R^2_{Langmuir}$ values were made (Figure 13). In most nanobiochar publications, the Langmuir and the Freundlich isotherm models were used to describe the adsorption data. The better fits were given by the Langmuir isotherm model (Figure 13). In addition, pseudo-first order and pseudo-second order models[173] are most often used to fit the kinetic data obtained for contaminant sorption on nanobiochar. The regression coefficients (R^2) were collected for both the kinetic models and a $R^2_{first\ order}$ versus $R^2_{second\ order}$ plot of this data is given (Figure 14). The pseudo second order rate equation better fitted the kinetic eq (Figure 14).

5.1.4. Desorption and Adsorbent Regeneration. Regenerating exhausted adsorbents is essential to make adsorption economical.[148,218] The effectiveness of a contaminant's desorption can be increased by using the appropriate regeneration procedure. The viability of industrial-scale use depends on several factors, including the type of adsorbent, the pollutant, the toxicity of used adsorbents, pH dependences and the cost and energy requirements of the regeneration.[148] The reusability of spent adsorbents is determined via its high aquatic stability (easy to separate from water), contaminant recovery, and regeneration potency (number of regeneration cycles).[219] The adsorbents with favorable properties may lower the production cost for commercial and industrial applications.[218,220]

Nanobiochar regeneration studies are not very common in literature (Table 6). NaOH and HCl were commonly used desorbing agents for many contaminants, including Cd (II), Cu (II), Cr (VI), phosphate, reactive red 120, and tetracycline. Organic compounds are frequently desorbed by ethanol. Most studies, summarized in Table 6, have shown high retention (>75%) of original capacity after multiple desorption and regeneration cycles. For example, >80% of the original methylene blue sorption capacity was achieved using Fe_3O_4 ball-milled biochar after 5 anhydrous ethanol desorption cycles.[87] β-FeOOH-loaded ball milled hickory chip biochar also had good regeneration capacity and reuse potential.[111] NaOH was a better eluent than HCl for reactive red desorption with a 73.6% desorption and subsequent reuse after three

https://doi.org/10.1021/acsomega.3c07804
ACS Omega 2024, 9, 12331−12379

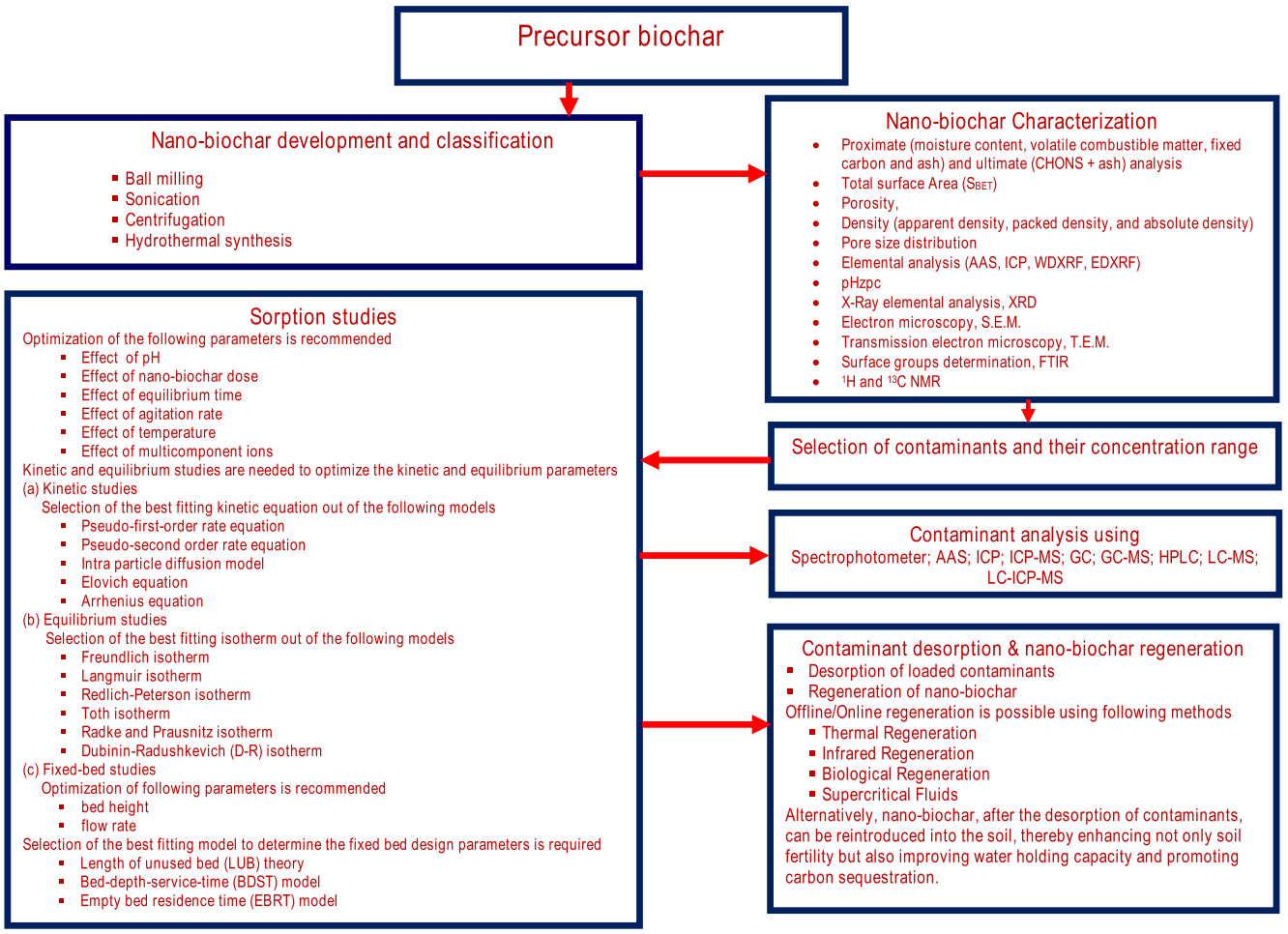

Figure 15. Nanobiochar selection protocol for aqueous contaminant removal. Table adapted and modified with permission from ref 148. Copyright 2019 American Chemical Society.

cycles.[111] HCl also produced high desorption, but the readsorption capacity dropped drastically because β-FeOOH dissolution occurred during acidic stripping.[111] Most nanobiochar regenerations were performed in batch studies. Proper column nanobiochar regeneration studies are absent in the current literature and very few parameters have been explored.

A protocol for nanobiochar preparation, characterization, and utilisation for aqueous contaminant removal is summarized in Figure 15.

5.2. Soil and Agriculture. Beyond sorptive applications, nanobiochar can provide agronomic plant growth and development benefits by improving soil properties. Nanobiochar has enhanced soil moisture content, improved plant nutrients (P, K, and N) availability, reduced nutrient leaching, generated better water-stable soil aggregates, lowered water runoff and soil erosion, and improved plant growth and yields.[18,39,44,94,158] These benefits are due to nanobiochar's surface morphology, porosity, functionality, and ion exchange capacities.[39] A recent review has summarized nanobiochar applications that can significantly enhance overall soil properties and support plant growth.[44] Although these beneficial properties have also been reported for bulk biochars, nanobiochars are expected to produce different effects owing to their greater specific surface area, difference in particle size, more negative zeta potential, and higher polar functional group content versus their bulk counterparts.[44] For instance, rice straw-derived nanobiochar showed much higher surface activity, polar index, and porosity (easier release of volatiles owing to less steric hindrance) versus its bulk counterpart.

5.2.1. Soil Health Enhancer. Nanobiochar soil amendments can alter soil porosity,[44,224] increase water holding capacity,[44,224] enhance soil moisture content,[44] foster better soil particle aggregates,[18,44,94,158,224] better nutrient retention,[18,44,158] increased soil carbon content,[18,44,94,158,224] provide contaminant immobilization,[44] and enhance soil cation and anion exchange capacities.[18,44,94,158,224] Nanobiochar or its engineered analogs can add nutrients to the soil.[39,42,224] All these properties contribute to enhance microbial and plant growth in the soil.[39,44,224]

Application of nanobiochar alters the soil pore structures through a reduction in macropores and an increase in micropores, which increased soil moisture content.[94] Soil moisture content rises as the amount of nanobiochar amendment goes up with least value near the surface region, owing to evapo-transpiration.[94] The enhancement in the soil moisture content is further aided by an the increase in the water infiltration rate, thereby lowering both water runoff by 0.57−43.5% and soil loss by 10−11%.[18,225] Increased soil pore volume and micropores with nanobiochar treatment led to enhanced capillary action, where more water is absorbed. This lowers runoff. This is evident with the increase in water absorption capacity from 39.7 to 74.4% with rise in nanobiochar soil application rates from 0.1 to 1%, respectively.[225] In this case, nanobiochar also helped stabilize soil aggregates and strengthen

https://doi.org/10.1021/acsomega.3c07804
ACS Omega 2024, 9, 12331−12379

soil structures. Stabilization occurs because various minerals and organic matter adhere to nanobiochar surfaces, which act as the binding material for the soil aggregates to form. This strengthened and stabilized soil structure making soil particles less susceptible to erosion loss.[94,225] Nanobiochar application also reduced the crack intensity factor in soil.[226] For example, application of nanostructured chalk and wheat residue biochar reduced the crack intensity factor of densely compacted soil from 3.9 to 0.4%. Reducing the crack intensity factor can significantly reduce water evaporation rates, enhance water retention, and promote soil stability.[226]

Nanobiochar amendments have resulted in significant reductions of nutrient loss from soil.[18,225] This is correlated with the reduction of surface runoff and soil erosion loss. For example, a reduction of 29.9−42.7% in nitrate loss with the application of oak tree branch-derived nanobiochar at 0.7−1% (~0.184−0.268 t/ha) application rates were observed. This was performed on a sandy soil with four types of vegetations (alfalfa, bean, *Caragana microphylla*, and corn)[18] Similarly, reductions in phosphorus and potassium loss via runoff were also reported with nanobiochar application.[18,94,225] Nanobiochar was mixed with soil to form a 5 cm thick soil-nanobiochar layer and then applied in bands 10 cm below the surface. Then the remaining top 5 cm was covered with another 5 cm layer of only soil. This reduction is facilitated by the enhanced migration of nutrients into deeper soil layers by nanobiochar, causing lesser nutrient availability near the surface for runoff. This is evident with the shift in the peak nitrate concentration values from the upper 5−10 cm soil layer to the 10−15 cm layer of soil after nanobiochar amendments. A 40 min simulated rainfall experiment was performed and the nitrate concentrations were then measured.[225] Nanobiochar application also increased nutrient availability and fertilizer use efficiency because of its high cation exchange capacity, specific surface area, and water holding capacity.[94,225] The International Biochar Initiative (IBI) recommends a bulk biochar application rate of 5−50 t/ha for positive crop response, but as mentioned above, nanobiochar can provide beneficial results with application rates as low as 0.184−0.268 t/ha.[18,227]

Enhancement of soil potassium concentration also occurs with nanobiochar amendment because the potassium in that biomass is concentrated and retained in the resulting biochar. Also, K^+ ions are trapped in the large number of nanobiochar-induced soil micropores.[94] This impedes the transportability of highly soluble and mobile potassium ions and holds them in the soil-biochar agglomerated layer. This helps in keeping them available to plant systems for a longer duration.[94] Accumulation of phosphorus in the soil root zone occurs in nanobiochar amended soil because of its adsorption on nanobiochar (owing to its greater porosity). This assists greater phosphorus availability for plant growth and development.[94] Compared to conventional biochar, nanobiochar application achieved greater nutrient use efficiency at a lower application rate (0.5−1% as opposed to 2−8% for conventional biochar).[225] That study was performed on 1m × 1m plots using nanobiochar only, in a sandy soil using maize and caragana vegetation. Another study also reported 0.7% and 1.0% as the best amendment level for nanobiochar, giving the highest reduction in water runoff, maximum soil particles, and nutrient conservation.[18] Thus, nanobiochar may be a more economical and efficient way of nutrient application in soil. Overall, one must define the cost required to make nano-BC versus the regular BC to see if the lower nano-BC weight is an advantageous way to apply nutrients to the soil.

5.2.2. Controlled-Release Fertilizer and Plant Growth Promoter. The ability of nanobiochar to maintain nutrients in the soil profile makes it a probable candidate for a sustainable, environmentally friendly controlled or slow-release fertilizer. The same concepts apply to biochars in general. Several studies demonstrated the controlled release of nutrients from nanobiochar and biochar-based nanofertilizers. These were derived from pyrolyzed feedstocks of corncob, wheat straw, pine needles, *Lantana camara*, and others.[142,157,228,229] Nanobiochar showed a typical nutrient release pattern of comparatively rapid nutrient release in the initial phase, which slowed and reduced/plateaued afterward, ensuring a more steady nutrient supply.[142] This release pattern correlates to the nutritional needs of plants during their growth stages. The initial growth stage requires a greater nutrient supply, while the remaining stages require a steady supply to maintain proper development and productivity.[142] For instance, macro (NO_3^-, P_2O_5, K_2O, Mg^{2+}, Ca^{2+}, and micro (Fe^{2+}, Fe^{3+}, Zn^{2+}, and Na_2O) nutrients show a hurried pace at the beginning. This eventually shifts to a gradual pace and then to a constant value toward the end.[157] All nutrients except NO_3^- and P_2O_5, showed a slower release pattern until the fifth day, eventually increasing until the 14th day where it reaches a plateau. While NO_3^- and P_2O_5 were released a bit faster than the rest until the fifth day and then reached plateau.[157]

Different biomass feeds have different pore and morphological characteristics, along with different ion adsorption and binding capacities.[142] For example, different nutrient release speeds by biochar-based nanofertilizers derived from pine-needle, *Lantana camara*, wheat stalk, and black gram biochars were determined.[228] The biochar-based nanofertilizers derived from pine needle biochars showed the highest nutrient (iron, magnesium, calcium, and sodium) retentions and sorption capacities.[228]

Nanobiochar also enhances plant nutrient uptake, leading to greater growth parameters including plant height, stem diameter, leaf area, and crop yield.[44] For example, coconut shell nanobiochar application led to a 4.4−5.7% increase in the maize crop yield versus unamended soil.[94] Goat manure derived nanobiochar increased wheat plant height (11%) and crop dry weight (25%), while enhancing plant nitrogen and copper uptake.[114] Similarly, several other reports exist where significant increases in biomass weights and plant heights occurred with nanobiochar addition.[114,153,229−231]

Nanobiochar application can affect seed germination.[229] Wheat seed germination, when tested using nanobiochar applications at 10−150 mg/L concentrations, exhibited the highest germination success at 50 mg/L.[229] A decrease in germination and a reduction in the shoot length occurred at higher application rates (>80 ppm). This deleterious effect did not show any improvement beyond a 50 mg/L application. This may be attributed to the excessive release and accumulation of nutrients into the root zone.[229] Hence, optimization of dosage for efficient nutrient delivery is essential. Wheat straw nanobiochar was reported to increase the germination percentage of cucumbers, tomatoes, lettuce, and carrots by 11.0, 10.0, 17.5, and 10.3%, respectively, versus unamended cultivated soil.[230]

Rice plant biomass weight, height, and root vitality benefited more with rice husk-derived nanobiochar addition versus addition of its precursor bulk biochar.[153] To enhance plant

https://doi.org/10.1021/acsomega.3c07804
ACS Omega 2024, 9, 12331−12379

growth, nanobiochar can be applied through foliar and soil application techniques.[63] Both foliar and soil applications significantly improved the root and shoot biomass of carrot plants via improvements in their pigments, nutrient status, and physiological indices.[63] Nanobiochar application leads to significant increases in total soluble sugars, free amino acids, flavonoids, total free proteins, and total free phenolics.[63] Greater below the soil-plant growth also occurred. Higher above soil plant growth through foliar nanobiochar application was achieved. However, the highest plant growth was observed when nanobiochar was applied with a combination of foliar (0.3%) and soil (3%) additions.[63]

5.2.3. Contaminant Immobilization and Reduction of Pollutant Toxicity. High surface area, porosity, cation, and anion exchange capacities make nanobiochar suitable for contaminant immobilization in soil. Nanobiochar applications have achieved immobilization, reduced bioavailability, and lowered phytotoxicity of both organic and inorganic contaminants.[42,44,153,230] For instance, rice husk nanobiochar significantly reduced cadmium bioavailability and toxicity in rice plants versus its bulk biochar counterpart.[153] This was enabled by nanobiochar's higher surface reactivity and greater dispersibility, which allowed it to attach to plant root surfaces easily. This, in turn, provides protection for roots and helps in cadmium immobilization.[153] The growth parameters of rice plants grown under cadmium stress exhibited the best results using amendments in the order, nanobiochar 600 °C ≈ nanobiochar 500 °C > nanobiochar 400 °C > nanobiochar 300 °C > bulk biochar 600 °C > control. This is attributed to an increase in surface area and pore volume at a higher pyrolysis temperature, leading to more cadmium adsorption, thereby lowering its negative effect on plant growth.[153] These results confirm that nanobiochar is clearly superior at reducing cadmium's negative effects on plant growth. This type of comparison of plant growth, if conducted in uncontaminated soil, might show nanobiochar could offer benefits versus the precursor rice husk bulk biochar, of larger particle sizes. The tiny nanobiochar particle size was also established as an advantage in seed germination.

Additional research reported a reduction in cadmium content in plant tissues by 86.5−95.1% after nanobiochar soil amendment.[230] This was ascribed to the reduction in the exchangeable cadmium forms, limiting their availability for plant absorption.[230] Cadmium usually exists in soil in four forms: exchangeable, reducible, oxidizable, and residual fractions. The exchangeable fraction is easily available to plants while residual fractions are recalcitrant and not utilizable by plants. Nanobiochar helps transform the soluble cadmium form into a stable form [$CdCO_3$ and $Cd(OH)_2$], thereby reducing plant uptake.[232] The high cadmium adsorption by nanobiochar is promoted by its high surface area, many oxy functional groups, and mineral constituents in the char, which promote surface complexation, ion exchange, and electrostatic attraction.[153,230]

Nanobiochar application reduced physiological plant damage induced by toxic soil contaminants.[116,153,233] Physiological damage was indicated by lowered levels of chlorophyll,[116] higher leaf membrane permeability,[153] and elevated malondialdehyde (MDA),[116] antioxidative enzyme activities of superoxide dismutase (SOD),[116] peroxidase (POD),[234] and catalase (CAT)[234] levels. All of these are indicators of stress-induced cellular damage.[116,153,233] Nanobiochar application increases the chlorophyll content,[116,233] reduces leave membrane permeability,[233] and MDA content.[116] One study reported chlorophyll *a* and *b* contents increased by 69−79% and 79−91%, respectively, while, MDA content dropped by 15%, upon nanobiochar application to cadmium contaminated soil.[233] When plants are exposed to a heavy metal stress, they initiate defense mechanisms through the actions of SOD, CAT, and POD.[234] SOD, POD, and CAT are antioxidative enzymes that deactivate harmful reactive oxygen species arising from oxidative stress. The higher the stress, the higher will be the activity of these enzymes. Nanobiochar application diminishes the activity of these enzymes, thereby modulating oxidative stress. This could be ascribed to reduced adsorption of the contaminant by the plant via nanobiochar addition, which diminishes the stress. Hence enzyme activity is lowered.[116,153,233] Nanobiochar addition can also alleviate heavy metal toxicity to soil microbes. This is corroborated by an increase in soil microbe diversity and microbial biomass with an increase of nanobiochar application under soil cadmium toxicity conditions. The most abundant microbe present at the lower nanobiochar application rate was *Proteobacteria*, because of its high cadmium tolerance.[230] As nanobiochar application rose, *Actinobacteria* and *Bacteroidetes* appeared in the soil samples, as cadmium toxicity dropped upon its complexation by nanobiochar. Greater microbial diversity occurs as cadmium toxicity drops and biochar's pores provide microbial habitat. Also, the nanobiochar may serve as microbes food sources, providing a suitable environment for microbial growth.[230]

5.2.4. Enhanced Crop Resistance and Allelopathic Effects. Nanobiochar application can also promote increased crop resistance to pathogens and allelopathic effects (a phenomenon where one species releases certain chemicals that can have detrimental effect on another species).[116,235] Nanobiochar application can mitigate negative effects of allelopathic species on crop plants.[116] One example is the detoxification of ferulic acid, which is a common root exudate of the invasive allelopathic plant *Imperata cylindrica*.[236] Nanobiochar addition led to a 435% rise in the biomass of seedlings grown in the presence of ferulic acid. Nanobiochar likely adsorbed ferulic acid, which was indicated by the reduction of MDA, SOD, and rise in chlorophyll levels.[116]

The corn straw biochar nanoparticles played a beneficial role in enhancing immunity of *Nicotiana benthamiana* in soil against infection by the *Phytophthora nicotianae*.[235] A 10-fold increase in immunity occurred after two biochar nanoparticle treatments.[235] Rice straw nanobiochar's effect on plant growth and disease resistance was evaluated against the Gram-negative bacterium Xanthomonas *campestris pv Vesicatoria*.[237] Plant leaves were first inoculated with the bacteria via the needle prick method (leaves were injured to provide a passageway for bacteria). Rice straw nanobiochar was applied via direct drenching of the root zone of plants. Plants treated with rice straw nanobiochar had a significant reduction in disease incidence and disease severity versus plants grown in the control soil.[237] This induction of nanoparticles resulted in an up-regulation of the innate immunity response of the plants against the pathogens.[237]

5.3. Miscellaneous Applications of Nanobiochar. Beyond water treatment, soil, and agriculture applications, nanobiochars have been investigated for many other potential uses. These involve sensing, additive and filler use, enzyme immobilization, targeted drug delivery, fuel additives, and catalysts. Altogether, nanobiochars can contribute to a wide range of problems. Only a handful of studies have been

https://doi.org/10.1021/acsomega.3c07804
ACS Omega 2024, 9, 12331−12379

conducted to date in these fields, but they are worth mentioning to understand the scope of nanobiochar applications.

5.3.1. Immobilization Supports for Enzymes and Microbes. Nanobiochar serves as a support for laccase enzyme immobilization, capitalizing on its high porosity, abundance of surface functional groups, and good surface to volume ratio.[53] Nitric acid plus sulfuric acid activation of nanobiochar benefits enzyme immobilization by significantly increasing surface −COOH groups and by removing impurities.[53] Surface carboxyl groups are attachment sites for covalently binding enzymes to the nanobiochar support.[53] Laccases are multi copper oxidase enzymes that can be classified as green catalysts as they produce only water as a byproduct.[57] In their unbound state, they undergo a rapid decline in catalytic activity during storage and have limited reusability.[55−57] To improve their stability and preserve activity upon storage under different pH and thermal conditions, enzymes are commonly immobilized onto supports.[53,238]

Laccase immobilization on nanobiochar achieved enhanced enzyme stability and activity.[53,55,238,239] For example, nanobiochar-immobilized laccase retained 15% of its initial activity whereas unbound laccase retained no activity after a 1-month storage.[53] Immobilized laccase also exhibited better stability and activity under extreme pH conditions, retaining up to 70% and 36% activity at pH 3−6 and pH > 8, respectively. Unbound laccase retained only 40% (pH 3−6) and 0% (pH > 8) activity. Similarly, at higher temperature (50−70 °C) the immobilized enzyme retained 42% of its activity versus only <11% in the unbound form.[53]

Immobilization also enhances the operational stability of enzymes by retaining significant catalytic activity even after many usage cycles. For example, nanobiochar-immobilized laccase retained catalytic activity for up to 7 cycles.[53,55,238] The stability and activity of nanobiochar-immobilized toluene/*o*-xylene monooxygenase and catechol 1,2-dioxygenase increased significantly (50% initial activity retained after 30 days storage at 4 ± 1 °C) versus only 10% retained activity for the unbound enzyme.[240] Immobilization increases enzyme stability by enhancing structural rigidity and protection from denaturation and unfolding via stabilization on the nanobiochar support. The enhanced pH and thermal stability result from the molecular rigidification experienced by the numerous enzymatic proteins, which interact through attractive forces with the surface functional groups of nanobiochar. These reduce unfolding and uncoiling, protecting the enzyme from denaturation. This shifts the denaturation pH and temperature making it hard to denature.[53,55,241] The improved operational ability of the enzymes after immobilization on nanobiochar results from synergism between enzyme binding and nanobiochar's good adsorbent properties, which help concentrate the substrate together.[53,240] However, the loss in enzyme activity after repeated use points toward leaching loss of enzymes from the immobilized support through repeated washing and denaturation via blockage of the enzymatic active sites by radicals formed during the process.[241] A covalently bonded enzyme is more difficult to remove from the support compared to noncovalent attachments (physical adsorption).[55,241] Hence, the selection of a proper bonding chemistry between enzyme and support improves operational stability.

Nanobiochar can also serve as an immobilization support to immobilize some microorganisms that can degrade complex contaminants.[242] *Rhodococcus opacus*, a Gram-positive actinomycetes, is one such bacterium. It can break down many recalcitrant organic compounds present in various industrial wastewater systems.[242] *Rhodococcus opacus*, when immobilized in a polyurethane/nanobiochar support, gave better COD removal capacity from industrial wastewater (up to 95%) versus only using a polyurethane support (81% removal).[242] This enhanced removal capacity was attributed to synergism between the nanobiochar and the immobilized bacterium. The bacterium degrades the contaminant, while the nanobiochar adsorbs contaminants via its high sorption capacity and supplies minerals that aid the microbes. For instance, the iron present in nanobiochar improves microbial stress tolerance and serves as a micronutrient source. Iron is a crucial component in both microbial enzyme systems and contaminant degradation.[242]

5.3.2. Catalysts. Nanobiochar catalyzes reactions, including esterification and photoreactions, to provide better product yield.[45,46,159] One sulfonated nanobiochar had a high catalytic ability for esterifying oleic acid with methanol, leading to a 64% methyl oleate yield as opposed to a merely 4% yield in its absence.[159] Catalysis was due to immobilized sulfonic acid sites on the nanobiochar's surface.[159] The highly porous nature and hydrophobic nanobiochar carbonaceous regions further enhanced catalytic activity by raising reactant accessibility to these acidic sites. The hydrophobic regions speed water removal required to drive the esterification equilibrium.[45,46]

Catalysts derived from biochar and nanobiochar are green catalysts. They are biodegradable and derived from waste biomass. They show good thermal and mechanical stability and can be separated and recycled.[243] One engineered nanobiochar was reported that exhibits photocatalytic activity due to the incorporation of ZnO.[125] This nanobiochar/ZnO composite was able to degrade and remove 99% phenol within 90 min under light irradiation. Nanobiochar/ZnO retained 95% of its ability to photodegrade phenol versus 69% for the ZnO alone, after five use cycles. This suggests the protection of ZnO particles by nanobiochar from photo corrosion.[125]

5.3.3. Fuel Additives. Some fuel additives reduce toxic emissions formation (e.g., particulate matter and NOx) during combustion.[244] Waste biomass-derived fusel oil is a common additive for lowering NOx emissions. However, increased unburnt hydrocarbon and carbon monoxide (CO) emissions have been reported using fusel oil blended into fuel. Other additives that can lower CO and unburnt hydrocarbon emissions are required. Nanobiochar-derived additives provide a good alternative to replace pre-existing nanometal additives (e.g., aluminum, boron, cerium, copper, manganese, and platinum), which have been widely used.[245] These metal-containing additives pose serious health hazards to living organisms and the environment.[244] Nanobiochar has found application as a fuel additive, owing to its low preparation cost and easy raw material availability. For instance, a sugar cane bagasse-derived nanobiochar and fusel oil blend was found to reduce NOx and hydrocarbon emissions by ∼20.5% and 14.6%, respectively.[244] For this additive, the desired concentration of nanobiochar is blended with the fuel via ultrasonication.[246,247] Further, increasing percentage of nanobiochar additive can provide additional NOx emissions reduction by increasing viscosity of the fuel blend. This, in turn lowers the combustion temperature.[244] The reduction in CO and unburnt hydrocarbons can be attributed to enhanced combustion efficiency of fuel owing to the nanobiochar's catalytic ability, high surface to volume ratio, and surface area, thus lowering the emission of unburnt particles.[246,247] Incomplete combustion is the main cause of unburnt hydrocarbon emissions, which was mainly

https://doi.org/10.1021/acsomega.3c07804
ACS Omega 2024, 9, 12331−12379

attributed to the high water content of the fusel oil additive.[244] However, with the addition of nanobiochar, an enhancement in the surface-to-volume ratio of the fuel induced a greater heat transfer rate, thereby aiding in better combustion.[244]

5.3.4. Additives and Fillers in Polymers and Rubber. Nanobiochar could serve as environmentally friendly and inexpensive additives or fillers by replacing some of those used now in the polymer and rubber industries. Additives and fillers enhance product stability and properties universally in these industries.[109,162] For example, carbon black and silica are commonly used fillers in tires to prevent abrasion and wet-skid resistance.[109,162] Nanobiochar derived from rice husk biomass, is composed of both carbon and silica which is formed when pyrolyzing lignocellulosic rice husks which have high silica content. Thus, it can serve as the source for both carbon black and silica fillers.[162] Rice husk nanobiochar fillers significantly reinforced natural rubber (NR). The ball-milled EM-400 (prepared using ethanol at 400 rpm) demonstrated the most significant reinforcement. EM 400/NR vulcanizates demonstrated improvements of 44% in tensile strength, 18% in 300% modulus, and 9% in tear strength compared to unmilled/NR vulcanizates.[162] A lignin-based nanobiochar filler used in tires gave similar reinforcing properties to carbon black, with a significant increase in both tensile strength (7 time increment) and the vulcanization rate.[109]

Nanobiochar has also been applied in the polymer industry as a filler to obtain enhanced properties.[113] Recently, a nanobiochar prepared via ball-milling of biochar obtained from the *Digitalis purpueres* plant pyrolyzed at 400 °C was used as a filler in the thermoplastic polyurethane.[113] This thermoplastic polyurethane nanobiochar composite was prepared via the fused deposition modeling (FDM) process, and it was used for mulching.[113] Nanobiochar addition effectively improved the surface color, contact angle, porosity, tensile strength, tear strength, water vapor transmission rate, and oxygen transmission rate for the nanobiochar composite mulching films.[113] Just the 10% nanobiochar addition into polyurethane achieved a 21% reduction in light transmittance. This is desirable to reduce the passage of photosynthetic active radiation and hence reduces weed growth in the agricultural fields.[113] The tear strength was 4 MPa and the tensile strength reached 38 MPa.[113] The tear strength increase resulted from slippage restriction and scissoring of the thermoplastic polyurethane chain, leading to longer tear paths.[113] Moreover, an increase in penetration resistance to 27.1 N versus only 21.4 N in pure polyurethane and a rise in matrix toughening effect and crack propagation was also achieved.[113] Nanobiochar filling also improves barrier properties. It led to a reduction in the water vapor transmission and oxygen transmission rates by increasing the diffusion's path length.[113] Nanobiochar-loaded thermoplastic polyurethane also exhibited a better thermal preservation effect than transparent mulch films, which can cause increases in soil temperature. . This is because nanobiochar-polyurethane mulch films can cause variation in the diurnal temperature of soil owing to its lesser light transmittance ability. This reduction in high soil temperature is highly beneficial for plant growth.[113]

5.3.5. Sensors. Nanobiochar has been successfully integrated into sensing technology.[123,161] The high specific surface area, oxygen-rich surface functional groups and ability to modify nanobiochar's high electrical conductivity makes it an excellent candidate for use in sensing technologies and electrochemical applications.[123] A few studies have used nanobiochar for the sensing and detection of heavy metals,[123] nitrites and sulfites,[248] nitrobenzene,[249] and microcystin.[161]

A microcystin sensor was developed using nanobiochar having a detection limit of 0.017 μg/L within 5 min, which had good reproducibility, specificity and storage stability.[161] Another study reported using sugar cane bagasse nanobiochar to prepare an electrochemical sensor for the ultrasensitive detection of Cd^{2+} and Pb^{2+}.[123] In situ electro-polymerization of L-cysteine was used to make an ion imprinted ball milled nanobiochar enhanced sensing signal electrode.[123] This sensor achieved a lower detection limit of 0.883 aM and 5.86 fM, respectively, and a linear range of 0.1 fM−1 μM, and 25 fM−1 μM, respectively, for Cd^{2+} and Pb^{2+}.[123] This electrode showed no interference from K^+, Na^+, Mg^{2+}, Fe^{3+}, Hg^{2+}, Cu^{2+}, Cl^-, and NO_3^- and organic compounds. Overall, the nanobiochar based electrochemical sensor was recycled at least seven times without reduction in sensing potential.[123] Ferlazzo et al. also developed a sensor using orange peel-derived nanobiochar for the detection of nitrites and sulfites, which showed recoveries in the range 94−102% in spiked mineral water.[248]

5.3.6. Targeted Drug Delivery. Nanomaterials have recently been extensively tested for use in drug delivery.[250] Since nanobiochar can adsorb a variety of pharmaceuticals, it can also be applied for drug delivery.[6,17,53,100,191] Multifunctional nanobiochar properties have attracted attention for use in targeted drug delivery.[251] Orange peel nanobiochar derived via hydrothermal carbonization (at 240 °C for 1 h) was tested to deliver a drug used in cancer treatment.[251] A prepared nanobiochar can be covalently conjugated with riboflavin, folic acid, hyaluronic acid, and biotin using coupling reactions at room temperature.[251] Nanobiochar's biocompatibility and ability for a human alveolar cancer cell line (A549 cells) to take up the nanobiochar was studied with the most common targeted ligands like biotin (B, vitamin B7), hyaluronic acid (HA), folic acid (FA, vitamin B9), and riboflavin (R, vitamin B2). In vitro biological tests revealed the ability of the conjugated A549 cells/nanobiochar system to internalize the DHF drug (5,5-dimethyl-6a-phenyl-3-(trimethylsilyl)-6,6a-dihydrofuro[3,2-*b*]furan-2(5H)-one) in A549 cells. Biotin functionalized nanobiochar carrying DHF causes increased cancer cell death (almost twice) compared to using DHF alone.[251] It is a better candidate than the pristine drug for cancer treatment.[251] Oxygen-containing functional groups present on nanobiochar surface exhibited improved water dispersion stability during drug delivery. This helps overcome the limitations of DHF which is the most used cancer drug.[248,251] This study paved the path for further research on new nanobiochar-based nano carriers for cancer therapy that will minimize the associated side effects and systemic toxicity associated with the conventional chemotherapy.[251]

5.3.7. Landfill Cover Additive. Compacted kaolin is used to construct hydraulic barriers in landfill covers because of its low permeability to gas and water.[30,252] This reduces landfill gas emissions and rainfall percolation.[30,252] However, kaolin develops cracks during desiccation because of its volume shrinkage.[253,254] Eventually, this results in increased gas and water permeability, which reduces landfill cover effectiveness.[254] To overcome this issue, lime, quartz, and fibers have been used as soil amendments, but on the other hand, they increase the hydraulic conductivity of soil.[254,255] Nanobiochar addition decreases gas and water permeability of kaolin by pore filling.[256,257] Nanobiochar amendment also increased the shrinkage limits of kaolin. Shrinkage limit is defined as the

https://doi.org/10.1021/acsomega.3c07804
ACS Omega 2024, 9, 12331−12379

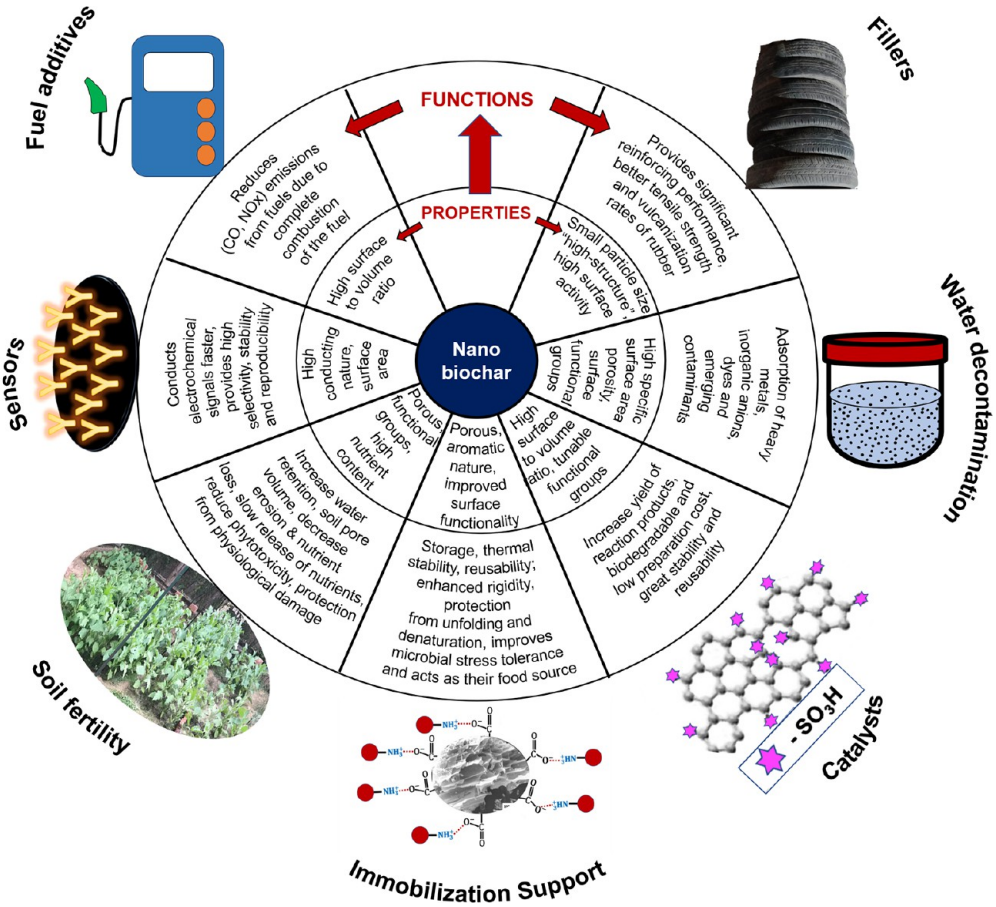

Figure 16. Diverse applications of nanobiochar: unveiling versatility and potential.

gravimetric water content below which the volume of soil remains constant as the water content decreases. In practical applications, the shrinkage limit is utilized to assess both the soil's potential for shrinkage and the formation of cracks. Adding nanobiochar, prepared from coconut shell biochar pyrolyzed at 600 °C (water vapor activated) at a 4% application rate, increases the shrinkage limit from 29.7 to 49.8%.[254] Total shrinkage volume of nanobiochar amended kaolin was nearly one-third larger versus pure kaolin, because nanobiochar addition fills pores, which decreases the macro pores.[254] This application will be helpful in landfill cover construction using kaolin or other fine-grained clay soils with lower shrinkage.[254]

5.3.8. Mixing with Cementitious Materials. Globally, the construction industry is one of the sectors where CO_2 pollution is a major issue. Energy-intensive cement production generates huge CO_2 emissions.[258,259] The cement industry accounts for roughly 8% of worldwide anthropogenic greenhouse gas emissions.[260] One ton of Portland cement can emit approximately one ton of CO_2 into the atmosphere.[259] Additionally, the cement sector is one of the biggest users of natural resources. Raw material extraction requires mining, processing, and transportation, all of which significantly contribute to the greenhouse gas production.[261] Carbon sequestration in cementitious materials might compensate for some emissions. Using biochar as an admixture in cementitious materials could sequester significant amounts of carbon in civil infrastructure given the fast growth throughout the world of new cities.[258]

Building materials including asphalt mixture,[262,263] red clay binder,[264] natural inorganic clay composites,[265] and geopolymers[266,267] have all been created which include biochar.[268] Per ton of dry feedstock, biochar can reduce greenhouse gas emissions by 870 kg of CO_2-equivalents.[269] Growing interest has been shown in nanoscale biochar as an admixture in cement composites.[270,271]

In one study, apricot kernel shell was pyrolyzed at 500 °C at a heating rate of 10 °C/min under N_2 flow (50 mL/min) for 1 h.[270] The obtained biochar was ground to the nanoscale (<500 nm) before mixing into mortar to enhance surface-active sites and surface area by performing ball-milling (Fritsch Premium Line Pulverisette 7). Mortar was mixed with nanoscale biochar at various volume percentages (0.0, 0.04, 0.06, 0.08, 0.12, and 0.15%).[270] In the case of a composite blend comprising 0.04% nanoscale biochar by volume, both flexural and compressive strengths increase by 5% and 15%, respectively, versus the standard mortar. Furthermore, the fracture energies for flexure and compression exhibited remarkable enhancement, soaring by 98% and 38%, respectively, versus reference mortar.[270] Nanoscale biochar within the mortar composite plays several pivotal roles, including crack bridging and redirection, which leads to greater participation of volume in the fracture process. The porous structure of the nanoscale biochars serves as a hydration nucleation site, and develops internal curing, which increases strength and fracture energy.[270] However, at high volume percentages (0.15%), the aggregation and inadequate dispersion of nanoscale biochar can give rise to weak zones, consequently diminishing the overall strength.[270] Nanoscale biochar can be a promising additive for carbon sequestration as well as enhancing the mechanical properties of cement composites.[270]

https://doi.org/10.1021/acsomega.3c07804
ACS Omega 2024, 9, 12331−12379

Table 7. Comparative Remediation Performance of Nanobiochar versus Its Bulk Counterpart[a]

Adsorbate	Feedstock (Pyrolysis temperature; °C)	Particle size		Surface area (m^2/g)		Adsorption capacity (mg/g)		Adsorption capacity per surface area (mg/m^2)	
		Nanobiochar (nm)	Precursor biochar (μm)	Nanobiochar	Precursor (bulk) biochar	Nanobiochar	Precursor (bulk) biochar	Nanobiochar	Precursor (bulk) biochar
Methylene blue[102]	Sugar cane bagasse (300)	242	500−1000	10.8	NA	169[b]	9.9[b]	15.6	NA
	Sugar cane bagasse (450)	170	500−1000	331	51	298[b]	14.5[b]	0.9	0.28
	Sugar cane bagasse (600)	140	500−1000	364	359	268[b]	12.2[b]	0.74	0.03
	Bamboo (300)	250	500−1000	8.3	2	202[b]	9.2[b]	24.3	4.6
	Bamboo (450)	165	500−1000	299	4.7	246[b]	13.2[b]	0.82	2.8
	Bamboo (600)	140	500−1000	276	59	225[b]	6.9[b]	0.82	0.12
	Hickory wood (300)	333	500−1000	5.6	0.8	114[b]	7.9[b]	20.4	9.9
	Hickory wood (450)	158	500−1000	309	9.8	253[b]	6.6[b]	0.82	0.67
	Hickory wood (600)	133	500−1000	270	222	234[b]	14.1[b]	0.87	0.063
Sulfamethoxazole[191]	Hickory chips (450)	NA	NA	309	9.8	100.3[c]	NA[c]	NA	NA
Sulfapyridine[191]	Bamboo (450)	NA	NA	299	4.7	57.9[c]	NA[c]	0.19	NA
Tetracycline[6]	Wheat straw (700)	57−200	1.33−5.26	296.3	198.6	268.3[c]	NA[c]	0.91	NA
17β-estradiol[192]	Bagasse (800)	245.4	3.6	321.7	22.2	8.94[b]	7.8[b]	0.03	0.35
Phthalate esters[75]	Corn straw (500)	100−600	10−60	364	185	33.87[c]	12.68[c]	0.09	0.06
	Rice husk (500)	100−600	10−60	298	96	27.65[c]	11.93[c]	0.09	0.12
Lead[105]	Wheat straw (600)	1300	14.7	130	0.41	119.5[b]	134.7[b]	0.92	328.5
Lead[103]	Cow bone (300)	100−2500	1−20	35.5	2.7	339.3[c]	209.5[c]	9.6	75.9
	Cow bone (450)	100−2500	1−20	199.5	22.9	428.8[c]	301.8[c]	2.1	13.2
	Cow bone (600)	100−1000	1−20	313.1	52.8	558.9[c]	389.5[c]	1.8	7.4
Copper[103]	Cow bone (300)	100−2500	1−20	35.5	2.7	159.3[c]	86.3[c]	4.5	31.3
	Cow bone (450)	100−2500	1−20	199.5	22.9	184.3[c]	120.6[c]	0.92	5.3
	Cow bone (600)	100−1000	1−20	313.1	52.8	217.6[c]	163.8[c]	0.69	3.1
Cadmium[103]	Cow bone (300)	100−2500	1−20	35.5	2.7	66.3[c]	31.1[c]	1.87	11.3
	Cow bone (450)	100−2500	1−20	199.5	22.9	122[c]	44.6[c]	0.61	1.95
	Cow bone (600)	100−1000	1−20	313.1	52.8	165.7[c]	75.1[c]	0.53	1.4
Mercury[6]	Wheat straw (700)	57−200	1.33−5.26	296.3	198.6	127.4[c]	NA[c]	0.43	NA
Antibiotic resistance genes: Extracellular DNA (eDNA) adsorption[68]	Rice straw (400)	403	50−250	93.2	141.2	278.4[c]	1.7[c]	2.99	0.01
	Rice straw (700)	234	50−250	253.9	155.3	295.8[c]	2.6[c]	1.17	0.02

[a]NA = not available. [b]Experimental adsorption capacity (mg/g). [c]Langmuir adsorption capacity (mg/g).

Biochar nanoparticles derived from softwood biochar pyrolyzed at 700 °C (from the UK Biochar Centre) have also been evaluated for possible cement composites.[271] Mortars were prepared using ordinary portland cement, superplasticizer, deionized water, and biochar nanoparticles. Softwood biochar nanoparticles were incorporated into the cementitious composites at 0.8% and 1% by weight of cement.[271] Samples with biochar nanoparticles exhibited 20% higher flexural strength compared to the control.[271] Furthermore, no significant difference was observed between 0.8% and 1% of added biochar nanoparticles. Three-point bending (TPB) test, studies of fracture energy in the experimental specimens revealed a slight increase when biochar nanoparticles were introduced into the cement paste, both at 7 and 28 days.[271] Load-CMOD (crack mouth opening displacement) curve graphs revealed that the incorporation of biochar nanoparticles into the cement-based composites resulted in improved mechanical performance in terms of both toughness and flexural strength.[271] Feedstock type, heating rate, pyrolysis temperature, and pressure are important to determine the potential of biochar nanoparticles as

https://doi.org/10.1021/acsomega.3c07804
ACS Omega 2024, 9, 12331−12379

a construction material for carbon capture and sequestration.[270,271]

Apart from its potential use as an adsorbent, nanobiochar can also be used as a filler, sensor, capacitor, electrode, fuel additive, admixture in cement, soil conditioner, immobilization supporter, and catalyst. The diverse application possibilities of nanobiochar are illustrated in Figure 16.

6. ADVANTAGES OF NANOBIOCHAR OVER PRISTINE BIOCHAR

Similar to its bulk counterpart, the nanobiochar proved to be a suitable candidate for carbon sequestration, agriculture, and environmental remediation.[39] Further, nanobiochar's diverse applications can also be extended to catalysts, sensors, the battery industry, biomolecule carriers, fillers, additives, and electrode materials, as discussed at length in the previous sections.[17,39] Biochar and nanobiochar possess similar properties and applications since they are derived from the same feedstock. However, developing nanobiochar over pristine biochar can introduce enhanced properties and application advantages (Table 7). Basically, nanobiochar offers enhancements in surface area, porosity, pore volume, surface functional groups, and surface-active sites per unit weight (Table 7). This, of course, comes at the expense of the size reduction step. Nanobiochars have provided enhancements in contaminant removal capacity versus to their corresponding bulk biochars (Table 7). A few comparative studies between bulk and nanobiochar are highlighted in this section.

Nanobiochar has been reported as a better contaminant adsorbent than "regular" biochar from same source and pyrolytic origin, with particle size and surface area often influencing adsorption.[75,78,192] Carbamazepine, a recalcitrant pharmaceutical, was removed (95%) by pinewood nanobiochar prepared at 525 °C.[57] Using methylene blue as a model contaminant, ball-milled sugar cane bagasse nanobiochar gave higher partition coefficient values compared to its corresponding pristine biochar prepared at 450 °C.[102] The Langmuir adsorption capacity increased from 17.2 for the pristine case to 354 mg/g for the nanobiochar.[102] In another case, the removal of ammonium from water was more efficient with ball milled bamboo biochar, which had a three-times higher Langmuir maximum adsorption capacity (22.9 mg/g) than its pristine counterpart (7 mg/g).[92] A comparative study was reported of three different biochar particle sizes (200−600 μm, 10−60 μm and 0.1−0.6 μm) on the adsorption of phthalate esters.[75] Pore filling dominated uptake, which favored adsorption in nanosized biochar. The Langmuir adsorption capacity increased from 12.68 to 33.87 mg/g going from the largest to the smallest particle size.[75] Fluoride was removed using rice husk biochar versus its nanoscale counterpart. Nanobiochar achieved 59.4% removal versus 27% by the bulk biochar within 10 min.[272] Nanobiochar produced from tea waste removed more cadmium and chromium at 99.7 and 98.2%, respectively, compared to 85.8 and 88.4% for their corresponding bulk biochar.[273]

Another very interesting study pointed out how nanobiochar inhibited DNA replication of antibiotic resistance genes.[68] The abundance of persistent free radicals in nanobiochar induced fragmentation of extracellular DNA.[68] In a plant growth experiment, rice was grown in Cd(II) polluted soil.[153] Nanobiochar application helped to reduce the heavy metal uptake in the rice plant due to its high affinity for Cd(II). Nanobiochar was able to attach to the roots, forming a protective barrier that protected them from the intake of Cd(II).[153]

7. NANOBIOCHAR CIRCULAR ECONOMY AND SUSTAINABILITY

Growing environmental challenges are driving research and innovative applications toward a more sustainable future.[274,275] Climate changes require swift strides toward transitioning to a carbon-neutral or carbon-negative future, alleviating the environmental strain induced by human activities.[42,276] In this scenario, the circular economy approach is gaining increasing momentum by bolstering the economy, building dual use paths for existing materials, encouraging biomass feedstock replacement of fossil fuels, while also safeguarding the environment.[274,276] By employing circular economy principles,, it is possible to diminish pollution and waste through effective recycling and optimized utilization. Then by using renewable resources to replace nonrenewable starting materials additional gains toward carbon neutrality can be made.[42,275,276] The manufacturing of nanobiochar derived from waste biomass and its subsequent use in multiple applications has emerged as another method to apply within the realm of the circular economy.[42,276] Potential nanobiochar applicability extends across fields such as water pollution remediation, agriculture, rubber filler, cement additives, and targeted drug delivery in a sustainable manner due to its heightened efficiency when compared to pristine biochar.[42,93,276] It can be viewed as one subsection of broader contribution that the sum of all biochar uses can contribute.[3] Increasing nanobiochar use holds promise for boosting the economic potential of biomass pyrolysis where its advantages over pristine biochar are sufficient. These applications might contribute to the carbon neutral economy.[42,276] Nanobiochar use to eliminate harmful contaminants from water could help conserve precious water resources if its cost and operational practicality can be improved.[40] Similar considerations apply to nanobiochar in agriculture where it could serve side by side with pristine biochar as a pragmatic circular economy strategy addressing the challenges posed by climate change.[44] Using nanobiochar to augment and lower chemical fertilizer use has the potential to enhance crop productivity and growth. It can function as a further extension of larger biochar particle sizes to change pH, promote microbial changes, release fertilizers more slowly, all of which might reduce nutrient loss through leaching.[142,142] Enhancing crop productivity, alleviating soil pollution and reducing CO_2 and NO emissions all fit circular economy goals.[44] Converting waste biomass into nanobiochar and using it as a solid fuel additive to liquid fuels could allow plant carbon to be burned in liquid fossil-derived fuels to lower their net CO_2 foot print.[244] Hence, nanobiochar could assist in fostering the circular economy and attaining sustainability.

8. NANOBIOCHAR'S ROLE IN PROMOTING SUSTAINABLE DEVELOPMENT GOALS (SDGS)

The Sustainable Development Goals (SDGs), a set of 17 interlinked objectives established by the United Nations, are designed to tackle a spectrum of global challenges encompassing poverty, inequality, environmental degradation, climate change, peace, and justice.[277] Achieving sustainable development highlights the importance of preserving natural resources, producing energy more efficiently, providing access to clean water and sanitation facilities, and reducing greenhouse gas

https://doi.org/10.1021/acsomega.3c07804
ACS Omega 2024, 9, 12331−12379

emissions.[277] Nanobiochar generation from biomass fits several objectives of SDGs.[276] For instance, **SDG 1** seeks to eliminate poverty. Nanobiochar fits this objective as a waste biomass product applied as a soil amendments to improve farm economies.[276] Likewise, the zero hunger objective of **SDG 2** may be achieved through the nanobiochar use as a soil amendment slow-release fertilizer to enhance crop productivity to meet the food demands of a growing population.[142,278] Utilizing nanobiochar in addressing soil and water pollution, as well as facilitating targeted drug delivery, would contribute to achieving good health and well-being, aligning with **SDG 3** objective.[40,251,276] Nanobiochar has potential to contribute to achieving **SDG 6**, focusing on clean water and sanitation.[40,93] Adding nanobiochar to fuels improves fuel combustion efficiency while decreasing NOx, CO and unburned hydrocarbon emissions which corresponds to the aiding in **SDG 7** objectives (ensuring access to affordable and clean energy).[244] Incorporating nanobiochar into cementitious materials not only aids in carbon sequestration but also enhances the mechanical properties of cement composites. This innovative approach contributes to achieving **SDG 11**, promoting sustainable cities and communities.[279] Producing nanobiochar from waste biomass and using it across many applications, corresponds to **SDG 12**-responsible consumption and production. Nanobiochar sequesters carbon and reduces greenhouse gas emissions, which are consistent with addressing climate action (**SDG 13**).[142,276,280]

9. ECONOMIC FEASIBILITY

The economic feasibility of nanobiochar application is understood in terms of production and application costs. No robust nanobiochar techno-economic analysis is available. There are no available data on commercial production. A recent review conducted a tentative techno-economic nanobiochar analysis based on the preparation method and estimated per kg values of nanobiochar production ranging from $8.2 to 103 for ball milling, $6.6−22 for carbonization, $34−438 for centrifugation, and $2.3−434 for sonication.[38] While these estimates did not include solvent cost and raw material cost fluctuations, they are lower than the market value of activated charcoal and graphene oxide.[38] Nanobiochar when compared to biochar for use as a sensor, is valued 18-times higher, given that the price was estimated at 1.29 £/kg which is 1% that of the cost of carbon dot-based sensors.[281] In comparison to activated carbon, silica gel, zeolite, and carbon-based nanofibers, nanobiochar like biochar appears cost-effective and carbon neutral.[39] The use of nanobiochar as a fuel additive reportedly cuts down costs incurred by damage from the release of toxic fumes, NOx, and hydrocarbons emission.[244]

Reducing particles to the nanoscale opens multiple avenues for upgrading the surface functionality and overcoming limitations of conventional adsorbents and even macro-biochar. However, nanobiochar yield research is still in its infancy. Ball-milling technique, an energy intensive process is identified to give the highest yield. This presents a major challenge in product commercialization.[17,38] Hydrothermal synthesis is another nanoscale biochar particle production method shown to produce a sizable yield (8.6−10.1%) compared to sonication (0.47−15.3%), and a combination of grinding, sonication, and centrifugation (2.16−3.19%).[69] To date, process optimization, feedstock selection, and heterogeneity of product remain factors impeding its feasibility.[74]

10. POTENTIAL TOXICITY OF NANOBIOCHAR APPLICATIONS

Nanobiochars behave differently in the environment than their macro counterparts with regards to the retention, distribution, and bioavailability of certain nutrients and/or contaminants.[64] The size conformity of nanobiochar with carbonaceous nanomaterials suggests that similar risks can be expected.[38] Sporadic documentation of the toxicity of biochar nanoparticles is found on mammalian cells,[95] algal growth,[282] and seed germination.[153,160]

The dispersibility of nanobiochar in air is significantly higher than its bulk counterpart, which has been a suggested area of concern.[42] Large-scale applications to farm fields could cause dust clouds with conventional application machinery. Gao and colleagues studied the implications of grinding biochar, which gave useful insights on the aerodynamic properties of biochar.[283] The travel distance and settling time were inversely proportional to its particle size. Given the potential toxicity associated with biochar, the concerns arising with increased mobility cannot be ignored.[283] An in vitro study on human lung epithelial cells revealed that tobacco stem-derived nano biochar elicits inflammatory and oxidative stress in pulmonary cells in higher concentrations of 100 μg/mL.[95] The study, however, asserted that, unless exposure is chronic, nanobiochar is relatively safe.

Biochar at the nanoscale passes through granular media seamlessly, meaning that the sorbed contaminants would be transported deeper into sediments.[118] The propensity of nanobiochar to contain contaminants with its large surface area will have far reaching consequences for a diverse group of organisms.[42] The free radical content reported in nanobiochar could also pose certain risks to microorganisms.[282] It reportedly inhibited the growth of algae by inducing oxidative stress and limiting the available nutrients for growth.[282] Biochar nanoparticles were shown to enhance the antioxidative enzymes in rice plants, indicating oxidative stress.[153] It is integral for nanobiochar use that PAH profiling and trace metal assessments must be made in line with International Biochar Initiative (IBI) and European Biochar Certificate (EBC) standards, given the growing utility of nanobiochar in the market.

11. CONCLUSIONS AND PROSPECTS

Nanobiochar, the tiny particle size version of pristine biochar, has shown promising results in a variety of areas, such as water pollution remediation, soil health promoter, plant growth enhancer, slow-release fertilizer, sensors, catalysts, fuel additives and fillers and/or additives for polymers, rubber, and landfill covers. Feedstocks (i.e., rice husk, wheat straw, bagasse, okra stem, etc.) were used to prepare nanobiochars. Among the different available synthetic methods, ball milling was the first choice for researchers, followed by sonication, centrifugation, and conventional carbonization. Nanobiochar demonstrates different characteristics than macro-biochar; the most common examples are enlarged surface areas, pore volumes, pore sizes, and zeta potentials.

Nanobiochar, as an emerging field, is witnessing growing attention among researchers. Nevertheless, a few areas urgently need to be addressed, including (a) the large-scale production yield of nanobiochar is a concern, (b) optimization of nanobiochar preparation processes, (c) lack of data for toxic/negative impacts of nanobiochar applications, and (d) nanobiochar applications must be evaluated through integrated economic and life cycle assessment.

https://doi.org/10.1021/acsomega.3c07804
ACS Omega 2024, 9, 12331−12379

AUTHOR INFORMATION

Corresponding Author

Dinesh Mohan − *School of Environmental Sciences, Jawaharlal Nehru University, New Delhi 110067, India;* orcid.org/0000-0002-3251-2946; Phone: 0091-11-26704616; Email: dm_1967@hotmail.com; Fax: 0091-11-26704616

Authors

Abhishek Kumar Chaubey − *School of Environmental Sciences, Jawaharlal Nehru University, New Delhi 110067, India;* orcid.org/0000-0001-8265-3125

Tej Pratap − *School of Environmental Sciences, Jawaharlal Nehru University, New Delhi 110067, India*

Brahmacharimayum Preetiva − *School of Environmental Sciences, Jawaharlal Nehru University, New Delhi 110067, India*

Manvendra Patel − *School of Environmental Sciences, Jawaharlal Nehru University, New Delhi 110067, India;* orcid.org/0000-0002-5801-5526

Jonathan S. Singsit − *School of Environmental Sciences, Jawaharlal Nehru University, New Delhi 110067, India*

Charles U. Pittman, Jr. − *Department of Chemistry, Mississippi State University, Mississippi State, Mississippi 39762, United States*

Complete contact information is available at: https://pubs.acs.org/10.1021/acsomega.3c07804

Notes

The authors declare no competing financial interest.

ACKNOWLEDGMENTS

DM is thankful to PSA, GOI for financial assistance under the project "Delhi Cluster-Delhi Research Implementation and Innovation" (DRIIV).

REFERENCES

(1) Ahmad, M.; Rajapaksha, A. U.; Lim, J. E.; Zhang, M.; Bolan, N.; Mohan, D.; Vithanage, M.; Lee, S. S.; Ok, Y. S. Biochar as a sorbent for contaminant management in soil and water: A review. *Chemosphere* **2014**, *99*, 19−33.

(2) Mohan, D.; Abhishek, K.; Sarswat, A.; Patel, M.; Singh, P.; Pittman, C. U., Jr Biochar production and applications in soil fertility and carbon sequestration - a sustainable solution to crop-residue burning in India. *RSC Adv.* **2018**, *8* (1), 508−520.

(3) Mohan, D.; Pittman, C. U. Jr.; Mlsna, T. E. *Sustainable Biochar for Water and Wastewater Treatment*; Elsevier Science, 2022.

(4) Patel, M.; Chaubey, A. K.; Navarathna, C.; Mlsna, T. E.; Pittman, C. U.; Mohan, D. Chapter 11 - Sorptive removal of pharmaceuticals using sustainable biochars. In *Sustainable Biochar for Water and Wastewater Treatment*; Mohan, D., Pittman, C. U. Jr.; Mlsna, T. E., Eds.; Elsevier, 2022; pp 395−427.

(5) Patel, M.; Chaubey, A. K.; Pittman, C. U., Jr; Mohan, D. Aqueous ibuprofen sorption by using activated walnut shell biochar: process optimization and cost estimation. *Environmental Science: Advances* **2022**, *1* (4), 530−545.

(6) Li, R.; Zhang, Y.; Deng, H.; Zhang, Z.; Wang, J. J.; Shaheen, S. M.; Xiao, R.; Rinklebe, J.; Xi, B.; He, X.; et al. Removing tetracycline and Hg(II) with ball-milled magnetic nanobiochar and its potential on polluted irrigation water reclamation. *J. Hazard. Mater.* **2020**, *384*, 121095.

(7) Xiang, W.; Zhang, X.; Chen, K.; Fang, J.; He, F.; Hu, X.; Tsang, D. C.W.; Ok, Y. S.; Gao, B. Enhanced adsorption performance and governing mechanisms of ball-milled biochar for the removal of volatile organic compounds (VOCs). *Chem. Eng. J.* **2020**, *385*, 123842.

(8) Wang, J.; Wang, S. Preparation, modification and environmental application of biochar: A review. *Journal of Cleaner Production* **2019**, *227*, 1002−1022.

(9) Mohan, D.; Sarswat, A.; Ok, Y. S.; Pittman, C. U., Jr Organic and inorganic contaminants removal from water with biochar, a renewable, low cost and sustainable adsorbent - A critical review. *Bioresour. Technol.* **2014**, *160*, 191−202.

(10) *IBI, Standardized product definition and product testing guidelines for biochar that is used in soil*; International Biochar Initiative, 2015; Vol. *23*.

(11) Van Nguyen, T. T.; Phan, A. N.; Nguyen, T.-A.; Nguyen, T. K.; Nguyen, S. T.; Pugazhendhi, A.; Ky Phuong, H. H. Valorization of agriculture waste biomass as biochar: As first-rate biosorbent for remediation of contaminated soil. *Chemosphere* **2022**, *307*, 135834.

(12) Huang, Q.; Song, S.; Chen, Z.; Hu, B.; Chen, J.; Wang, X. Biochar-based materials and their applications in removal of organic contaminants from wastewater: state-of-the-art review. *Biochar* **2019**, *1* (1), 45−73.

(13) Xiang, W.; Zhang, X.; Chen, K.; Fang, J.; He, F.; Hu, X.; Tsang, D. C. W.; Ok, Y. S.; Gao, B. Enhanced adsorption performance and governing mechanisms of ball-milled biochar for the removal of volatile organic compounds (VOCs). *Chem. Eng. J.* **2020**, *385*, 123842.

(14) Xiang, W.; Wan, Y.; Zhang, X.; Tan, Z.; Xia, T.; Zheng, Y.; Gao, B. Adsorption of tetracycline hydrochloride onto ball-milled biochar: Governing factors and mechanisms. *Chemosphere* **2020**, *255*, 127057.

(15) Li, N.; He, M.; Lu, X.; Yan, B.; Duan, X.; Chen, G.; Wang, S.; Hou, L. a. Municipal solid waste derived biochars for wastewater treatment: Production, properties and applications. *Resources, Conservation and Recycling* **2022**, *177*, 106003.

(16) Wei, X.; Wang, X.; Gao, B.; Zou, W.; Dong, L. Facile Ball-Milling Synthesis of CuO/Biochar Nanocomposites for Efficient Removal of Reactive Red 120. *ACS Omega* **2020**, *5* (11), 5748−5755.

(17) Ramanayaka, S.; Vithanage, M.; Alessi, D. S.; Liu, W.-J.; Jayasundera, A. C. A.; Ok, Y. S. Nanobiochar: production, properties, and multifunctional applications. *Environmental Science: Nano* **2020**, *7* (11), 3279−3302.

(18) Zhou, B.; Chen, X.; Henry, L. The Effect of nano-biochar on soil, water, and nutrient loss of a sloping land with different vegetation covers on Loess plateau of China. *Appl. Ecol. Envirn. Res.* **2020**, *18*, 2845−2861.

(19) Lehmann, J.; Gaunt, J.; Rondon, M. Bio-char Sequestration in Terrestrial Ecosystems - A Review. *Mitigation and Adaptation Strategies for Global Change* **2006**, *11* (2), 403−427.

(20) Lehmann, J.; Rillig, M. C.; Thies, J.; Masiello, C. A.; Hockaday, W. C.; Crowley, D. Biochar effects on soil biota - A review. *Soil Biol. Biochem.* **2011**, *43* (9), 1812−1836.

(21) Preetiva, B.; Chaubey, A. K.; Singsit, J. S. Chapter 9 - Biochar-mediated nutrients and microbial community dynamics in montane landscapes. In *Understanding Soils of Mountainous Landscapes*; Bhadouria, R., Singh, S., Tripathi, S., Singh, P., Eds.; Elsevier, 2023; pp 165−181.

(22) Mohan, D.; Preetiva, B.; Chaubey, A. K.; Singsit, J. S.; Mina, U.; Pittman, C. U., Jr Eggplant growth in wheat straw-, wheat straw biochar- and compost-amended soils: a field study of CO_2 emission dynamics, soil physicochemical, microbial, and nutrient effects. *Waste Management Bulletin* **2024**, *1* (4), 143−157.

(23) Bartoli, M.; Giorcelli, M.; Jagdale, P.; Rovere, M.; Tagliaferro, A. A review of non-soil biochar applications. *Materials* **2020**, *13* (2), 261.

(24) Bolan, N.; Hoang, S. A.; Beiyuan, J.; Gupta, S.; Hou, D.; Karakoti, A.; Joseph, S.; Jung, S.; Kim, K.-H.; Kirkham, M. B.; et al. Multifunctional applications of biochar beyond carbon storage. *Int. Mater. Rev.* **2022**, *67* (2), 150−200.

(25) Zhang, Y.; He, M.; Wang, L.; Yan, J.; Ma, B.; Zhu, X.; Ok, Y. S.; Mechtcherine, V.; Tsang, D. C. W. Biochar as construction materials for achieving carbon neutrality. *Biochar* **2022**, *4* (1), 59.

(26) Qin, C.; Wang, H.; Yuan, X.; Xiong, T.; Zhang, J.; Zhang, J. Understanding structure-performance correlation of biochar materials in environmental remediation and electrochemical devices. *Chem. Eng. J.* **2020**, *382*, 122977.

(27) Lehmann, J.; Cowie, A.; Masiello, C. A.; Kammann, C.; Woolf, D.; Amonette, J. E.; Cayuela, M. L.; Camps-Arbestain, M.; Whitman, T. Biochar in climate change mitigation. *Nature Geoscience* **2021**, *14* (12), 883−892.
(28) Li, R.; Deng, H.; Zhang, X.; Wang, J. J.; Awasthi, M. K.; Wang, Q.; Xiao, R.; Zhou, B.; Du, J.; Zhang, Z. High-efficiency removal of Pb(II) and humate by a CeO_2-MoS_2 hybrid magnetic biochar. *Bioresour. Technol.* **2019**, *273*, 335−340.
(29) Tan, X.-f.; Liu, Y.-g.; Gu, Y.-l.; Xu, Y.; Zeng, G.-m.; Hu, X.-j.; Liu, S.-b.; Wang, X.; Liu, S.-m.; Li, J. Biochar-based nano-composites for the decontamination of wastewater: A review. *Bioresour. Technol.* **2016**, *212*, 318−333.
(30) Liu, M.; Almatrafi, E.; Zhang, Y.; Xu, P.; Song, B.; Zhou, C.; Zeng, G.; Zhu, Y. A critical review of biochar-based materials for the remediation of heavy metal contaminated environment: Applications and practical evaluations. *Sci. Total Environ.* **2022**, *806*, 150531.
(31) Ling, L.-L.; Liu, W.-J.; Zhang, S.; Jiang, H. Magnesium Oxide Embedded Nitrogen Self-Doped Biochar Composites: Fast and High-Efficiency Adsorption of Heavy Metals in an Aqueous Solution. *Environ. Sci. Technol.* **2017**, *51* (17), 10081−10089.
(32) Kim, Y.; Oh, J.-I.; Vithanage, M.; Park, Y.-K.; Lee, J.; Kwon, E. E. Modification of biochar properties using CO_2. *Chem. Eng. J.* **2019**, *372*, 383−389.
(33) Karunanayake, A. G.; Todd, O. A.; Crowley, M.; Ricchetti, L.; Pittman, C. U., Jr; Anderson, R.; Mohan, D.; Mlsna, T. Lead and cadmium remediation using magnetized and nonmagnetized biochar from Douglas fir. *Chem. Eng. J.* **2018**, *331*, 480−491.
(34) Cui, J.; Jin, Q.; Li, Y.; Li, F. Oxidation and removal of As(III) from soil using novel magnetic nanocomposite derived from biomass waste. *Environmental Science: Nano* **2019**, *6* (2), 478−488.
(35) Chaubey, A. K.; Patel, M.; Mohan, D. *Synthesis of engineered biochar for aqueous pharmaceutical removal*; European Geosciences Union General Assembly 2021, online, 19−30 Apr 2021, EGU21-9358, https://doi.org/10.5194/egusphere-egu21-9358, 2021.
(36) Singh, A. K.; Chaubey, A. K.; Kaur, I. Remediation of water contaminated with antibiotics using biochar modified with layered double hydroxide: Preparation and performance. *Journal of Hazardous Materials Advances* **2023**, *10*, 100286.
(37) Chaubey, A. K.; Patel, M.; Pittman, C. U., Jr; Mohan, D. Acetaminophen and trimethoprim batch and fixed-bed sorption on MgO/Al_2O_3-modified rice husk biochar. *Colloids Surf., A* **2023**, *677*, 132263.
(38) Anupama; Khare, P. A comprehensive evaluation of inherent properties and applications of nano-biochar prepared from different methods and feedstocks. *Journal of Cleaner Production* **2021**, *320*, 128759.
(39) Chausali, N.; Saxena, J.; Prasad, R. Nanobiochar and biochar based nanocomposites: Advances and applications. *Journal of Agriculture and Food Research* **2021**, *5*, 100191.
(40) Pratap, T.; Chaubey, A. K.; Patel, M.; Mlsna, T. E.; Pittman, C. U., Jr.; Mohan, D. 20 - Nanobiochar for aqueous contaminant removal. In *Sustainable Biochar for Water and Wastewater Treatment*; Mohan, D., Pittman, C. U., Jr., Mlsna, T. E., Eds.; Elsevier, 2022; pp 667−704.
(41) Liu, G.; Zheng, H.; Jiang, Z.; Zhao, J.; Wang, Z.; Pan, B.; Xing, B. Formation and physicochemical characteristics of nano biochar: insight into chemical and colloidal Stability. *Environ. Sci. Technol.* **2018**, *52* (18), 10369−10379.
(42) Song, B.; Cao, X.; Gao, W.; Aziz, S.; Gao, S.; Lam, C.-H.; Lin, R. Preparation of nano-biochar from conventional biorefineries for high-value applications. *Renewable and Sustainable Energy Reviews* **2022**, *157*, 112057.
(43) Jiang, M.; He, L.; Niazi, N. K.; Wang, H.; Gustave, W.; Vithanage, M.; Geng, K.; Shang, H.; Zhang, X.; Wang, Z. Nanobiochar for the remediation of contaminated soil and water: challenges and opportunities. *Biochar* **2023**, *5* (1), 2.
(44) Rajput, V. D.; Minkina, T.; Ahmed, B.; Singh, V. K.; Mandzhieva, S.; Sushkova, S.; Bauer, T.; Verma, K. K.; Shan, S.; van Hullebusch, E. D.; et al. Nano-biochar: A novel solution for sustainable agriculture and environmental remediation. *Environ. Res.* **2022**, *210*, 112891.
(45) Goswami, L.; Kushwaha, A.; Singh, A.; Saha, P.; Choi, Y.; Maharana, M.; Patil, S. V.; Kim, B. S. Nano-biochar as a sustainable catalyst for anaerobic digestion: A synergetic closed-loop approach. *Catalysts* **2022**, *12* (2), 186.
(46) Goswami, S.; Kushwaha, A.; Goswami, L.; Gupta, N. R.; Kumar, V.; Bhan, U.; Reddy, B. S.; Tripathi, K. M. Chapter 7 - Nanobiochar—a green catalyst for wastewater remediation. In *Bio-Based Nanomaterials*; Mishra, A. K., Hussain, C. M., Eds.; Elsevier, 2022; pp 109−132.
(47) Wu, P.; Wang, Z.; Bolan, N. S.; Wang, H.; Wang, Y.; Chen, W. Visualizing the development trend and research frontiers of biochar in 2020: a scientometric perspective. *Biochar* **2021**, *3* (4), 419−436.
(48) Mohan, D.; Pittman, C. U., Jr; Bricka, M.; Smith, F.; Yancey, B.; Mohammad, J.; Steele, P. H.; Alexandre-Franco, M. F.; Gómez-Serrano, V.; et al. Sorption of arsenic, cadmium, and lead by chars produced from fast pyrolysis of wood and bark during bio-oil production. *J. Colloid Interface Sci.* **2007**, *310* (1), 57−73.
(49) Wang, D.; Zhang, W.; Zhou, D. Antagonistic effects of humic acid and iron oxyhydroxide grain-coating on biochar nanoparticle transport in saturated sand. *Environ. Sci. Technol.* **2013**, *47* (10), 5154−5161.
(50) van Eck, N.; Waltman, L. Software survey: VOSviewer, a computer program for bibliometric mapping. *Scientometrics* **2010**, *84* (2), 523−538.
(51) Aria, M.; Cuccurullo, C. bibliometrix: An R-tool for comprehensive science mapping analysis. *Journal of Informetrics* **2017**, *11* (4), 959−975.
(52) Sahu, M. K. Bibliographic coupling and co-citation networking analysis determining research contributions of business school between 1965-June, 2020: With special reference to Indian Institute of Management, India. *Library Philosophy and Practice* **2021**, 1−14.
(53) Naghdi, M.; Taheran, M.; Brar, S. K.; Kermanshahi-pour, A.; Verma, M.; Surampalli, R. Y. Immobilized laccase on oxygen functionalized nanobiochars through mineral acids treatment for removal of carbamazepine. *Sci. Total Environ.* **2017**, *584*−*585*, 393−401.
(54) Naghdi, M.; Taheran, M.; Brar, S. K.; Rouissi, T.; Verma, M.; Surampalli, R. Y.; Valero, J. R. A green method for production of nanobiochar by ball milling- optimization and characterization. *Journal of Cleaner Production* **2017**, *164*, 1394−1405.
(55) Naghdi, M.; Taheran, M.; Brar, S. K.; Kermanshahi-pour, A.; Verma, M.; Surampalli, R. Y. Pinewood nanobiochar: A unique carrier for the immobilization of crude laccase by covalent bonding. *Int. J. Biol. Macromol.* **2018**, *115*, 563−571.
(56) Naghdi, M.; Taheran, M.; Brar, S. K.; Kermanshahi-pour, A.; Verma, M.; Surampalli, R. Y. Fabrication of nanobiocatalyst using encapsulated laccase onto chitosan-nanobiochar composite. *Int. J. Biol. Macromol.* **2019**, *124*, 530−536.
(57) Naghdi, M.; Taheran, M.; Pulicharla, R.; Rouissi, T.; Brar, S. K.; Verma, M.; Surampalli, R. Y. Pine-wood derived nanobiochar for removal of carbamazepine from aqueous media: Adsorption behavior and influential parameters. *Arabian Journal of Chemistry* **2019**, *12* (8), 5292−5301.
(58) Nath, B. K.; Chaliha, C.; Kalita, E. Iron oxide permeated mesoporous rice-husk nanobiochar (IPMN) mediated removal of dissolved arsenic (As): chemometric modelling and adsorption dynamics. *Journal of Environmental Management* **2019**, *246*, 397−409.
(59) Ramanayaka, S.; Tsang, D. C. W.; Hou, D.; Ok, Y. S.; Vithanage, M. Green synthesis of graphitic nanobiochar for the removal of emerging contaminants in aqueous media. *Sci. Total Environ.* **2020**, *706*, 135725.
(60) Amusat, S. O.; Kebede, T. G.; Dube, S.; Nindi, M. M. Ball-milling synthesis of biochar and biochar-based nanocomposites and prospects for removal of emerging contaminants: A review. *Journal of Water Process Engineering* **2021**, *41*, 101993.
(61) Zhang, Y.; Zheng, Y.; Yang, Y.; Huang, J.; Zimmerman, A. R.; Chen, H.; Hu, X.; Gao, B. Mechanisms and adsorption capacities of hydrogen peroxide modified ball milled biochar for the removal of methylene blue from aqueous solutions. *Bioresour. Technol.* **2021**, *337*, 125432.

https://doi.org/10.1021/acsomega.3c07804
ACS Omega 2024, 9, 12331−12379

(62) Mahmoud, M. E.; Abou-Ali, S. A. A.; Elweshahy, S. M. T. Efficient and ultrafast removal of Cd(II) and Sm(III) from water by leaves of Cynara scolymus derived biochar. *Mater. Res. Bull.* **2021**, *141*, 111334.
(63) Khaliq, H.; Anwar, S.; Shafiq, F.; Ashraf, M.; Zhang, L.; Haider, I.; Khan, S. Interactive effects of soil and foliar-applied nanobiochar on growth, metabolites, and nutrient composition in Daucus carota. *Journal of Plant Growth Regulation* **2023**, *42* (6), 3715−3729.
(64) Oleszczuk, P.; Cwikła-Bundyra, W.; Bogusz, A.; Skwarek, E.; Ok, Y. S. Characterization of nanoparticles of biochars from different biomass. *J. Anal. Appl. Pyrolysis* **2016**, *121*, 165−172.
(65) Sajjadi, B.; Chen, W.-Y.; Mattern, D. L.; Hammer, N.; Dorris, A. Low-temperature acoustic-based activation of biochar for enhanced removal of heavy metals. *Journal of Water Process Engineering* **2020**, *34*, 101166.
(66) Shan, Y.; Yang, W.; Li, Y.; Liu, Y.; Pan, J. Preparation of microwave-activated magnetic bio-char adsorbent and study on removal of elemental mercury from flue gas. *Sci. Total Environ.* **2019**, *697*, 134049.
(67) Song, B.; Chen, M.; Zhao, L.; Qiu, H.; Cao, X. Physicochemical property and colloidal stability of micron- and nano-particle biochar derived from a variety of feedstock sources. *Sci. Total Environ.* **2019**, *661*, 685−695.
(68) Lian, F.; Yu, W.; Zhou, Q.; Gu, S.; Wang, Z.; Xing, B. Size matters: nano-biochar triggers decomposition and transformation inhibition of antibiotic resistance genes in aqueous environments. *Environ. Sci. Technol.* **2020**, *54* (14), 8821−8829.
(69) Guo, F.; Bao, L.; Wang, H.; Larson, S. L.; Ballard, J. H.; Knotek-Smith, H. M.; Zhang, Q.; Su, Y.; Wang, X.; Han, F. A simple method for the synthesis of biochar nanodots using hydrothermal reactor. *MethodsX* **2020**, *7*, 101022.
(70) Gao, Y.; Pramanik, A.; Begum, S.; Sweet, C.; Jones, S.; Alamgir, A.; Ray, P. C. Multifunctional biochar for highly efficient capture,identification, and removal of toxic metals and superbugs from water samples. *ACS Omega* **2017**, *2* (11), 7730−7738.
(71) Behnam, H.; Firouzi, A. F. Effects of synthesis method, feedstock type, and pyrolysis temperature on physicochemical properties of biochar nanoparticles. *Biomass Conversion and Biorefinery* **2023**, *13*, 13859.
(72) Genovese, M.; Jiang, J.; Lian, K.; Holm, N. High capacitive performance of exfoliated biochar nanosheets from biomass waste corn cob. *Journal of Materials Chemistry A* **2015**, *3* (6), 2903−2913.
(73) Haris, M.; Usman, M.; Su, F.; Lei, W.; Saleem, A.; Hamid, Y.; Guo, J.; Li, Y. Programmable synthesis of exfoliated biochar nanosheets for selective and highly efficient adsorption of thallium. *Chem. Eng. J.* **2022**, *434*, 134842.
(74) Kumar, M.; Xiong, X.; Wan, Z.; Sun, Y.; Tsang, D. C. W.; Gupta, J.; Gao, B.; Cao, X.; Tang, J.; Ok, Y. S. Ball milling as a mechanochemical technology for fabrication of novel biochar nanomaterials. *Bioresour. Technol.* **2020**, *312*, 123613.
(75) Ma, S.; Jing, F.; Sohi, S. P.; Chen, J. New insights into contrasting mechanisms for PAE adsorption on millimeter, micron- and nano-scale biochar. *Environmental Science and Pollution Research* **2019**, *26* (18), 18636−18650.
(76) Lyu, H.; Gao, B.; He, F.; Zimmerman, A. R.; Ding, C.; Huang, H.; Tang, J. Effects of ball milling on the physicochemical and sorptive properties of biochar: Experimental observations and governing mechanisms. *Environ. Pollut.* **2018**, *233*, 54−63.
(77) Shan, D.; Deng, S.; Zhao, T.; Wang, B.; Wang, Y.; Huang, J.; Yu, G.; Winglee, J.; Wiesner, M. R. Preparation of ultrafine magnetic biochar and activated carbon for pharmaceutical adsorption and subsequent degradation by ball milling. *J. Hazard. Mater.* **2016**, *305*, 156−163.
(78) Lyu, H.; Xia, S.; Tang, J.; Zhang, Y.; Gao, B.; Shen, B. Thiol-modified biochar synthesized by a facile ball-milling method for enhanced sorption of inorganic Hg^{2+} and organic CH_3Hg^+. *J. Hazard. Mater.* **2020**, *384*, 121357.
(79) Lyu, H.; Gao, B.; He, F.; Ding, C.; Tang, J.; Crittenden, J. C. Ball-milled carbon nanomaterials for energy and environmental applications. *ACS Sustainable Chem. Eng.* **2017**, *5* (11), 9568−9585.
(80) Wang, B.; Gao, B.; Wan, Y. Entrapment of ball-milled biochar in Ca-alginate beads for the removal of aqueous Cd(II). *Journal of Industrial and Engineering Chemistry* **2018**, *61*, 161−168.
(81) Ullah, M.; Ali, M.; Hamid, S. Structure-controlled nanomaterial synthesis using surfactant-assisted ball milling-a review. *Curr. Nanosci.* **2014**, *10* (3), 344−354.
(82) Lyu, H.; Gong, Y.; Tang, J.; Huang, Y.; Wang, Q. Immobilization of heavy metals in electroplating sludge by biochar and iron sulfide. *Environmental Science and Pollution Research* **2016**, *23* (14), 14472−14488.
(83) Hick, S. M.; Griebel, C.; Restrepo, D. T.; Truitt, J. H.; Buker, E. J.; Bylda, C.; Blair, R. G. Mechanocatalysis for biomass-derived chemicals and fuels. *Green Chem.* **2010**, *12* (3), 468−474.
(84) Boldyreva, E. Mechanochemistry of inorganic and organic systems: what is similar, what is different? *Chem. Soc. Rev.* **2013**, *42* (18), 7719−7738.
(85) Karinkanta, P.; Ämmälä, A.; Illikainen, M.; Niinimäki, J. Fine grinding of wood - Overview from wood breakage to applications. *Biomass Bioenergy* **2018**, *113*, 31−44.
(86) Naghdi, M.; Taheran, M.; Brar, S. K.; Verma, M.; Surampalli, R. Y.; Valero, J. R. Green and energy-efficient methods for the production of metallic nanoparticles. *Beilstein Journal of Nanotechnology* **2015**, *6*, 2354−2376.
(87) Li, Y.; Zimmerman, A. R.; He, F.; Chen, J.; Han, L.; Chen, H.; Hu, X.; Gao, B. Solvent-free synthesis of magnetic biochar and activated carbon through ball-mill extrusion with Fe_3O_4 nanoparticles for enhancing adsorption of methylene blue. *Sci. Total Environ.* **2020**, *722*, 137972.
(88) Richard, S.; Selwin Rajadurai, J.; Manikandan, V. Influence of particle size and particle loading on mechanical and dielectric properties of biochar particulate-reinforced polymer nanocomposites. *Int. J. Polym. Anal. Charact.* **2016**, *21* (6), 462−477.
(89) Yuan, Y.; Zhang, N.; Hu, X. Effects of wet and dry ball milling on the physicochemical properties of sawdust derived-biochar. *Instrumentation Science & Technology* **2020**, *48* (3), 287−300.
(90) Lu, L. *Iron ore: mineralogy, processing and environmental sustainability*; Elsevier, 2015.
(91) Li, W.; Zhu, X.; He, Y.; Xing, B.; Xu, J.; Brookes, P. C. Enhancement of water solubility and mobility of phenanthrene by natural soil nanoparticles. *Environ. Pollut.* **2013**, *176*, 228−233.
(92) Qin, Y.; Zhu, X.; Su, Q.; Anumah, A.; Gao, B.; Lyu, W.; Zhou, X.; Xing, Y.; Wang, B. Enhanced removal of ammonium from water by ball-milled biochar. *Environ. Geochem. Health* **2020**, *42* (6), 1579−1587.
(93) Pratap, T.; Patel, M.; Pittman, C. U., Jr.; Nguyen, T. A.; Mohan, D. Chapter 23 - Nanobiochar: A sustainable solution for agricultural and environmental applications. In *Nanomaterials for Soil Remediation*; Amrane, A., Mohan, D., Nguyen, T. A., Assadi, A. A., Yasin, G., Eds.; Elsevier, 2021; pp 501−519.
(94) Yang, Y.; Zhou, B.; Hu, Z.; Lin, H. The effects of nano-biochar on maize growth in northern Shaanxi Province on the Loess Plateau. *Appl. Ecol Environ. Res.* **2020**, *18*, 2863−2877.
(95) Dong, C. D.; Lung, S. C. C.; Chen, C. W.; Lee, J. S.; Chen, Y. C.; Wang, W. C. V.; Chen, C. J.; Hung, C. M.; Lin, C. H. Assessment of the pulmonary toxic potential of nano-tobacco stem-pyrolyzed biochars. *Environmental Science: Nano* **2019**, *6* (5), 1527−1535.
(96) Ullmann, C.; Babick, F.; Koeber, R.; Stintz, M. Performance of analytical centrifugation for the particle size analysis of real-world materials. *Powder Technol.* **2017**, *319*, 261−270.
(97) Xu, X.; Cölfen, H. Ultracentrifugation techniques for the ordering of nanoparticles. *Nanomaterials* **2021**, *11* (2), 333.
(98) Tang, Z.; Wu, L.; Luo, Y.; Christie, P. Size fractionation and characterization of nanocolloidal particles in soils. *Environ. Geochem. Health* **2009**, *31* (1), 1−10.
(99) Xu, Y.; Bai, T.; Yan, Y.; Zhao, Y.; Yuan, L.; Pan, P.; Jiang, Z. Enhanced removal of hexavalent chromium by different acid-modified

https://doi.org/10.1021/acsomega.3c07804
ACS Omega 2024, 9, 12331−12379

biochar derived from corn straw: behavior and mechanism. *Water Sci. Technol.* **2020**, *81* (10), 2270−2280.
(100) Li, L.; Zhang, K.; Chen, L.; Huang, Z.; Liu, G.; Li, M.; Wen, Y. Mass preparation of micro/nano-powders of biochar with water-dispersibility and their potential application. *New J. Chem.* **2017**, *41* (18), 9649−9657.
(101) Peterson, S. C.; Jackson, M. A.; Kim, S.; Palmquist, D. E. Increasing biochar surface area: Optimization of ball milling parameters. *Powder Technol.* **2012**, *228*, 115−120.
(102) Lyu, H.; Gao, B.; He, F.; Zimmerman, A. R.; Ding, C.; Tang, J.; Crittenden, J. C. Experimental and modeling investigations of ball-milled biochar for the removal of aqueous methylene blue. *Chem. Eng. J.* **2018**, *335*, 110−119.
(103) Xiao, J.; Hu, R.; Chen, G. Micro-nano-engineered nitrogenous bone biochar developed with a ball-milling technique for high-efficiency removal of aquatic Cd(II), Cu(II) and Pb(II). *J. Hazard. Mater.* **2020**, *387*, 121980.
(104) Zhang, Q.; Wang, J.; Lyu, H.; Zhao, Q.; Jiang, L.; Liu, L. Ball-milled biochar for galaxolide removal: Sorption performance and governing mechanisms. *Sci. Total Environ.* **2019**, *659*, 1537−1545.
(105) Cao, Y.; Xiao, W.; Shen, G.; Ji, G.; Zhang, Y.; Gao, C.; Han, L. Carbonization and ball milling on the enhancement of Pb(II) adsorption by wheat straw: Competitive effects of ion exchange and precipitation. *Bioresour. Technol.* **2019**, *273*, 70−76.
(106) Ramezanzadeh, H.; Reyhanitabar, A.; Oustan, S.; Mohammadi, M. H.; van der Zee, S. E. A. T. M. Enhanced sorption of cadmium by using biochar nanoparticles from ball milling in a sandy soil. *Eurasian Soil Science* **2021**, *54* (2), 201−211.
(107) Mahmoud, E.; El Baroudy, A.; Ali, N.; Sleem, M. Spectroscopic studies on the phosphorus adsorption in salt-affected soils with or without nano-biochar additions. *Environ. Res.* **2020**, *184*, 109277.
(108) Chen, X.; Wu, W.; Han, L.; Gu, M.; Li, J.; Chen, M. Carbon stability and mobility of ball milled lignin- and cellulose-rich biochar colloids. *Sci. Total Environ.* **2022**, *802*, 149759.
(109) Jiang, C.; Bo, J.; Xiao, X.; Zhang, S.; Wang, Z.; Yan, G.; Wu, Y.; Wong, C.; He, H. Converting waste lignin into nano-biochar as a renewable substitute of carbon black for reinforcing styrene-butadiene rubber. *Waste Manage. (Oxford)* **2020**, *102*, 732−742.
(110) Xu, X.; Zheng, Y.; Gao, B.; Cao, X. N-doped biochar synthesized by a facile ball-milling method for enhanced sorption of CO2 and reactive red. *Chem. Eng. J.* **2019**, *368*, 564−572.
(111) Feng, K.; Xu, Z.; Gao, B.; Xu, X.; Zhao, L.; Qiu, H.; Cao, X. Mesoporous ball-milling iron-loaded biochar for enhanced sorption of reactive red: Performance and mechanisms. *Environ. Pollut.* **2021**, *290*, 117992.
(112) Zhao, L.; Zhang, Y.; Wang, L.; Lyu, H.; Xia, S.; Tang, J. Effective removal of Hg(II) and MeHg from aqueous environment by ball milling aided thiol-modification of biochars: Effect of different pyrolysis temperatures. *Chemosphere* **2022**, *294*, 133820.
(113) Mayakrishnan, V.; Mohamed, J. K.; Selvaraj, N.; SenthilKumar, D.; Annadurai, S. Effect of nano-biochar on mechanical, barrier and mulching properties of 3D printed thermoplastic polyurethane film. *Polym. Bull.* **2023**, *80* (6), 6725−6747.
(114) Rashid, M. I.; Shah, G. A.; Iqbal, Z.; Ramzan, M.; Rehan, M.; Ali, N.; Shahzad, K.; Summan, A.; Ismail, I. M. I.; Ondrasek, G. Nanobiochar associated ammonia emission mitigation and toxicity to soil microbial biomass and corn nutrient uptake from farmyard manure. *Plants* **2023**, *12* (9), 1740.
(115) Cao, X.; Meng, Z.; Sheng, L.; Hu, X.; Wang, T.; Sun, X.; Yu, Y.; Liu, Z. Double-edged sword effect of nano-biochar for Cd^{2+} adsorption on zeolite. *Journal of Environmental Chemical Engineering* **2023**, *11* (3), 109901.
(116) Shen, Y.; Tang, H.; Wu, W.; Shang, H.; Zhang, D.; Zhan, X.; Xing, B. Role of nano-biochar in attenuating the allelopathic effect from Imperata cylindrica on rice seedlings. *Environmental Science: Nano* **2020**, *7* (1), 116−126.
(117) Yang, X.; Wang, L.; Tong, J.; Shao, X.; Chen, R.; Yang, Q.; Li, F.; Xue, B.; Li, G.; Han, Y.; et al. Synthesis of hickory biochar via one-step acidic ball milling: characteristics and titan yellow adsorption. *Journal of Cleaner Production* **2022**, *338*, 130575.
(118) Wang, D.; Zhang, W.; Hao, X.; Zhou, D. Transport of Biochar Particles in Saturated Granular Media: Effects of Pyrolysis Temperature and Particle Size. *Environ. Sci. Technol.* **2013**, *47* (2), 821−828.
(119) Tan, M.; Li, Y.; Chi, D.; Wu, Q. Efficient removal of ammonium in aqueous solution by ultrasonic magnesium-modified biochar. *Chem. Eng. J.* **2023**, *461*, 142072.
(120) Vidal, J. L.; Gallant, S. M. V.; Connors, E. P.; Richards, D. D.; MacQuarrie, S. L.; Kerton, F. M. Green solvents for the liquid-phase exfoliation of biochars. *ACS Sustainable Chem. Eng.* **2021**, *9* (27), 9114−9125.
(121) Bukhari, Q. U. A.; Silveri, F.; Della Pelle, F.; Scroccarello, A.; Zappi, D.; Cozzoni, E.; Compagnone, D. Water-phase exfoliated biochar nanofibers from eucalyptus scraps for electrode modification and conductive film fabrication. *ACS Sustainable Chem. Eng.* **2021**, *9* (41), 13988−13998.
(122) Gu, S.; Lian, F.; Han, Y.; Taherymoosavi, S.; Mitchell, D.; Joseph, S.; Wang, Z.; Xing, B. Nano-biochar modulates the formation of iron plaque through facilitating iron-involved redox reactions on aquatic plant root surfaces. *Environmental Science: Nano* **2022**, *9* (6), 1974−1985.
(123) Mao, D.; Hu, J.; Duan, P.; Qin, C.; Piao, Y. Ultrasensitive and highly reusable electrochemical sensor with ion imprinted nanobiochar. *Sens. Actuators, B* **2022**, *371*, 132490.
(124) Lian, F.; Gu, S.; Han, Y.; Wang, Z.; Xing, B. Novel insights into the impact of nano-biochar on composition and structural transformation of mineral/nano-biochar heteroaggregates in the presence of root exudates. *Environ. Sci. Technol.* **2022**, *56* (13), 9816−9825.
(125) Zhang, Y.; Zhao, G.; Xuan, Y.; Gan, L.; Pan, M. Enhanced photocatalytic performance for phenol degradation using ZnO modified with nano-biochar derived from cellulose nanocrystals. *Cellulose* **2021**, *28* (2), 991−1009.
(126) Mahmoud, M. E.; Abdelfattah, A. M.; Tharwat, R. M.; Nabil, G. M. Adsorption of negatively charged food tartrazine and sunset yellow dyes onto positively charged triethylenetetramine biochar: optimization, kinetics and thermodynamic study. *J. Mol. Liq.* **2020**, *318*, 114297.
(127) Mahmoud, M. E.; El-Ghanam, A. M.; Saad, S. R.; Mohamed, R. H. A. Promoted removal of metformin hydrochloride anti-diabetic drug from water by fabricated and modified nanobiochar from artichoke leaves. *Sustainable Chemistry and Pharmacy* **2020**, *18*, 100336.
(128) Xiao, J.; Hu, R.; Chen, G. Micro-nano-engineered nitrogenous bone biochar developed with a ball-milling technique for high-efficiency removal of aquatic Cd(II), Cu(II) and Pb(II). *J. Hazard. Mater.* **2020**, *387*, 121980.
(129) Chen, B.; Yang, Z.; Ma, G.; Kong, D.; Xiong, W.; Wang, J.; Zhu, Y.; Xia, Y. Heteroatom-doped porous carbons with enhanced carbon dioxide uptake and excellent methylene blue adsorption capacities. *Microporous Mesoporous Mater.* **2018**, *257*, 1−8.
(130) Nguyen, M.-V.; Lee, B.-K. A novel removal of CO_2 using nitrogen doped biochar beads as a green adsorbent. *Process Safety and Environmental Protection* **2016**, *104*, 490−498.
(131) Zhu, S.; Huang, X.; Ma, F.; Wang, L.; Duan, X.; Wang, S. Catalytic removal of aqueous contaminants on N-doped graphitic biochars: inherent roles of adsorption and nonradical mechanisms. *Environ. Sci. Technol.* **2018**, *52* (15), 8649−8658.
(132) Xing, T.; Sunarso, J.; Yang, W.; Yin, Y.; Glushenkov, A. M.; Li, L. H.; Howlett, P. C.; Chen, Y. Ball milling: a green mechanochemical approach for synthesis of nitrogen doped carbon nanoparticles. *Nanoscale* **2013**, *5* (17), 7970−7976.
(133) Kundu, S.; Xia, W.; Busser, W.; Becker, M.; Schmidt, D. A.; Havenith, M.; Muhler, M. The formation of nitrogen-containing functional groups on carbon nanotube surfaces: a quantitative XPS and TPD study. *Phys. Chem. Chem. Phys.* **2010**, *12* (17), 4351−4359.
(134) Xue, Y.; Chen, H.; Qu, J.; Dai, L. Nitrogen-doped graphene by ball-milling graphite with melamine for energy conversion and storage. *2D Materials* **2015**, *2* (4), 044001.
(135) Huang, Y.; Gong, Y.; Tang, J.; Xia, S. Effective removal of inorganic mercury and methylmercury from aqueous solution using

https://doi.org/10.1021/acsomega.3c07804
ACS Omega 2024, 9, 12331−12379

novel thiol-functionalized graphene oxide/Fe-Mn composite. *J. Hazard. Mater.* **2019**, *366*, 130−139.
(136) Ji, J.; Chen, G.; Zhao, J. Preparation and characterization of amino/thiol bifunctionalized magnetic nanoadsorbent and its application in rapid removal of Pb (II) from aqueous system. *J. Hazard. Mater.* **2019**, *368*, 255−263.
(137) He, F.; Wang, W.; Moon, J.-W.; Howe, J.; Pierce, E. M.; Liang, L. Rapid Removal of Hg(II) from Aqueous Solutions Using Thiol-Functionalized Zn-Doped Biomagnetite Particles. *ACS Appl. Mater. Interfaces* **2012**, *4* (8), 4373−4379.
(138) Zhang, S.; Zhang, Y.; Liu, J.; Xu, Q.; Xiao, H.; Wang, X.; Xu, H.; Zhou, J. Thiol modified Fe_3O_4@SiO_2 as a robust, high effective, and recycling magnetic sorbent for mercury removal. *Chem. Eng. J.* **2013**, *226*, 30−38.
(139) de Mello Ferreira Guimarães, A.; Ciminelli, V. S. T.; Vasconcelos, W. L. Smectite organofunctionalized with thiol groups for adsorption of heavy metal ions. *Appl. Clay Sci.* **2009**, *42* (3), 410−414.
(140) Yu, B.; Wang, X.; Xing, W.; Yang, H.; Wang, X.; Song, L.; Hu, Y.; Lo, S. Enhanced thermal and mechanical properties of functionalized graphene/thiol-ene systems by photopolymerization technology. *Chem. Eng. J.* **2013**, *228*, 318−326.
(141) Xia, C.; Liang, Y.; Li, X.; Garalleh, H. A.; Garaleh, M.; Hill, J. M.; Pugazhendhi, A. Remediation competence of nanoparticles amalgamated biochar (nanobiochar/nanocomposite) on pollutants: A review. *Environ. Res.* **2023**, *218*, 114947.
(142) Khan, H. A.; Naqvi, S. R.; Mehran, M. T.; Khoja, A. H.; Khan Niazi, M. B.; Juchelková, D.; Atabani, A. A performance evaluation study of nano-biochar as a potential slow-release nano-fertilizer from wheat straw residue for sustainable agriculture. *Chemosphere* **2021**, *285*, 131382.
(143) Baig, S. A.; Zhu, J.; Tan, L.; Xue, X.; Sun, C.; Xu, X. Influence of calcination on magnetic honeycomb briquette cinders composite for the adsorptive removal of As(III) in fixed-bed column. *Chem. Eng. J.* **2014**, *257*, 1−9.
(144) Shao, B.; Guan, Y.; Tian, Z.; Guan, X.; Wu, D. Advantages of aeration in arsenic removal and arsenite oxidation by structural Fe(II) hydroxides in aqueous solution. *Colloids Surf., A* **2016**, *506*, 703−710.
(145) Singh, P.; Sarswat, A.; Pittman, C. U., Jr; Mlsna, T.; Mohan, D. Sustainable low-concentration arsenite [As(III)] removal in single and multicomponent systems using hybrid iron oxide-biochar nanocomposite adsorbents—a mechanistic study. *ACS Omega* **2020**, *5* (6), 2575−2593.
(146) He, R.; Peng, Z.; Lyu, H.; Huang, H.; Nan, Q.; Tang, J. Synthesis and characterization of an iron-impregnated biochar for aqueous arsenic removal. *Sci. Total Environ.* **2018**, *612*, 1177−1186.
(147) Moyano, D. B.; Paraiso, D. A.; González-Lezcano, R. A. Possible Effects on Health of Ultrasound Exposure, Risk Factors in the Work Environment and Occupational Safety Review. *Healthcare* **2022**, *10* (3), 423.
(148) Patel, M.; Kumar, R.; Kishor, K.; Mlsna, T.; Pittman, C. U., Jr; Mohan, D. Pharmaceuticals of emerging concern in aquatic systems: chemistry, occurrence, effects, and removal methods. *Chem. Rev.* **2019**, *119* (6), 3510−3673.
(149) Kloss, S.; Zehetner, F.; Dellantonio, A.; Hamid, R.; Ottner, F.; Liedtke, V.; Schwanninger, M.; Gerzabek, M. H.; Soja, G. Characterization of slow pyrolysis biochars: effects of feedstocks and pyrolysis temperature on biochar properties. *J. Environ. Qual.* **2012**, *41* (4), 990−1000.
(150) Yang, S.; Yang, C.; Hu, X.; Ding, Z.; Zhou, R.; Wei, H.; Wang, L. Aqueous norfloxacin removal by novel biochar adsorbent prepared through ethanol-combined ball milling. *Env. Pollut. Bioavail.* **2024**, *36* (1), 2311675.
(151) Liu, G. C.; Zheng, H.; Jiang, Z. X.; Zhao, J.; Wang, Z. Y.; Pan, B.; Xing, B. S. Formation and physicochemical characteristics of nano biochar: insight into chemical and colloidal stability. *Environ. Sci. Technol.* **2018**, *52* (18), 10369−10379.
(152) Oleszczuk, P.; Cwikla-Bundyra, W.; Bogusz, A.; Skwarek, E.; Ok, Y. S. Characterization of nanoparticles of biochars from different biomass. *Journal of Analytical and Applied Pyrolysis* **2016**, *121*, 165−172.
(153) Yue, L.; Lian, F.; Han, Y.; Bao, Q.; Wang, Z.; Xing, B. The effect of biochar nanoparticles on rice plant growth and the uptake of heavy metals: implications for agronomic benefits and potential risk. *Sci. Total Environ.* **2019**, *656*, 9−18.
(154) Liu, C.-H.; Chu, W.; Li, H.; Boyd, S. A.; Teppen, B. J.; Mao, J.; Lehmann, J.; Zhang, W. Quantification and characterization of dissolved organic carbon from biochars. *Geoderma* **2019**, *335*, 161−169.
(155) Raja, P. M. V.; Barron, A. R. *Chapter 2 - Zeta Potential Analysis. In Physical Methods in Chemistry and Nano Science*; Rice University, 2019.
(156) Munkhbayar, B.; Nine, M. J.; Jeoun, J.; Bat-Erdene, M.; Chung, H.; Jeong, H. Influence of dry and wet ball milling on dispersion characteristics of the multi-walled carbon nanotubes in aqueous solution with and without surfactant. *Powder Technol.* **2013**, *234*, 132−140.
(157) Lateef, A.; Nazir, R.; Jamil, N.; Alam, S.; Shah, R.; Khan, M. N.; Saleem, M.; Rehman, S.-U. Synthesis and characterization of environmental friendly corncob biochar based nano-composite - A potential slow release nano-fertilizer for sustainable agriculture. *Environmental Nanotechnology, Monitoring & Management* **2019**, *11*, 100212.
(158) Chen, X.; Zhou, B. Synergistic effects of nano-biochar and crop on reducing rainwater runoff and phosphorus loss from sloping farmland. *Arabian Journal of Geosciences* **2022**, *15* (1), 43.
(159) Jenie, S. N. A.; Kristiani, A.; Kustomo; Simanungkalit, S.; Mansur, D. Preparation of nanobiochar as magnetic solid acid catalyst by pyrolysis-carbonization from oil palm empty fruit bunches. *AIP Conf. Proc.* **2017**, *1904* (1), 020018.
(160) Zhang, K.; Wang, Y.; Mao, J.; Chen, B. Effects of biochar nanoparticles on seed germination and seedling growth. *Environ. Pollut.* **2020**, *256*, 113409.
(161) Yao, L.; He, L.; Yang, Y.; Zhang, Y.; Liu, Z.; Liang, L.; Piao, Y. Nanobiochar paper based electrochemical immunosensor for fast and ultrasensitive detection of microcystin-LR. *Sci. Total Environ.* **2021**, *750*, 141692.
(162) Xue, B.; Wang, X.; Sui, J.; Xu, D.; Zhu, Y.; Liu, X. A facile ball milling method to produce sustainable pyrolytic rice husk bio-filler for reinforcement of rubber mechanical property. *Industrial Crops and Products* **2019**, *141*, 111791.
(163) Hu, R.; Xiao, J.; Wang, T.; Chen, G.; Chen, L.; Tian, X. Engineering of phosphate-functionalized biochars with highly developed surface area and porosity for efficient and selective extraction of uranium. *Chem. Eng. J.* **2020**, *379*, 122388.
(164) Deng, J.; Liu, Y.; Liu, S.; Zeng, G.; Tan, X.; Huang, B.; Tang, X.; Wang, S.; Hua, Q.; Yan, Z. Competitive adsorption of Pb(II), Cd(II) and Cu(II) onto chitosan-pyromellitic dianhydride modified biochar. *J. Colloid Interface Sci.* **2017**, *506*, 355−364.
(165) Chen, S.; Ma, Y.; Chen, L.; Wang, L.; Guo, H. Comparison of Pb(II) Immobilized by bone char meal and phosphate rock: characterization and kinetic study. *Arch. Environ. Contam. Toxicol.* **2010**, *58* (1), 24−32.
(166) Wang, H.; Gao, B.; Wang, S.; Fang, J.; Xue, Y.; Yang, K. Removal of Pb(II), Cu(II), and Cd(II) from aqueous solutions by biochar derived from $KMnO_4$ treated hickory wood. *Bioresour. Technol.* **2015**, *197*, 356−362.
(167) Zhang, M.; Gao, B. Removal of arsenic, methylene blue, and phosphate by biochar/AlOOH nanocomposite. *Chem. Eng. J.* **2013**, *226*, 286−292.
(168) Zhao, G.; Li, J.; Ren, X.; Chen, C.; Wang, X. Few-layered graphene oxide nanosheets as superior sorbents for heavy metal Ion pollution management. *Environ. Sci. Technol.* **2011**, *45* (24), 10454−10462.
(169) Kołodyńska, D.; Wnetrzak, R.; Leahy, J. J.; Hayes, M. H. B.; Kwapiński, W.; Hubicki, Z. Kinetic and adsorptive characterization of biochar in metal ions removal. *Chem. Eng. J.* **2012**, *197*, 295−305.

https://doi.org/10.1021/acsomega.3c07804
ACS Omega 2024, 9, 12331−12379

(170) Tang, J.; Zhao, B.; Lyu, H.; Li, D. Development of a novel pyrite/biochar composite (BM-FeS_2@BC) by ball milling for aqueous Cr(VI) removal and its mechanisms. *J. Hazard. Mater.* **2021**, *413*, 125415.
(171) Wang, K.; Liu, X.; Tang, J.; Wang, L.; Sun, H. Ball milled Fe0@FeS hybrids coupled with peroxydisulfate for Cr(VI) and phenol removal: Novel surface reduction and activation mechanisms. *Sci. Total Environ.* **2020**, *739*, 139748.
(172) Zou, H.; Zhao, J.; He, F.; Zhong, Z.; Huang, J.; Zheng, Y.; Zhang, Y.; Yang, Y.; Yu, F.; Bashir, M. A.; et al. Ball milling biochar iron oxide composites for the removal of chromium [Cr(VI)] from water: Performance and mechanisms. *J. Hazard. Mater.* **2021**, *413*, 125252.
(173) Mohan, D.; Chaubey, A. K.; Patel, M.; Navarathna, C.; Mlsna, T. E.; Pittman, C. U., Jr. Chapter 5 - Biochar adsorption system designs. In *Sustainable Biochar for Water and Wastewater Treatment*, Mohan, D., Pittman, C. U., Jr.; Mlsna, T. E., Eds.; Elsevier, 2022; pp 153−203.
(174) Wang, T.; Qian, T.; Huo, L.; Li, Y.; Zhao, D. Immobilization of hexavalent chromium in soil and groundwater using synthetic pyrite particles. *Environ. Pollut.* **2019**, *255*, 112992.
(175) Kantar, C. Role of low molecular weight organic acids on pyrite dissolution in aqueous systems: implications for catalytic chromium (VI) treatment. *Water Sci. Technol.* **2016**, *74* (1), 99−109.
(176) Sun, H.; Chen, M.; Zou, L.; Shu, R.; Ruan, R. Study of the kinetics of pyrite oxidation under controlled redox potential. *Hydrometallurgy* **2015**, *155*, 13−19.
(177) Kantar, C.; Bulbul, M. S. Effect of pH-buffering on Cr(VI) reduction with pyrite in the presence of various organic acids: Continuous-flow experiments. *Chem. Eng. J.* **2016**, *287*, 173−180.
(178) Kantar, C.; Ari, C.; Keskin, S.; Dogaroglu, Z. G.; Karadeniz, A.; Alten, A. Cr(VI) removal from aqueous systems using pyrite as the reducing agent: batch, spectroscopic and column experiments. *J. Contam. Hydrol.* **2015**, *174*, 28−38.
(179) Guo, J.; Chen, B. Insights on the molecular mechanism for the recalcitrance of biochars: interactive effects of carbon and silicon components. *Environ. Sci. Technol.* **2014**, *48* (16), 9103−9112.
(180) Park, J.-H.; Wang, J. J.; Zhou, B.; Mikhael, J. E. R.; DeLaune, R. D. Removing mercury from aqueous solution using sulfurized biochar and associated mechanisms. *Environ. Pollut.* **2019**, *244*, 627−635.
(181) Hanandeh, A. E.; Abu-Zurayk, R. A.; Hamadneh, I.; Al-Dujaili, A. H. Characterization of biochar prepared from slow pyrolysis of Jordanian olive oil processing solid waste and adsorption efficiency of Hg^{2+} ions in aqueous solutions. *Water Sci. Technol.* **2016**, *74* (8), 1899−1910.
(182) Vishnu, D.; Dhandapani, B.; Vaishnavi, G.; Preethi, V. Synthesis of tri-metallic surface engineered nanobiochar from cynodon dactylon residues in a single step - Batch and column studies for the removal of copper and lead ions. *Chemosphere* **2022**, *286*, 131572.
(183) El-Shafey, E.I.; Ali, S. N.F.; Al-Busafi, S.; Al-Lawati, H. A.J. Preparation and characterization of surface functionalized activated carbons from date palm leaflets and application for methylene blue removal. *Journal of Environmental Chemical Engineering* **2016**, *4* (3), 2713−2724.
(184) Bradder, P.; Ling, S. K.; Wang, S.; Liu, S. Dye adsorption on layered graphite oxide. *Journal of Chemical & Engineering Data* **2011**, *56* (1), 138−141.
(185) Zhang, M.; Gao, B.; Yao, Y.; Xue, Y.; Inyang, M. Synthesis, characterization, and environmental implications of graphene-coated biochar. *Sci. Total Environ.* **2012**, *435*−*436*, 567−572.
(186) Žic, M.; Ristić, M.; Musić, S. Microstructural changes in particles detected during the transformation from β-FeOOH to α-Fe_2O_3 in dense aqueous suspensions. *J. Alloys Compd.* **2008**, *464* (1), 81−88.
(187) Yao, X.; Ji, L.; Guo, J.; Ge, S.; Lu, W.; Cai, L.; Wang, Y.; Song, W.; Zhang, H. Magnetic activated biochar nanocomposites derived from wakame and its application in methylene blue adsorption. *Bioresour. Technol.* **2020**, *302*, 122842.
(188) Mahmoud, M. E.; El-Ghanam, A. M.; Saad, S. R. Sequential removal of chromium (VI) and prednisolone by nanobiochar-enriched-diamine derivative. *Biomass Conversion and Biorefinery* **2022**, DOI: 10.1007/s13399-022-02888-1.
(189) Makshut, N. A.; Ngaini, Z.; Wahi, R.; Hussain, H.; Mahmut, N. I.; Bahrin, N. Q. Nano-sized adsorbent from pyrolysed sago activated sludge forremoval of Pb (II) from aqueous solution. *Pertanika Journal of Science Technology* **2020**, *28* (3).
(190) Ma, W.; Xu, Y.; Zhou, D.; Wang, L.; Liang, X.; Sun, Y. Development and optimization of high-performance nano-biochar for efficient removal Cd in aqueous: Absorption performance and interaction mechanisms. *Chem. Eng. Res. Des.* **2023**, *189*, 516−529.
(191) Huang, J.; Zimmerman, A. R.; Chen, H.; Gao, B. Ball milled biochar effectively removes sulfamethoxazole and sulfapyridine antibiotics from water and wastewater. *Environ. Pollut.* **2020**, *258*, 113809.
(192) Dong, X.; He, L.; Hu, H.; Liu, N.; Gao, S.; Piao, Y. Removal of 17β-estradiol by using highly adsorptive magnetic biochar nanoparticles from aqueous solution. *Chem. Eng. J.* **2018**, *352*, 371−379.
(193) Ahmed, M. B.; Zhou, J. L.; Ngo, H. H.; Guo, W.; Johir, M. A. H.; Sornalingam, K. Single and competitive sorption properties and mechanism of functionalized biochar for removing sulfonamide antibiotics from water. *Chem. Eng. J.* **2017**, *311*, 348−358.
(194) Zheng, H.; Wang, Z.; Zhao, J.; Herbert, S.; Xing, B. Sorption of antibiotic sulfamethoxazole varies with biochars produced at different temperatures. *Environ. Pollut.* **2013**, *181*, 60−67.
(195) Inyang, M.; Gao, B.; Zimmerman, A.; Zhou, Y.; Cao, X. Sorption and cosorption of lead and sulfapyridine on carbon nanotube-modified biochars. *Environmental Science and Pollution Research* **2015**, *22* (3), 1868−1876.
(196) Amarasinghe, B. M. W. P. K.; Williams, R. A. Tea waste as a low cost adsorbent for the removal of Cu and Pb from wastewater. *Chem. Eng. J.* **2007**, *132* (1), 299−309.
(197) Garg, V. K.; Gupta, R.; Anu; Kumar, R. Dye removal from aqueous solution by adsorption on treated sawdust. *Bioresour. Technol.* **2003**, *89* (2), 121−124.
(198) Zeng, Z.; Ye, S.; Wu, H.; Xiao, R.; Zeng, G.; Liang, J.; Zhang, C.; Yu, J.; Fang, Y.; Song, B. Research on the sustainable efficacy of g-MoS2 decorated biochar nanocomposites for removing tetracycline hydrochloride from antibiotic-polluted aqueous solution. *Sci. Total Environ.* **2019**, *648*, 206−217.
(199) Yang, W.; Zheng, F.; Lu, Y.; Xue, X.; Li, N. Adsorption interaction of tetracyclines with porous synthetic resins. *Ind. Eng. Chem. Res.* **2011**, *50* (24), 13892−13898.
(200) Keiluweit, M.; Nico, P. S.; Johnson, M. G.; Kleber, M. Dynamic molecular structure of plant biomass-derived black carbon (Biochar). *Environ. Sci. Technol.* **2010**, *44* (4), 1247−1253.
(201) Sun, K.; Jin, J.; Keiluweit, M.; Kleber, M.; Wang, Z.; Pan, Z.; Xing, B. Polar and aliphatic domains regulate sorption of phthalic acid esters (PAEs) to biochars. *Bioresour. Technol.* **2012**, *118*, 120−127.
(202) Zhu, D.; Pignatello, J. J. Characterization of aromatic compound sorptive interactions with black carbon (charcoal) assisted by graphite as a model. *Environ. Sci. Technol.* **2005**, *39* (7), 2033−2041.
(203) Langmuir, I. The adsorption of gases on plane surfaces of glass, mica and platinum. *Journal of the American Chemical society* **1918**, *40* (9), 1361−1403.
(204) Freundlich, H. Over the adsorption in solution. *J. Phys. Chem.* **1906**, *57* (385471), 1100−1107.
(205) Temkin, M. Kinetics of ammonia synthesis on promoted iron catalysts. *Acta physiochim. URSS* **1940**, *12*, 327−356.
(206) Sips, R. On the structure of a catalyst surface. *J. Chem. Phys.* **1948**, *16* (5), 490−495.
(207) Toth, J. State equation of the solid-gas interface layers. *Acta Chimica Hungarica* **1971**, *69*, 311−328.
(208) Redlich, O.; Peterson, D. L. A useful adsorption isotherm. *J. Phys. Chem.* **1959**, *63* (6), 1024−1024.
(209) Radke, C.; Prausnitz, J. Adsorption of organic solutes from dilute aqueous solution of activated carbon. *Industrial Engineering Chemistry Fundamentals* **1972**, *11* (4), 445−451.
(210) Freundlich, H. M. F. Over the adsorption in solution. *J. Phys. Chem.* **1906**, *57*, 385−471.

https://doi.org/10.1021/acsomega.3c07804
ACS Omega 2024, 9, 12331−12379

(211) Langmuir, I. The constitution and fundamental properties of solids and liquids. Part 1. Solids. *J. Am. Chem. Soc.* **1916**, *38* (11), 2221−2295.
(212) Temkin, M. J.; Pyzhev, V. Recent modifications to Langmuir isotherms. *Acta Physicochimica URSS* **1940**, *12*, 217−222.
(213) Sips, R. Combined form of Langmuir and Freundlich equations. *J. Chem. Phys.* **1948**, *16*, 490−495.
(214) Toth, J. State equations of the solid gas interface layer. *Acta Chem. Acad. Hung* **1971**, *69*, 311−317.
(215) Redlich, O.; Peterson, D. L. A useful adsorption isotherm. *J. Phys. Chem.* **1959**, *63*, 1024.
(216) Radke, C. J.; Prausnitz, J. M. Adsorption of organic solutes from dilute aqueous solution on activated carbon. *Industrial and Engineering Chemistry Fundamental* **1972**, *11*, 445−451.
(217) Koble, R. A.; Corrigan, T. E. Adsorption isotherms for pure hydrocarbons. *Ind. Eng. Chem.* **1952**, *44* (2), 383−387.
(218) Baskar, A. V.; Bolan, N.; Hoang, S. A.; Sooriyakumar, P.; Kumar, M.; Singh, L.; Jasemizad, T.; Padhye, L. P.; Singh, G.; Vinu, A.; et al. Recovery, regeneration and sustainable management of spent adsorbents from wastewater treatment streams: A review. *Sci. Total Environ.* **2022**, *822*, 153555.
(219) Yang, H.; Ye, S.; Zeng, Z.; Zeng, G.; Tan, X.; Xiao, R.; Wang, J.; Song, B.; Du, L.; Qin, M.; et al. Utilization of biochar for resource recovery from water: A review. *Chem. Eng. J.* **2020**, *397*, 125502.
(220) Gupta, S.; Sireesha, S.; Sreedhar, I.; Patel, C. M.; Anitha, K. L. Latest trends in heavy metal removal from wastewater by biochar based sorbents. *Journal of Water Process Engineering* **2020**, *38*, 101561.
(221) Anush, S. M.; Chandan, H. R.; Gayathri, B. H.; Asma; Manju, N.; Vishalakshi, B.; Kalluraya, B. Graphene oxide functionalized chitosan-magnetite nanocomposite for removal of Cu(II) and Cr(VI) from waste water. *Int. J. Biol. Macromol.* **2020**, *164*, 4391−4402.
(222) Begna Sisay, G.; Belege Atisme, T.; Admassu Workie, Y.; Worku Negie, Z.; Leul Mekonnen, M. Mg/Zr modified nanobiochar from spent coffee grounds for phosphate recovery and its application as a phosphorous release fertilizer. *Environmental Nanotechnology, Monitoring & Management* **2023**, *19*, 100766.
(223) Yan, N.; Hu, B.; Zheng, Z.; Lu, H.; Chen, J.; Zhang, X.; Jiang, X.; Wu, Y.; Dolfing, J.; Xu, L. Twice-milled magnetic biochar: A recyclable material for efficient removal of methylene blue from wastewater. *Bioresour. Technol.* **2023**, *372*, 128663.
(224) Shafiq, F.; Anwar, S.; Firdaus e, B.; Zhang, L.; Ashraf, M. Nano-biochar: properties and prospects for sustainable agriculture. *Land Degradation & Development* **2023**, *34* (9), 2445−2463.
(225) Chen, X.; Zhou, B.; Wang, Q.; Tao, W.; Lin, H. Nano-biochar reduced soil erosion and nitrate loss in sloping fields on the Loess Plateau of China. *CATENA* **2020**, *187*, 104346.
(226) Kumar, H.; Cai, W.; Lai, J.; Chen, P.; Ganesan, S. P.; Bordoloi, S.; Liu, X.; Wen, Y.; Garg, A.; Mei, G. Influence of in-house produced biochars on cracks and retained water during drying-wetting cycles: comparison between conventional plant, animal, and nano-biochars. *Journal of Soils and Sediments* **2020**, *20* (4), 1983−1996.
(227) Major, J. Guidelines on practical aspects of biochar application to field soil in various soil management systems. *International Biochar Initiative* **2010**, *8*, 5−7.
(228) Das, S. K.; Ghosh, G. K. Development and evaluation of biochar-based secondary and micronutrient enriched slow release nano-fertilizer for reduced nutrient losses. *Biomass Conversion and Biorefinery* **2023**, *13*, 12193.
(229) Saxena, M.; Maity, S.; Sarkar, S. Carbon nanoparticles in 'biochar' boost wheat (Triticum aestivum) plant growth. *RSC Adv.* **2014**, *4* (75), 39948−39954.
(230) Liu, W.; Li, Y.; Feng, Y.; Qiao, J.; Zhao, H.; Xie, J.; Fang, Y.; Shen, S.; Liang, S. The effectiveness of nanobiochar for reducing phytotoxicity and improving soil remediation in cadmium-contaminated soil. *Sci. Rep.* **2020**, *10* (1), 858.
(231) Khader, A.; Ibrahim, M.; Alkhathami, F.; Elsawy, H.; El-Kader, N. A.; Shaker, E.; Sedky, A.; Mahmoud, E. Properties of Nano-Amendments and Their Effect on Some Soil Properties and Root-Knot Nematode and Yield Attributes of Tomato Plant. *Agriculture* **2023**, *13* (2), 366.
(232) Xu, W.; Xiao, L.; Hou, S.; Rukh, G.; Xu, M.; Pan, Y.; Xu, J.; Lan, W.; Ruan, Z.; Zhong, B.; et al. Bioavailability and speciation of Cadmium in contaminated paddy soil as alleviated by biochar from co-pyrolysis of peanut shells and maize straw. *Environmental Sciences Europe* **2022**, *34* (1), 69.
(233) Ramzan, M.; Zia, A.; Naz, G.; Shahid, M.; Shah, A. A.; Farid, G. Effect of nanobiochar (nBC) on morpho-physio-biochemical responses of black cumin (*Nigella sativa* L.) in Cr-spiked soil. *Plant Physiol. Biochem.* **2023**, *196*, 859−867.
(234) Ren, T.; Chen, N.; Wan Mahari, W. A.; Xu, C.; Feng, H.; Ji, X.; Yin, Q.; Chen, P.; Zhu, S.; Liu, H.; et al. Biochar for cadmium pollution mitigation and stress resistance in tobacco growth. *Environ. Res.* **2021**, *192*, 110273.
(235) Kong, M.; Liang, J.; White, J. C.; Elmer, W. H.; Wang, Y.; Xu, H.; He, W.; Shen, Y.; Gao, X. Biochar nanoparticle-induced plant immunity and its application with the elicitor methoxyindole in nicotiana benthamiana. *Environmental Science: Nano* **2022**, *9* (9), 3514−3524.
(236) Xuan, T. D.; Toyama, T.; Fukuta, M.; Khanh, T. D.; Tawata, S. Chemical interaction in the invasiveness of Cogongrass (Imperata cylindrica (L.) Beauv.). *J. Agric. Food. Chem.* **2009**, *57* (20), 9448−9453.
(237) Aftab, Z.-e.-H.; Aslam, W.; Aftab, A.; Shah, A. N.; Akhter, A.; Fakhar, U.; Siddiqui, I.; Ahmed, W.; Majid, F.; Wróbel, J.; et al. Incorporation of engineered nanoparticles of biochar and fly ash against bacterial leaf spot of pepper. *Sci. Rep.* **2022**, *12* (1), 8561.
(238) Datta, S.; Veena, R.; Samuel, M. S.; Selvarajan, E. Immobilization of laccases and applications for the detection and remediation of pollutants: a review. *Environmental Chemistry Letters* **2021**, *19* (1), 521−538.
(239) Lonappan, L.; Liu, Y.; Rouissi, T.; Pourcel, F.; Brar, S. K.; Verma, M.; Surampalli, R. Y. Covalent immobilization of laccase on citric acid functionalized micro-biochars derived from different feedstock and removal of diclofenac. *Chem. Eng. J.* **2018**, *351*, 985−994.
(240) Miri, S.; Perez, J. A. E.; Brar, S. K.; Rouissi, T.; Martel, R. Sustainable production and co-immobilization of cold-active enzymes from Pseudomonas sp. for BTEX biodegradation. *Environ. Pollut.* **2021**, *285*, 117678.
(241) Taheran, M.; Naghdi, M.; Brar, S. K.; Knystautas, E. J.; Verma, M.; Surampalli, R. Y. Degradation of chlortetracycline using immobilized laccase on Polyacrylonitrile-biochar composite nanofibrous membrane. *Sci. Total Environ.* **2017**, *605−606*, 315−321.
(242) Goswami, L.; Pakshirajan, K.; Pugazhenthi, G. Biological treatment of biomass gasification wastewater using hydrocarbonoclastic bacterium Rhodococcus opacus in an up-flow packed bed bioreactor with a novel waste-derived nano-biochar based bio-support material. *Journal of Cleaner Production* **2020**, *256*, 120253.
(243) Velusamy, K.; Devanand, J.; Senthil Kumar, P.; Soundarajan, K.; Sivasubramanian, V.; Sindhu, J.; Vo, D.-V. N. A review on nano-catalysts and biochar-based catalysts for biofuel production. *Fuel* **2021**, *306*, 121632.
(244) Safieddin Ardebili, S. M.; Taghipoor, A.; Solmaz, H.; Mostafaei, M. The effect of nano-biochar on the performance and emissions of a diesel engine fueled with fusel oil-diesel fuel. *Fuel* **2020**, *268*, 117356.
(245) Saxena, V.; Kumar, N.; Saxena, V. K. A comprehensive review on combustion and stability aspects of metal nanoparticles and its additive effect on diesel and biodiesel fuelled C.I. engine. *Renewable and Sustainable Energy Reviews* **2017**, *70*, 563−588.
(246) Mirbagheri, S. A.; Safieddin Ardebili, S. M.; Kiani Deh Kiani, M. Modeling of the engine performance and exhaust emissions characteristics of a single-cylinder diesel using nano-biochar added into ethanol-biodiesel-diesel blends. *Fuel* **2020**, *278*, 118238.
(247) Ramachandran, S.; Thangavelu, M.; Kamaraj, L.; Sorakka Ponnappan, V.; Arumugam, R. Ignition analysis of diesel engine propelled with neat biodiesel containing nanoparticles. *Energy Sources, Part A: Recovery, Utilization, and Environmental Effects* **2021**, 1−13.

https://doi.org/10.1021/acsomega.3c07804
ACS Omega 2024, 9, 12331−12379

(248) Ferlazzo, A.; Bressi, V.; Espro, C.; Iannazzo, D.; Piperopoulos, E.; Neri, G. Electrochemical determination of nitrites and sulfites by using waste-derived nanobiochar. *J. Electroanal. Chem.* **2023**, *928*, 117071.
(249) Bressi, V.; Chiarotto, I.; Ferlazzo, A.; Celesti, C.; Michenzi, C.; Len, T.; Iannazzo, D.; Neri, G.; Espro, C. Voltammetric sensor based on waste-derived carbon nanodots for enhanced detection of nitrobenzene. *ChemElectroChem.* **2023**, *10*, No. e202300004.
(250) Liu, Y.; Sun, M.; Wang, T.; Chen, X.; Wang, H. Chitosan-based self-assembled nanomaterials: their application in drug delivery. *VIEW* **2021**, *2* (1), 20200069.
(251) Iannazzo, D.; Celesti, C.; Espro, C.; Ferlazzo, A.; Giofrè, S. V.; Scuderi, M.; Scalese, S.; Gabriele, B.; Mancuso, R.; Ziccarelli, I.; et al. Orange-peel-derived nanobiochar for targeted cancer therapy. *Pharmaceutics* **2022**, *14* (10), 2249.
(252) Ng, C. W. W.; Coo, J. L.; Chen, Z. K.; Chen, R. Water infiltration into a new three-layer landfill cover system. *J. Environ. Eng.* **2016**, *142* (5), 04016007.
(253) Chen, S.; Lu, X.; Wang, T.; Zhang, Z. Preparation and characterization of urea-formaldehyde resin/reactive kaolinite composites. *Particuology* **2016**, *24*, 203−209.
(254) Liu, H.; Feng, S. Effects of nano-biochar of different particle sizes on the shrinkage properties of kaolin. *Journal of Soils and Sediments* **2022**, *22* (5), 1511−1520.
(255) Zhang, Y.; Schaap, M. G. Estimation of saturated hydraulic conductivity with pedotransfer functions: A review. *Journal of Hydrology* **2019**, *575*, 1011−1030.
(256) Jeffery, S.; Meinders, M. B. J.; Stoof, C. R.; Bezemer, T. M.; van de Voorde, T. F. J.; Mommer, L.; van Groenigen, J. W. Biochar application does not improve the soil hydrological function of a sandy soil. *Geoderma* **2015**, *251*−*252*, 47−54.
(257) Liu, H. W.; Feng, S.; Leung, A. K. Effects of nano-activated carbon on water and gas permeability and hydrogen sulphide removal in compacted kaolin. *Appl. Clay Sci.* **2019**, *172*, 80−84.
(258) Gupta, S.; Kua, H. W.; Low, C. Y. Use of biochar as carbon sequestering additive in cement mortar. *Cem. Concr. Compos.* **2018**, *87*, 110−129.
(259) Worrell, E.; Price, L.; Martin, N.; Hendriks, C.; Meida, L. O. Carbon dioxide emissions from the global cement industry. *Annu. Rev. Energy Environ.* **2001**, *26* (1), 303−329.
(260) Andrew, R. M. Global CO_2 emissions from cement production, 1928−2018. *Earth Syst. Sci. Data* **2019**, *11* (4), 1675−1710.
(261) Mehta, P. K. Greening of the concrete industry for sustainable development. *Concr. Int.* **2002**, *24* (7), 23−28.
(262) Zhao, S.; Huang, B.; Shu, X.; Ye, P. Laboratory investigation of biochar-modified asphalt mixture. *Transportation Research Record* **2014**, *2445* (1), 56−63.
(263) Walters, R. C.; Fini, E. H.; Abu-Lebdeh, T. Enhancing asphalt rheological behavior and aging susceptibility using bio-char and nano-clay. *American Journal of Engineering and Applied Sciences* **2014**, *7* (1), 66.
(264) Yang, S.; Wi, S.; Lee, J.; Lee, H.; Kim, S. Biochar-red clay composites for energy efficiency as eco-friendly building materials: thermal and mechanical performance. *J. Hazard. Mater.* **2019**, *373*, 844−855.
(265) Lee, H.; Yang, S.; Wi, S.; Kim, S. Thermal transfer behavior of biochar-natural inorganic clay composite for building envelope insulation. *Construction and Building Materials* **2019**, *223*, 668−678.
(266) Farges, R.; Gharzouni, A.; Ravier, B.; Jeulin, P.; Rossignol, S. Insulating foams and dense geopolymers from biochar by-products. *Journal of Ceramic Science Technology* **2018**, *9* (2), 193−200.
(267) Novais, R. M.; Saeli, M.; Caetano, A. P. F.; Seabra, M. P.; Labrincha, J. A.; Surendran, K. P.; Pullar, R. C. Pyrolysed cork-geopolymer composites: a novel and sustainable EMI shielding building material. *Construction and Building Materials* **2019**, *229*, 116930.
(268) Maljaee, H.; Madadi, R.; Paiva, H.; Tarelho, L.; Ferreira, V. M. Incorporation of biochar in cementitious materials: A roadmap of biochar selection. *Construction and Building Materials* **2021**, *283*, 122757.
(269) Woolf, D.; Amonette, J. E.; Street-Perrott, F. A.; Lehmann, J.; Joseph, S. Sustainable biochar to mitigate global climate change. *Nat. Commun.* **2010**, *1* (1), 56.
(270) Sisman, M.; Teomete, E.; Yanik, J.; Malayoglu, U.; Tac, G. The effects of apricot kernel shell nanobiochar on mechanical properties of cement composites. *Cement-Wapno-Beton = Cement Lime Concrete* **2023**, *28* (1), 2.
(271) Cosentino, I.; Restuccia, L.; Ferro, G. A.; Tulliani, J.-M. Influence of pyrolysis parameters on the efficiency of the biochar as nanoparticles into cement-based composites. *Procedia Structural Integrity* **2018**, *13*, 2132−2136.
(272) Goswami, R.; Kumar, M. Removal of fluoride from aqueous solution using nanoscale rice husk biochar. *Groundwater for Sustainable Development* **2018**, *7*, 446−451.
(273) Elbehiry, F.; Darweesh, M.; Al-Anany, F. S.; Khalifa, A. M.; Almashad, A. A.; El-Ramady, H.; El-Banna, A.; Rajput, V. D.; Jatav, H. S.; Elbasiouny, H. Using biochar and nanobiochar of water hyacinth and black tea waste in metals removal from aqueous solutions. *Sustainability* **2022**, *14* (16), 10118.
(274) Tan, E. C. D.; Lamers, P. Circular bioeconomy concepts—A perspective. *Front. Sustain.* **2021**, *2*, 701509.
(275) Casau, M.; Dias, M. F.; Matias, J. C. O.; Nunes, L. J. R. Residual biomass: A comprehensive review on the importance, uses and potential in a circular bioeconomy approach. *Resources* **2022**, *11* (4), 35.
(276) Sani, M. N. H.; Amin, M.; Siddique, A. B.; Nasif, S. O.; Ghaley, B. B.; Ge, L.; Wang, F.; Yong, J. W. H. Waste-derived nanobiochar: A new avenue towards sustainable agriculture, environment, and circular bioeconomy. *Sci. Total Environ.* **2023**, *905*, 166881.
(277) Arora, N. K.; Mishra, I. United Nations Sustainable Development Goals 2030 and environmental sustainability: race against time. *Environmental Sustainability* **2019**, *2* (4), 339−342.
(278) Mazarji, M.; Bayero, M. T.; Minkina, T.; Sushkova, S.; Mandzhieva, S.; Tereshchenko, A.; Timofeeva, A.; Bauer, T.; Burachevskaya, M.; Kızılkaya, R.; et al. Realizing United Nations Sustainable Development Goals for greener remediation of heavy metals-contaminated soils by biochar: emerging trends and future directions. *Sustainability* **2021**, *13* (24), 13825.
(279) Neogi, S.; Sharma, V.; Khan, N.; Chaurasia, D.; Ahmad, A.; Chauhan, S.; Singh, A.; You, S.; Pandey, A.; Bhargava, P. C. Sustainable biochar: A facile strategy for soil and environmental restoration, energy generation, mitigation of global climate change and circular bioeconomy. *Chemosphere* **2022**, *293*, 133474.
(280) Ramadan, M. M.; Asran, A.; Abd-Elsalam, K. A. Chapter 16 - Micro/nano biochar for sustainable plant health: Present status and future prospects. In *Carbon Nanomaterials for Agri-Food and Environmental Applications*; Abd-Elsalam, K. A., Ed.; Elsevier, 2020; pp 323−357.
(281) Plácido, J. S.; Meissner, K. E.; Kelly, D. E.; Kelly, S. L.; et al. Multivariate analysis of biochar-derived carbonaceous nanomaterials for detection of heavy metal ions in aqueous systems. *Sci. Total Environ.* **2019**, *688*, 751−761.
(282) Huang, X.; Zhu, S.; Zhang, H.; Huang, Y.; Wang, X.; Wang, Y.; Chen, D. Biochar nanoparticles induced distinct biological effects on freshwater algae via oxidative stress, membrane damage, and nutrient depletion. *ACS Sustainable Chem. Eng.* **2021**, *9* (32), 10761−10770.
(283) Gao, X.; Wu, H. Aerodynamic properties of biochar particles: effect of grinding and implications. *Environmental Science & Technology Letters* **2014**, *1* (1), 60−64.
(284) Xiao, Y.; Lyu, H.; Tang, J.; Wang, K.; Sun, H. Effects of ball milling on the photochemistry of biochar: Enrofloxacin degradation and possible mechanisms. *Chem. Eng. J.* **2020**, *384*, 123311.

https://doi.org/10.1021/acsomega.3c07804
ACS Omega 2024, 9, 12331−12379